TECHNICAL REPORT STANDARD TITLE PAGE

1. Report No.	2. Government Accession No.	3. Recipient's Catalog No.
FHWA/TX-86/59+384-1F		

4. Title and Subtitle	5. Report Date
DEVELOPMENT OF A SIMPLE FATIGUE RESISTANT STAY CABLE ANCHORAGE	November 1985
	6. Performing Organization Code
7. Author(s)	8. Performing Organization Report No.
J. L. Lamb and K. H. Frank	Research Report 384-1F
9. Performing Organization Name and Address	10. Work Unit No.
Center for Transportation Research The University of Texas at Austin Austin, Texas 78712-1075	11. Contract or Grant No. Research Study 3-5-84-384
	13. Type of Report and Period Covered
12. Sponsoring Agency Name and Address Texas State Department of Highways and Public Transportation; Transportation Planning Division P. O. Box 5051 Austin, Texas 78763	Final
	14. Sponsoring Agency Code

15. Supplementary Notes

Study conducted in cooperation with the U. S. Department of Transportation, Federal Highway Administration. Research Study Title: "Development of a Simple Fatigue-Resistant Stay Cable Anchorage"

16. Abstract

A simple fatigue-resistant anchorage for seven wire prestressing strand was developed and studied. The fatigue test results indicate that an anchorage incorporating copper or aluminum wedges which have been formed to match the strand produce an anchorage which can attain the fatigue strength of the strand.

The fatigue test results were correlated with load distribution measurements, finite element analysis, electron microscopy of the fractures, and various wear models. A clear understanding of the factors relating to the fatigue performance of the wedges studies resulted from the correlation of the various studies.

A further optimization of the anchorage is possible based on the results of the theoretical studies. However, the anchorage as developed using copper wedges is adequate. The developed anchorage provides a simple anchorage which allows for individual insertion and removal of the strands making up a cable stay.

17. Key Words	18. Distribution Statement
anchorage, fatigue resistant, stay cable, prestressing strand, seven-wire, wedges, copper, aluminum	No restrictions. This document is available to the public through the National Technical Information Service, Springfield, Virginia 22161.

19. Security Classif. (of this report)	20. Security Classif. (of this page)	21. No. of Pages	22. Price
Unclassified	Unclassified	158	

Form DOT F 1700.7 (8-69)

DEVELOPMENT OF A SIMPLE FATIGUE RESISTANT STAY CABLE ANCHORAGE

by

J. L. Lamb and K. H. Frank

Research Report No. 384-1F

Research Study 3-5-84-384

Development of a Simple Fatigue-Resistant Stay Cable Anchorage

Conducted for

Texas
State Department of Highways and Public Transportation

In Cooperation with the
U.S. Department of Transportation
Federal Highway Administration

by

CENTER FOR TRANSPORTATION RESEARCH
BUREAU OF ENGINEERING RESEARCH
THE UNIVERSITY OF TEXAS AT AUSTIN

November 1985

The contents of this report reflect the views of the authors who are responsible for the facts and accuracy of the data presented herein. The contents do not necessarily reflect the views of policies of the Federal Highway Administration. This report does not constitute a standard, specification or regulation.

There was no invention or discovery conceived or first actually reduced to practice in the course of or under this contract, including any art, method, process, machine, manufacture, design or composition of matter, or any new and useful improvement thereof, or any variety of plant which is or may be patentable under the patent laws of the United States of America or any foreign country.

PREFACE

This report presents the results of Research Project 3-5-84-384, "Development of a Simple Fatigue-Resistant Stay Cable Anchorage." This research was sponsored by the Texas State Department of Highways and Public Transportation and the Federal Highway Administration. Specimen testing was performed at the Phil M. Ferguson Structural Engineering Laboratory of The University of Texas at Austin.

The authors are grateful for the help of Blake Stasney and Richard Marshall, who built and maintained the test equipment. Maxine DeButts was invaluable for her editing and typing of this report. Laurie Golding helped by expediting the purchase and machining of the wedges used in the project.

S U M M A R Y

A simple fatigue resistant anchorage for seven wire prestressing strand was developed and studied. The fatigue test results indicate that ananchorage incorporating copper or aluminum wedges which have been formed to match the strand produce an anchorage which can attain the fatigue strength of the strand.

The fatigue test results were correlated with load distribution measurements, finite element analysis, electron microscopy of the fractures, and various wear models. A clear understanding of the factors relating to the fatigue performance of the wedges studied resulted from the correlation of the various studies.

A further optimization of the anchorage is possible based on the results of the theoretical studies. However, the anchorage as developed using copper wedges is adequate. The developed anchorage provides a simple anchorage which allows for individual insertion and removal of the strands making up a cable stay.

I M P L E M E N T A T I O N

A simple fatigue resistant anchorage was developed and studied in this project. The anchorage should be evaluated by designers and contractors to determine the feasibility of using the anchorage in actual construction. Full size or near full size tests should be performed on stays using this anchorage to determine if the construction of the stay may lead to unforeseen fatigue or static strength problems.

C O N T E N T S

F I G U R E S

Figure Page

T A B L E S

CHAPTER 1

INTRODUCTION

1.1 The Cable-Stayed Bridge: Historical Background

The stayed bridge concept was first offered by C. J. Loscher in 1784. His design consisted of a timber deck, tower, and stays. Later engineers built upon the concepts of Loscher. Other proposed design possibilities included steel bar stays, proposed in 1821, and chain stays, proposed in 1840. Failures of some of the early stayed bridges undoubtedly accounted for their fall from engineers' favor [23].

One of the main advantages of the cable-stayed bridge over the suspension type is its increased stiffness characteristics. The increased stiffness is a result of the direct transfer of load from the bridge deck to the tower. This mechanism has, however, been found to be responsible for severe fatigue problems in the anchorage zones, where the stay cable is connected to the tower and deck. Many research programs have attempted to alleviate the problem. The solutions, some quite successful, are complex and do not allow for inspection of the cable in the critical anchorage region. This point is discussed in more detail in the next section and Chapter 2.

1.2 Limitations of Existing Cable Stay Anchorages

The research program presented in this report was proposed to further investigate the problem of fatigue in the anchorage region. The final goal of the research is the development of a simple fatigue-resistant method of anchoring parallel strand cable stays.

Cable stay anchorages currently being studied and used in bridges around the world are presented in detail in Chapter 2. While the manufacturers claim the anchorages to be fatigue resistant, there are disadvantages in their systems. The anchorages are typically grouted with epoxy or cement which not only serves to carry most of the live load but also acts as corrosion protection for the individual wires or strands that make up the cable. Research programs aimed at studying the fatigue resistance of these cable stay anchors have not addressed the question of long-term effects of grout creep. Creep of the load-carrying grout could adversely affect the performance of the anchor if some of the dynamic live load reached the fatigue-sensitive

dead load anchors (standard prestressing chucks). The dead load anchor is placed behind the live load anchorage zone and serves to hold the individual wires or strands in place while the live load anchor is formed (cast). A typical anchorage arrangement is shown in Fig. 1.1. Since creep is a long-term phenomenon, it would not be observed in short-term laboratory testing. In addition to the problem of creep, cracking of the grout may compromise the grout's function as a barrier to the corrosive environment. Aggravating the problem further is the fact that the grout prevents the inspection of the strands or wires and consequently the replacement of a single strand should the need arise.

In summary, while laboratory tests may indicate that a given anchorage does not affect the fatigue performance of the cable, the time frame of laboratory tests does not allow for the possible detrimental effects of creep and corrosion. The inspection and possible replacement of strands or wires is made difficult since the strands or wires are encased.

1.3 Purpose of Research Program

The purpose of this research program is to develop a method of anchoring cable stays which will not only provide fatigue resistance but also allow for the visual inspection and replacement of the individual strands that make up the cable. To better understand and characterize the performance of the anchorages tested, three separate experimental and analytical methods were employed: (1) Laboratory testing, (2) Finite element stress analysis, and (3) Scanning electron microscope fractography.

The laboratory testing program consisted of two parts: the first, fatigue tests, and the second, load distribution tests. Rather than testing full-size cables, which would be both expensive and time consuming, only individual strands were tested. Since this research is primarily oriented to the parallel-strand cable systems, the specimens selected for testing in this program were 0.5 in. and 0.6 in. diameter, Grade 270 prestressing strands. The test methods and results are presented in Chapters 4, 5 and 6.

In addition to the fatigue tests, load distribution tests were performed. The anchorage method selected for this application is a two-stage grip technique. The applied load is shared between the two grips. Specific tests were performed which measured the load distribution between the two grips. The details of this two-stage grip and the results of the load distribution study are presented in Chapter 5.

The results from the load distribution study gave the total load carried by each of the grips, but did not provide information as

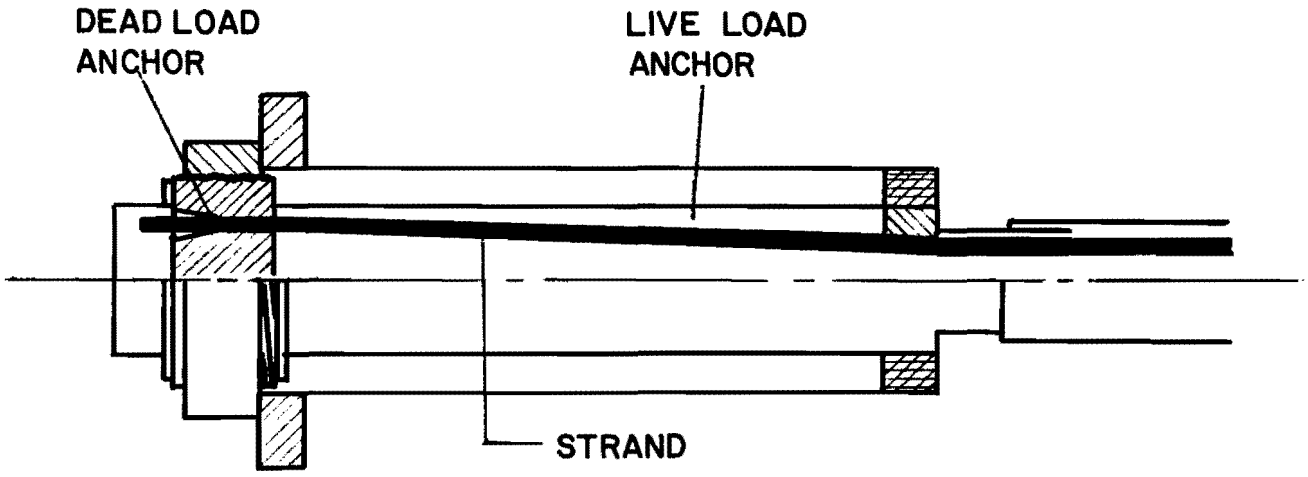

Fig. 1.1 Typical multi-strand anchorage

to how the load was distributed along the strand within each of the grips. To obtain this information, a finite element study was performed. The finite element stress analysis program, ABAQUS, donated to the University of Texas for research purposes by Hibbit, Karlsson, and Sorrenson Inc., was used for this analysis. In addition to the geometric and material variables tested experimentally, other grip geometries were also analyzed in the finite element study so that their probable experimental performance could be judged without actually testing them. The results of this analysis are presented in Chapter 5.

The quantitative information provided by the experimental work and the stress analysis is complimented by qualitative information from the fractography study. The fatigue-fractured pieces of wire were cut from the strands and viewed under a scanning electron microscope. The location of crack nucleation could be determined. Any surface damage (scratches, pits, etc.) could also be seen and compared to other failures. The photographs and discussion of the fractography study are presented in Chapter 6.

A complete synthesis of the experimental and analytical results is presented in Chapter 6 of this report. A wear model is proposed to explain the quantitative and qualitative data. The performance of each of the grips tested is discussed in relation to the wear model. Finally, in Chapter 7, a cable-stay anchorage is proposed which satisfies the goals set for this research program. The anchorage is simple to apply in the field, fatigue resistant, allows for inspection of the individual strands, and also provides for the replacement of individual strands should replacement be necessary.

CHAPTER 2

CURRENT ANCHORAGE METHODS AND RELATED RESEARCH

Some of the current methods employed in anchoring cable stays will be presented in this chapter. A primary function of all cable stay anchors is to produce failures away from the anchor regions, thus developing the full strength of the cable. It will be demonstrated that while some of the anchoring methods have proved successful in resisting fatigue, they are very complex, require a great deal of time to fabricate, and do not allow for inspection and individual replacement of component strands or wires. In addition to the current anchoring methods, a review of a research program [19] carried out at the Otto Graf Institute in Stuttgart, Germany will be presented.

2.1 Current Anchorage Methods

The four anchoring methods to be presented in this section include the zinc-filled socket, the HiAm socket, the BBRV-DINA socket, and the Freyssinet H15 anchorage. The procedure used in the fabrication process of each of the anchorages will be described as well as its performance with respect to fatigue.

2.1.1 Zinc-Filled Socket. The zinc-filled socket shown in Fig. 2.1 was very successful in suspension bridge applications so it was only natural to use the method for cable-stayed bridge applications. However, the susceptibility of the anchorage to fatigue loading has rendered this method useless in cable-stayed structures.

The zinc-filled anchorage is generally prefabricated. The individual wires are first splayed and then passed into the socket after being cleaned and coated with a flux solution. Molten zinc (heated to temperature of approximately 450) is poured into the socket surrounding each of the strands and allowed to cool. This process is tightly controlled so as to prevent premature hardening of the zinc and yet keep the heat-induced embrittlement of the cable to a minimum.

Applied tension in the cable causes the entire zinc/cable mass to move into the socket. As the socket is tapered, radial stresses develop with increasing tension and, together with the bond between the zinc and cable, hold the individual wires in place. A secondary standard anchorage and end plate applied at the rear of the socket has been used to help prevent strand pull-out.

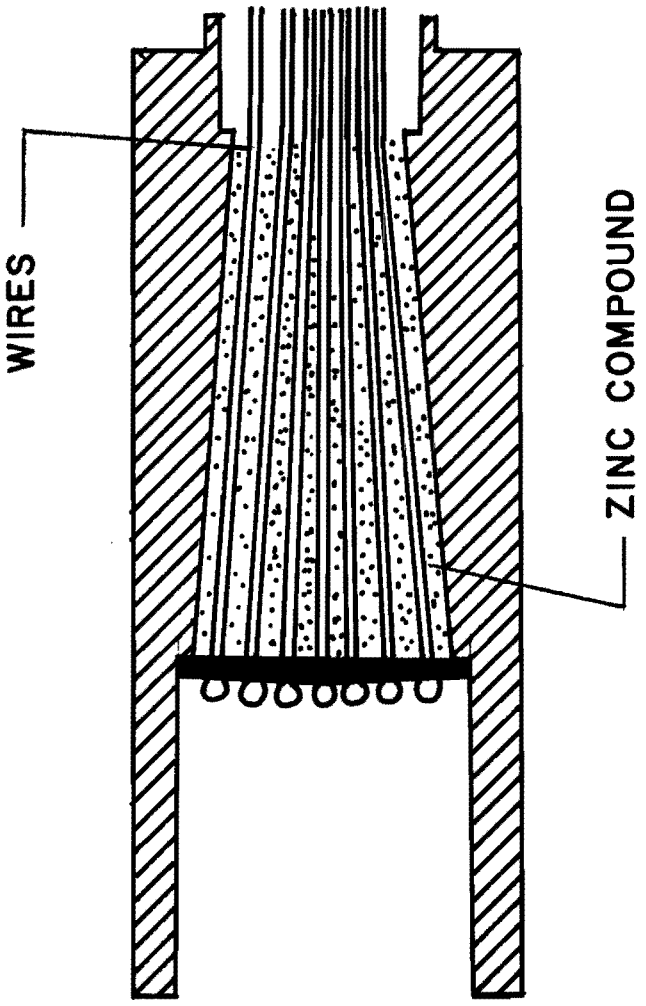

Fig. 2.1 Zinc-filled socket for wire

While this type of anchorage has performed satisfactorily in static load situations, fatigue loading has caused problems. Wire embrittlement is partially responsible for the poor fatigue performance. When the molten zinc comes into contact with the wires, embrittlement occurs which is known to reduce fatigue strength. The large stress concentrations that exist at the lead-in portion of the anchorage have also been cited as a cause of reduced fatigue lives.

2.1.2 HiAm Socket. Recognition of the negative side effects of the hot pouring process has led to the application of "cold-pouring" technology to anchorage fabrication. The HiAm socket (HiAm stands for high amplitude), illustrated in Fig. 2.2, makes use of this form of anchorage fabrication. Some similarities exist between the zinc-filled socket and the HiAm socket. Both anchorages are intended for use with parallel-wire cables. The sockets are also tapered and splaying of the individual wires is necessary. In the fabrication of the HiAm socket, the wires are passed through an endplate and button-headed which serves to hold the wires in place during the pouring process and provide initial load resistance.

The process of filling the socket is performed in three stages (two stages have been used as well). The first layer, where the cable enters the socket, is an epoxy compound. The second stage is composed of a combination of epoxy and zinc dust and the third, filling the majority of the socket, consists of epoxy and steel balls. The idea behind the three-stage filling process is to provide a gradient of stiffness along the length of the anchorage. It is believed that the stiffness gradient leads to a more uniform stress distribution along the cable and prevents stress concentrations forming at the base of the anchorage. After the process of filling the socket is completed, the entire socket is vibrated to ensure a homogeneous mixture. Voids in the socket could jeopardize the entire anchorage.

The wedging action described for the zinc-filled socket is also responsible for the load transfer in the HiAm socket. The stress distribution along the individual wires is, however, more complex due to the introduction of the steel balls. The fatigue performance has been encouraging. It is reported [12] that a majority of the wires that break, break in the free length of the stay cable.

2.1.3 BBRV-DINA Socket. The BBRV-DINA anchorage is intended for use with either parallel wire or parallel-strand cables. This socket intended for use with parallel strand is illustrated in Fig. 2.3 and is constructed by first splaying the individual strands and then passing them through an endplate. The initial process is similar to the previous methods. There is no conical socket in this form of cable anchorage. After the strands have been anchored (with buttonheads for wires and prestressing chucks for strands) behind the endplate an epoxy compound is poured around the wires.

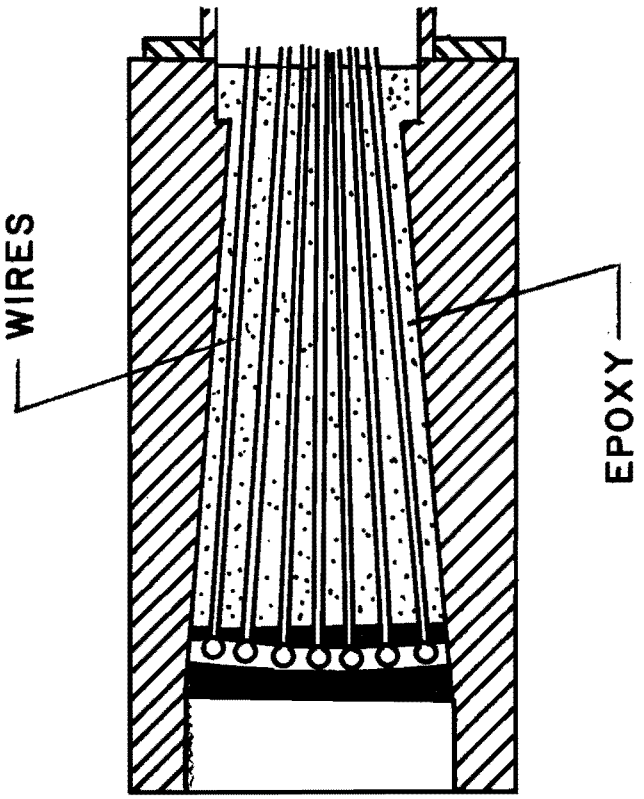

Fig. 2.2 Hi-Am socket for wire

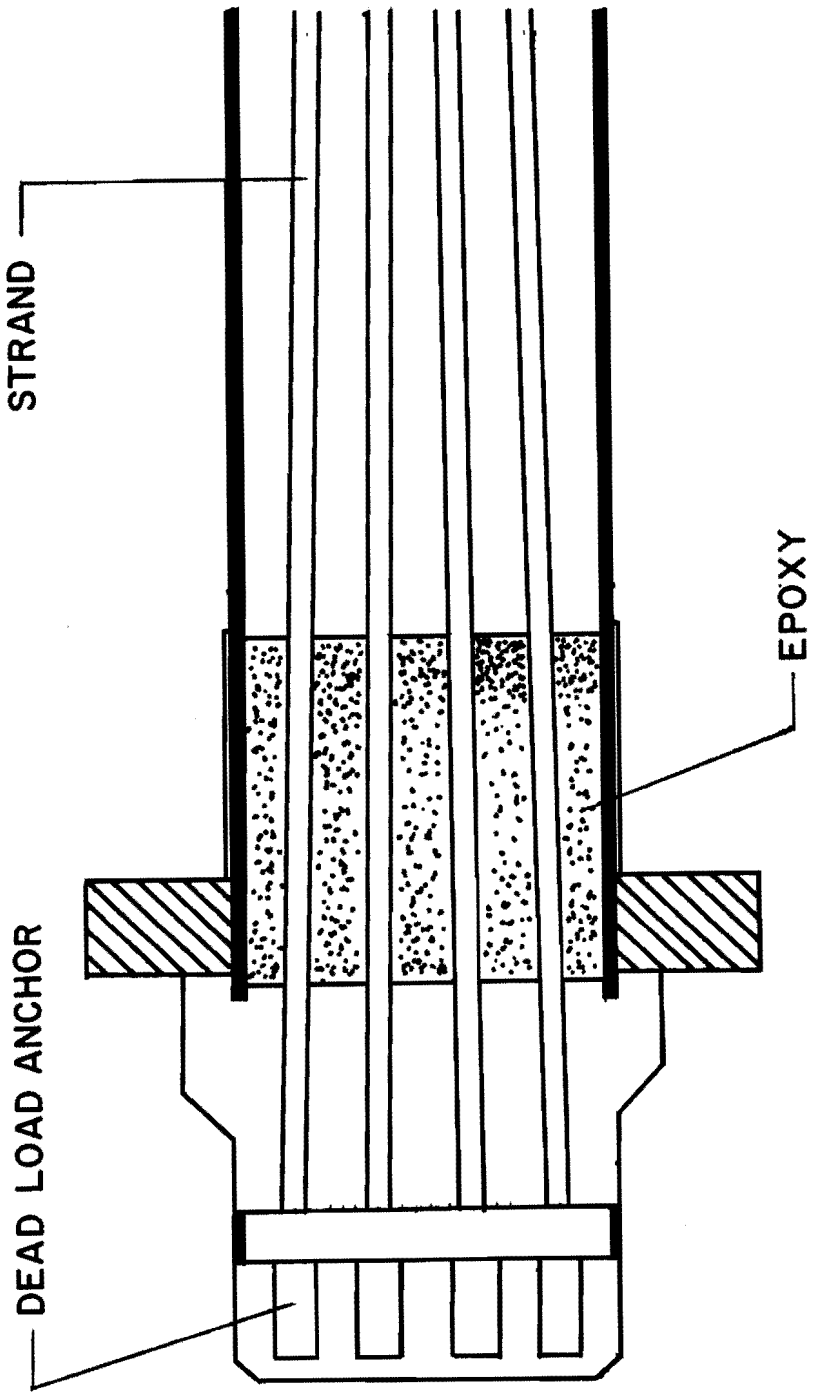

Fig. 2.3 BBRV-DINA socket for parallel wire strand

Since there is no tapered socket in this anchoring technique, the load transfer mechanism is different. The dead or static load is designed to be taken at the endplate while the dynamic load is carried by the epoxy compound.

2.1.4 Freyssinet H15 Anchor. The Freyssinet anchor is a relatively new method of anchoring parallel-strand cables. This anchorage, shown in Fig. 2.4, is designed for use with parallel strand cables. Fabrication of this anchorage requires that the strands be passed through a series of trumpets, each increasing in diameter toward the endplate. The strands are then splayed and held in place behind the endplate with standard prestressing chucks. Like the BBRV-DINA socket, the static and dynamic loads are separated. After the expected dead load has been applied to the cable, the prestressing chucks are adjusted to lock in this stress. An epoxy or cement grout is then poured into the trumpets. The dynamic load is carried by the epoxy.

The combination of long transitional trumpets and increasing diameter ensures that little dynamic load reaches the prestressing chucks. The dynamic stresses are transferred by friction into the grout and then by wedging action into the trumpets. The fatigue performance of this anchorage is good, allowing for the full development of the fatigue strength of the cable [17].

2.1.5 Summary. Four methods of anchoring stay cables have been described. The complexity of each of the anchorages can be readily seen. The HiAm, Freyssinet H15, and possibly the BBRV-DINA anchorages were discussed. Tests performed with the anchorages lead to development of the fatigue strength of the cable. These anchorages can be termed "fatigue resistant". An anchorage can therefore be defined as "fatigue resistant" if, as a result of fatigue testing, failures of component wires or strands occur between the anchored zones rather than in the anchorages themselves.

2.2 Related Research

The research of the fatigue problem using single strands or wires is relatively new, though the idea may not be. Most of the fatigue testing performed on individual strands and wires has as its main goal the determination of the fatigue characteristics of the strand. Failures occurring in the gripped region, while not giving an accurate index to the fatigue strength of the specimen itself, are regarded as an occupational hazard.

A research program [19] conducted at the Otto Graf Institute of the University of Stuttgart in Germany is the only research program

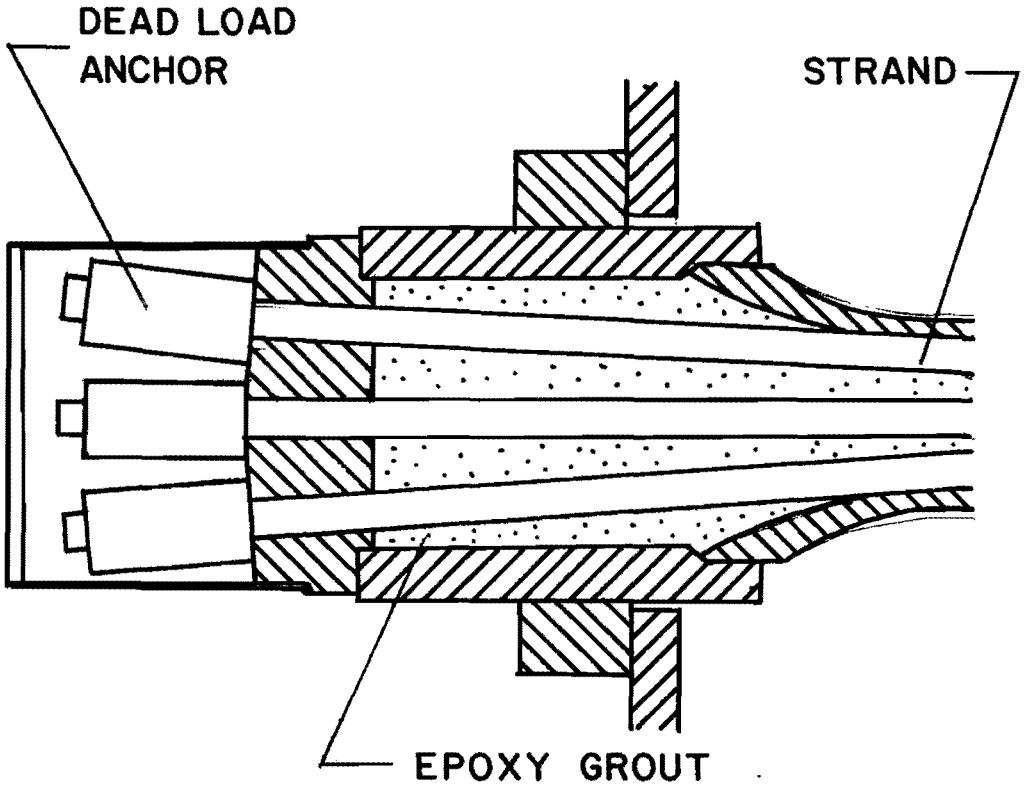

Fig. 2.4 Freyssinet H15 anchorage for parallel wire strand

in the literature which specifically investigated the fatigue problem of the anchorage. The portion of the research that dealt with wedge anchorages is presented in this section.

The goal of the research was the determination of the effects of the clamping stress, wedge-induced notches, and fretting on the fatigue strength of a single high strength steel bar 12 mm (0.5 in.) in diameter. The effect of the transverse (clamping) pressure on the fatigue life was investigated by two different methods. First, the load was applied as a uniformly distributed load of 5 kN/mm (28.55 kips/in.). The researchers used a bar of equal diameter placed along side the test specimen to apply the transverse load. In the second test, a near-concentrated force of 20 kN (4.5 kips.) was applied with 7 mm (0.25 in.) diameter bars arranged perpendicular to the axis of the test specimen. The test specimen was a 7 mm diameter bar. It was found that the lateral pressure, alone, had essentially no effect of the fatigue strength.

The second series of tests was designed to investigate the effect of the notches produced in the surface of the bars by the serrations on the inner surface of the wedges. A clamp with a single tooth was applied to bar specimens with clamping forces varying from 20 kN to 80 kN (18 kips). The assembly was then tested in fatigue. Failures consistently occurred in the clamped region but always away from the notch. They concluded the notches had little effect on the fatigue performance.

The last set of tests was intended to investigate the effect of fretting ("Reibkorrosion"). In these tests, two sets of mutually opposing clamping forces were applied to the 12 mm diameter bar specimens 100 mm (3.94 in.) apart. The loads were applied with 12 mm diameter bars set perpendicular to the axis of the test specimen. The magnitude of the forces varied from 6 kN (1.35 kips.) to 20 kN. The effect of fretting on the fatigue strength was significant. Reductions in the fatigue life were found to be more than 50%. They reported the effect was not as serious when a lubricant was used.

To test the validity of their results, the research team designed a new wedge. The wedge was designed to dig into the surface of the test bars and prevent the relative motion. The modifications to the old style wedge included fully-formed teeth at the beginning of the wedge (the teeth of the older version were smaller to reduce the size of the notch), and a taper angle which forced initial contact to occur at the first tooth as opposed to having all teeth contact simultaneously as in the older wedge. The goal of the researchers was to develop a wedge which would force the digging in of the first and subsequent teeth into the surface of the bar. This would tend to hold the wedge in place and prevent the relative displacement, and thus the fretting, from occurring. Tests performed with this wedge, reportedly,

proved to be successful as the bar consistently failed outside the anchored region.

A review of a research program performed at the Otto Graf Institute in Germany was presented in this subsection. The researchers found the fatigue lives of their 12 mm diameter bar specimens to be controlled by the fretting process rather than by any notching produced by the conventional wedge-type anchorage. A new wedge was designed to eliminate relative slip between the surface of the bar and the wedge and thus the fretting as well. The new wedge proved successful.

CHAPTER 3

FAILURE MECHANISMS IN THE ANCHORAGE ZONES

Researchers performing fatigue tests on prestressing strand have long been plagued by premature fatigue failures in the anchorage zones. Understanding the reasons for these consistent fatigue failures is of paramount interest if the goal of fatigue resistance is to be satisfied. The various modes of failure in the anchorage zone will be presented in this chapter. Each of the modes will be defined and its mechanism described. The variables affecting the mode of failure will also be presented as well as methods of preventing or controlling it. As a given mode of failure is highly case specific, the basic features of typical anchorage assemblies will be presented first.

Anchorage assemblies which rely on wedging action typically consist of three main elements: the strand, wedge (two or three pieces), and the collar (reacts wedging action through tensile hoop stress) (Fig. 3.1). Load is transferred from the strand into the wedges by friction and then into the collar. The force is then resisted by bearing between the end plate and the collar. Since the wedge and the strand are separate parts some relative displacement between the two is possible. Also the wedge and the strand are fabricated from different materials. In order to develop the necessary friction, a large clamping force is developed through the wedge/collar assembly leading to large surface tractions at the interface between the strand and the wedge. Finally, the entire system is loaded in fatigue so that all of the stress components vary with time.

Prior to discussing the various failure modes, the process of fatigue will be presented. A brief discussion of crack initiation and crack propagation will be presented. In studying a variety of failure modes, four specific cases appear to be particularly important. Abrasive and adhesive wear are active at the strand/wedge interface and must be considered. The mode of failure known as fretting (cited as the cause of failure in the research program reviewed in the previous chapter) is considered since it is a specialization and extension of the abrasive and adhesive modes. Corrosion fatigue is important in application environments and will also be discussed as well. These four modes are presented and their influence on crack initiation and crack propagation discussed.

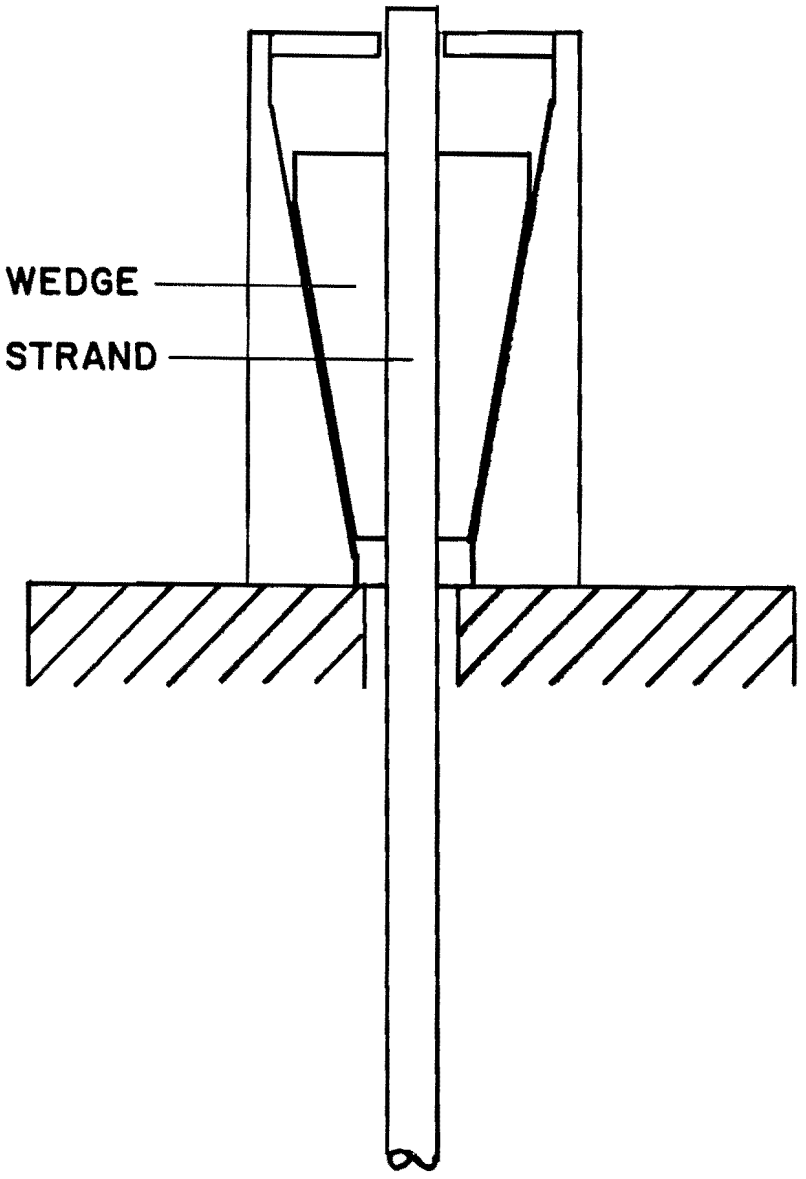

Fig. 3.1 Major components of wedge-type anchorage for single strands

3.1 Fatigue

It is beyond the scope of this chapter to give a complete description of the fatigue process; therefore, only those features which pertain to this specific case will be presented. In general, the fatigue mechanism consists of three separate parts: crack initiation, crack propagation, and fracture. This research was concerned with preventing the fracture stage from occurring and that could only be accomplished by (1) preventing a fatigue crack from initiating or (2) retarding crack growth after crack nucleation. Only the first possibility was feasible in this particular case.

3.1.1 Crack Initiation. The true crack initiation phase is not, as the name implies, the development of a single crack. The actual initiation stage consists of the development of many microcracks. A microcrack can be defined as a crack with a length in the range of 0.01 to 0.0001 in. A group of these microcracks may or may not coalesce into a larger crack known as a macrocrack. The macrocrack, if formed, may then propagate through the material in the crack propagation stage. The majority of the fatigue life, however, is spent in the development of macrocracks. The development of microcracks into a macrocrack will be considered as defining crack initiation.

Fatigue cracks are known to initiate at or near singularities on or just below the surface of metals. Singularities or stress raisers may develop as a result of nonmetallic inclusions, surface scratches, pits, notches, or slip bands. The surface condition of the fatigue specimen is, therefore, very important. However, even when extreme care is taken to prevent surface damage prior to testing and thereby eliminate stress concentrations, slip bands form during the fatigue process and microcracks develop at these sites (Fig. 3.2). Surface defects do tend to hasten the development of microcracks however.

The second prerequisite for the development of microcracks is dependent upon the state of stress and the distribution of that stress along the surface. Plastic deformation is necessary for crack nucleation. Consequently the hardness and yield stress of the material are important in determining fatigue resistance. While the nominal stress through the fatigue specimen may be below the yield point, surface stresses aggravated by surface flaws may be well above the yield point. The zone of plastic flow will increase with increasing applied stress. Increasing the zone of plasticity will provide more area for the development of microcracks and therefore an increase in the number of microcracks.

Some of the main factors influencing the crack initiation phase have been presented in this subsection. Crack initiation is a complex topic and many simplifications have been made in this

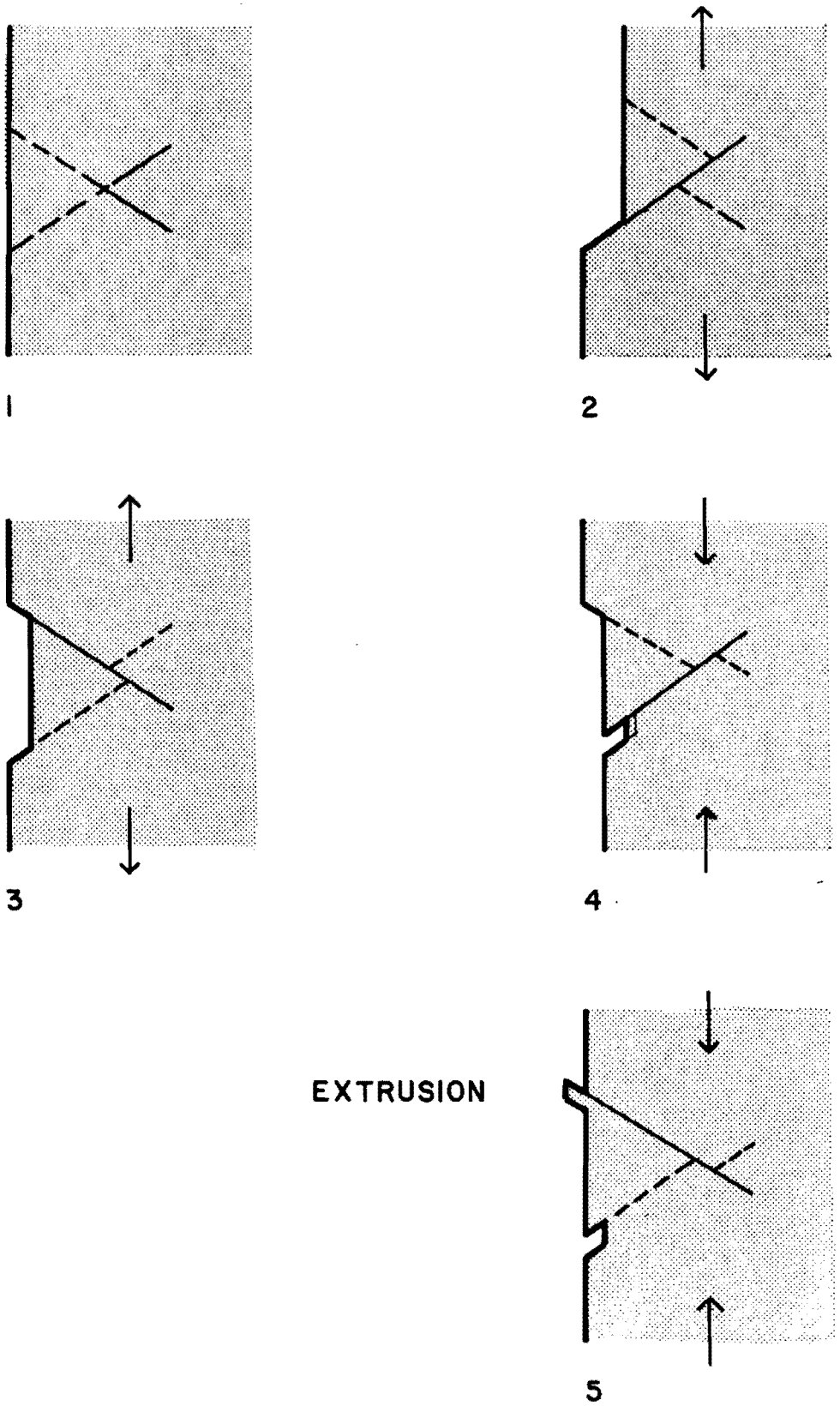

Fig. 3.2 Formation of persistent slip bands

presentation. The effects of the various wear modes and environmental conditions on the crack initiation stage will be discussed later in the chapter.

3.1.2 Crack Propagation. The crack growth phase of the fatigue process begins when the microcracks develop into macrocracks which can then grow into the specimen. The study of crack growth requires the various geometric parameters that define the crack be known. The important factors influencing the crack growth will be presented.

Crack propagation is primarily controlled by the range of stress at the crack tip. The crack tip stress field can be characterized by the fracture mechanics stress intensity factor, K. The stress intensity factor, K, relates the remotely applied stress to the local stress field at the crack tip. The variation in K is used in many models describing crack growth and is directly related to the stress range in fatigue testing. The variation in K is defined by the relation:

$$\Delta K = K_{MAX} - K_{MIN}$$

This relation can be interpreted as the K value due to the maximum stress in the cycle minus the K value due to the minimum stress in the cycle. A popular crack propagation model, known as the Paris Law, defines the rate of crack growth as:

$$da/dN = C (\Delta K)^{n}$$

where C in the equation is a material constant. The value of n is typically found to be in the range of two to four. It can be seen that the stress range in fatigue testing plays a large role in the growth rate of cracks. Testing at large stress ranges will thus lead to rapid failure once a propagating crack has formed.

The crack propagation life of a wire is quite small, due to the small diameter of the wire and the high mean stress the wires are subjected to. The crack size at fracture is of the order of the macrocracks found from coalescence of the microcracks. Efforts in prolonging fatigue life of prestressing strand in the anchorage zones should concentrate on the the crack initiation stage of the fatigue process. The remaining sections in this chapter concentrate, primarily, on mechanisms which tend to accelerate the crack initiation stage.

3.2 Wear

It was discussed in Section 3.1.1 that surface damage in the form of scratches, pits, etc. tend to accelerate the process of fatigue crack initiation. Any process that tends to damage surfaces could, therefore, result in a reduced fatigue life. The wear process, while not a common concern to civil engineers, is a process which can cause extensive damage to surfaces in contact. In general, the wear process can be defined as the undesired cumulative change in dimensions brought about by the gradual removal of discrete particles from contacting surfaces in motion, due predominately to mechanical action. Researchers in this area have recognized five main subcategories of wear of which only two are of importance in this particular case. The two forms of wear to be considered in this chapter are abrasive wear and adhesive wear.

3.2.1 Abrasive Wear. Abrasive wear can be defined as the displacement of material by hard particles or protuberances. The terms "two-body wear" and "three-body wear" are found in the literature. Two-body wear refers to the situation of two surfaces in sliding contact (Figs. 3.3a and 3.3b). In this case one surface abrades the other. The second term refers to the situation where hard particles exist between two surfaces. The particles may abrade both surfaces depending upon the relative hardness. It should be noted that while two-body wear may dominate at first, the constant abrasion will dislodge particles thus changing the dominate process to three-body wear. The particles released in the abrasive process may oxydize upon contact with the atmosphere. In many cases, the oxidized particles are harder than the original material thereby causing damage to both surfaces. The process of three-body wear will be concentrated upon in this section.

The mechanisms of three-body wear are complex as there are a variety of possibilities for particle geometry, particle loading, and attack angle. All of these variables have a profound influence on the mechanism of material removal and the wear rate. There are two extreme mechanisms used to describe the three-body wear process. Plastic deformation is the dominating process in one model while fracture dominates in the other.

In the model dominated by plastic deformation, two major processes take place when abrasive particles contact the surface of a ductile material: (1) The formation of grooves which do not involve direct material removal and (2) the separation of particles in the form of primary wear debris or microchips. Plastic deformation controls the rate at which material is removed. The volume of material removed is given by the equation [5]:

$$V = (k_1)(k_2)(k_3)(k_4)(L)(H^{-1})(S)$$

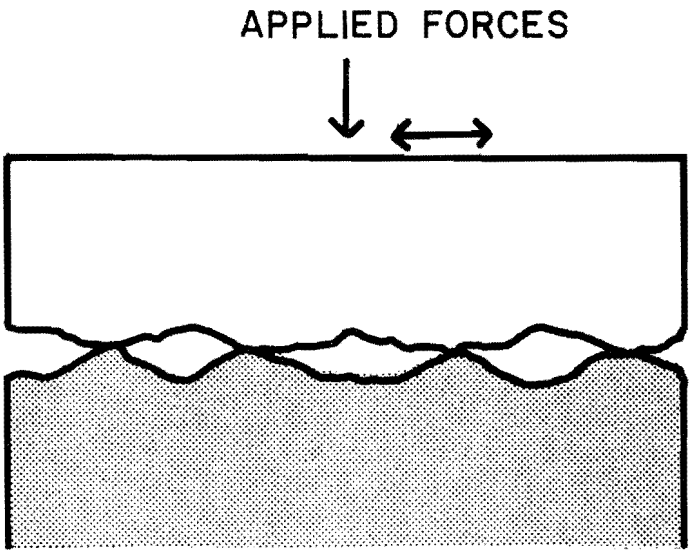

Fig. 3.3 (a) Two-body abrasive wear process

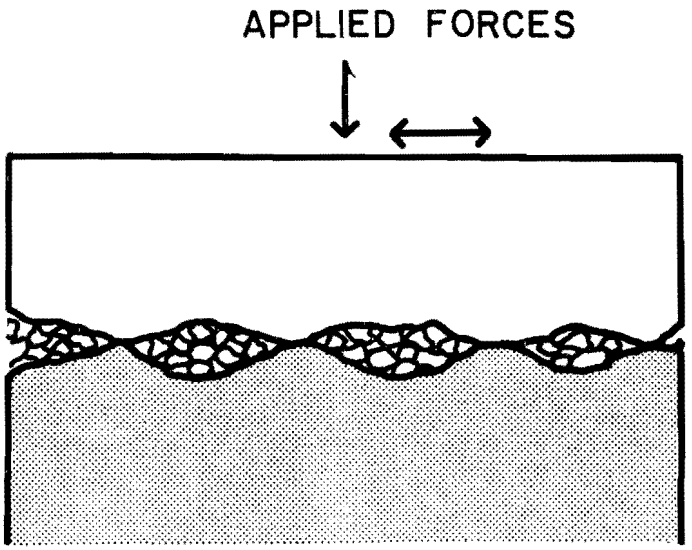

Fig. 3.3 (b) Three-body abrasive wear process

This equation will not be used in a quantitative sense, but it is important as it presents the relationship between important variables. The four constants (k_1 to k_4) depend upon the probability of material removal and particle shape. L in the above equation defines the load on the particles and is directly proportional to the applied stress. H is the hardness of the surface and S is the sliding distance. To reduce wear (i.e. the volume V) one must decrease the applied stress, increase the surface hardness, and/or decrease the sliding distance.

The second model, the fracture-dominated model, has some similarities with the previous model, but also has some important differences. For the case of abrasive wear in which brittle fracture is the predominate mechanism of material removal the volume of material removal is a function of the fracture toughness. As in the previous model the load on the particle and the hardness are also important. A model predicting the upper limit of material removal has been proposed [5] and is given by the equation:

$$W = (N)(L^{5/4})(K_c^{-3/4})(H^{-3/4})$$

This equation gives the volume of wear per unit sliding area per unit sliding distance, therefore the sliding distance parameter is implicit. L and H have the same definition as in the previous model (though their exponents are different). N is the number of particle contacts and K_c is the fracture toughness parameter. In order to decrease the wear damage one should decrease the sliding distance and applied stress. The fracture toughness and hardness should be increased.

The main variables in both of the mechanisms described are similar even though the mechanisms are quite different. The important variables presented here are hardness, fracture toughness, sliding distance, and applied stress. While it was mentioned that the particle size, number, and orientation were also important in determining the wear rate, it should be recognized that control over those variables is difficult.

3.2.2 Adhesive Wear. Adhesive wear occurs when two smooth bodies slide over each other, and fragments are pulled off one surface to adhere to the other. These fragments may, with time, develop into loose wear debris. This process is illustrated in Fig. 3.4. The strong atomic cohesive forces, brought about by the intimate contact of the two surfaces, is responsible for the adhesion. During sliding, a small patch from one surface may come into contact with a similar patch on the other surface, and there is a chance, though small (only 0.01% to 5.0% of the junctions formed during the sliding process break so as to form sizeable wear particles), that during the reverse cycle, a break

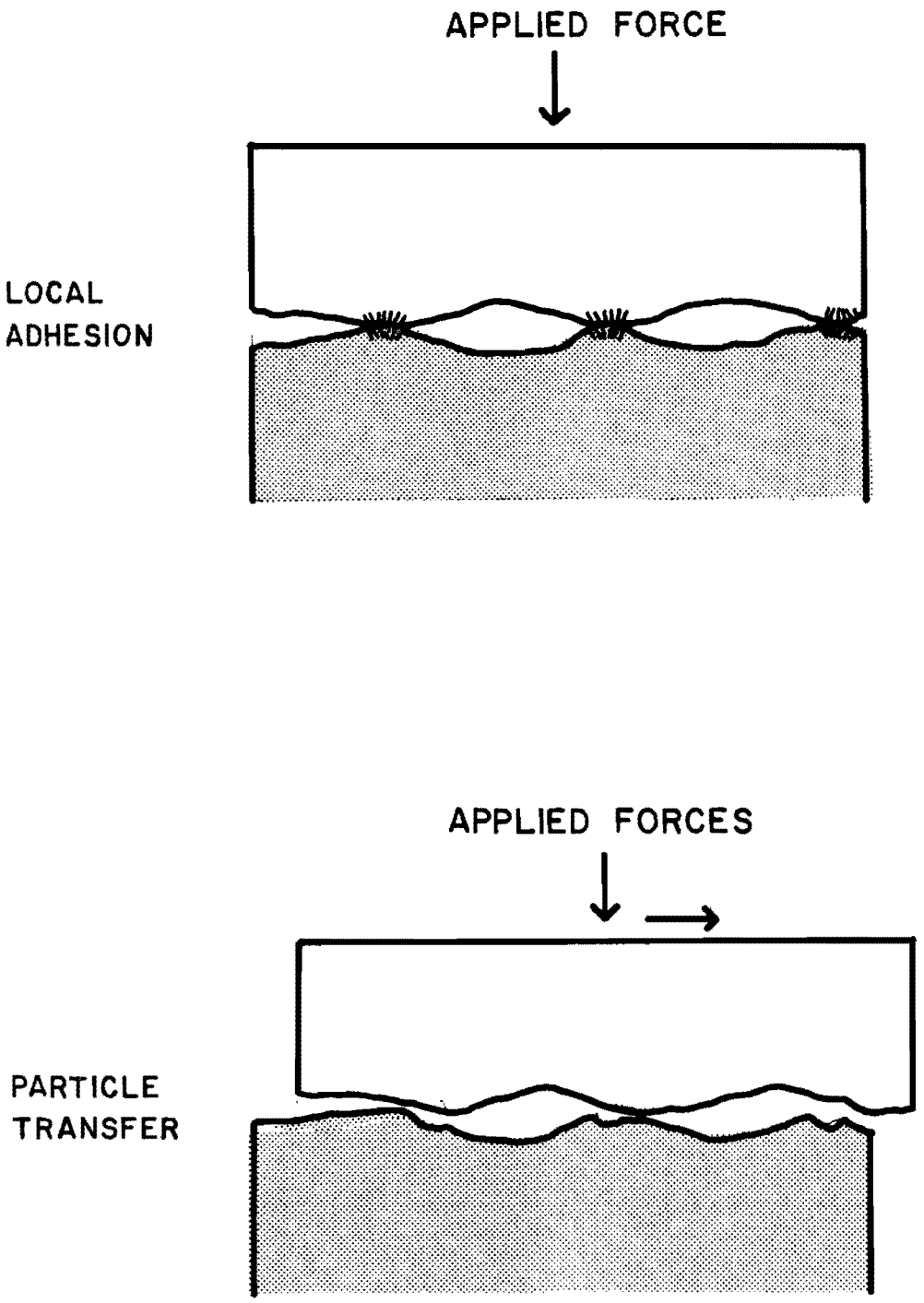

Fig. 3.4 Adhesive wear process

will occur at some location other than the bonded interface. The result is to transfer material from one surface to the other. Adhesive wear is, in fact, the most common form of wear and occurs to some degree whenever two surfaces are pressed together in sliding contact. The conditions at the interface of the adhering surfaces is quite similar to those found in the cold-welding process.

One of the major differences between adhesive wear and abrasive wear is that the harder of the two surfaces in contact can be damaged in the adhesive case. This is not true for abrasion. In adhesive wear, more particles will be transferred from the softer surface than the harder surface. Since particle removal is the mechanism of surface damage, both surfaces are subject to damage in the form of surface scratches, pits, etc. which, in turn, are the cause of stress raisers. This is an important point as the strand, in this research program, is harder than the contacting aluminum wedges. Were abrasion the only active mode of wear, the surface of the strand could not be damaged. However, since adhesion also exists, the surface of the strand can be damaged through particle removal. Surface damage can accelerate crack initiation due to the existence of the stress raisers.

Only a general discussion of the adhesive wear process has been presented up to this point. The remainder of this subsection will be devoted to the main variables and proposed numerical models. Three laws of adhesive wear have been developed [9] based on research using mostly metallic, unlubricated surfaces: (1) The amount of wear is directly proportional to the load L, (2) the amount of wear is proportional to the sliding distance X, and (3) the amount of wear is inversely proportional to the hardness H of the surface being worn away. These have been expressed [5] in a quantitative form by the equation:

$$V=(k)(L)(X)(H^{-1})$$

where V in the equation is the volume of material removed. This model is very similar to the formula in Subsection 3.2.1 for abrasive wear.

Aside from the variables mentioned in the previous paragraph, the surface energy parameter is also of importance when designing against adhesive wear. The equation derived to quantify the surface energy between two mating materials is given [4] by:

$$W_{ad} = e_1 + e_2 - e_{1,2}$$

where e_1 and e_2 are the values for the interfacial energy for materials 1 and 2 and $e_{1,2}$ represents the interaction between the two materials. In general, the interfacial energy is directly related to the hardness of the material. In order to decrease the effect of adhesive wear, the surface energy, W_{ad}, should be minimized. The selection of materials with low interaction is most effective. It is preferable to have one of the metals chosen from the B-subgroup of the Periodic Table since their covalent bonds are typically weaker than those of other metals. Tin and zinc are two examples of metals from the B-subgroup [3].

Adhesive wear has been presented in this section. Some of the important differences between adhesion and abrasion have been presented. Among those differences is the fact that adhesive wear is the more common and exists at some level in all wear situations. Secondly, it is known that both of the materials in contact will sustain damage during the wear process, not just the softer surface (as in abrasion).

Similarities exist between the abrasive and adhesive wear modes as well. The wear rates for both forms of wear are functions of the same material and load parameters. Another similarity is that of visual damage. Surfaces subjected to abrasive and adhesive wear would both have a variety of scratches and pits. In adhesive wear, however, material will have been transferred from one surface to the other. This is characteristic of adhesive wear and serves as a guide in distinguishing between the two modes.

The adhesive wear mode can be more effective in the initiation of fatigue cracks. As bonds break on reverse cycles, the break can occur at the bonded interface or in one of the two surfaces. If the bond breaks in one of the surfaces, the resulting crack may develop as a microcrack in subsequent cycles.

3.3 Fretting

The process of fretting is actually another form of wear. The seriousness of the consequences of a fretting-induced failure combined with the frequency of such occurrences, however, have led researchers to define the fretting process as an independent mode of failure. When two pieces of material are pressed together and cyclically displaced relative to one another, wear at the interface occurs. If the magnitude of relative displacement is small (around 0.004") [18] the process is defined as fretting. When fretting occurs simultaneously with fatigue the total process is termed "fretting fatigue".

The fretting fatigue process does not come about by a single mechanism. Four different possible mechanisms have been identified in

fretting fatigue. These mechanisms are: (1) Abrasive pit-digging, (2) Asperity-contact microcrack initiation, (3) Friction-generated cyclic stresses which lead to the development of microcracks, and (4) Subsurface cyclic shear stresses leading to delamination [3]. Each of these mechanisms will be discussed.

The abrasive pit-digging mechanism is thought to reduce fatigue strength by first leading to the development of a series of pits and grooves aligned parallel to the direction of fretting. This surface damage leads to stress concentrations and serves as probable fatigue crack nucleation points. This mechanism is quite similar to the abrasive two-body wear mode already described. This process is illustrated in Fig. 3.5.

The asperity-contact mechanism, shown in Fig. 3.6, is based on the inherent "out-of-flatness" of surfaces. Even a well-polished surface will have a wavy surface with peaks in the range of 50.0 to 100.0 A.U. in height [1]. When two surfaces are brought together, contact will initially occur at only a few points. Upon the application of a load, normal to the plane of contact, local deformation, possibly plastic, will tend to increase the real area of contact. Like the adhesive wear mode described previously, micro-welds form at the contact sites. If a cyclic stress is then superimposed over the normal load, fatigue stresses, transferred through the adhesive bonds, develop at the bases of the contacting asperities. Fatigue microcracks are believed to develop at these locations. This mechanism would tend to produce a series of microcracks oriented perpendicular to the direction of fretting.

The third mechanism, the friction-generated cyclic stress fretting hypothesis, is thought to be the result of compressive and tensile stresses formed in front and behind of the contacting surfaces. As one surface is moved over the other surface, tensile stresses develop in the material in the wake of the moving surface. Compressive stresses form in front of the moving surface. The sign of the stresses switches in the second half of the load cycle. That is to say that the material subjected to tensile stresses in the first half of a load cycle would be subjected to compressive stresses in the second half thus setting the stage for the development of fatigue microcracks ahead and behind of the fretting zone. These microcracks would tend to form perpendicular to the direction of fretting. This process is illustrated in Fig. 3.7. Again, adhesive bonding, provides the path of force transfer.

The final mechanism is the delamination theory of fretting. The combination of normal and tangential stresses and the fact that contact occurs only at the asperities leads to a complicated multiaxial state of stress in the materials. The cyclic variation of these stresses is believed to cause subsurface shear stress peaks and finally subsurface crack nucleation sites. These cracks tend to

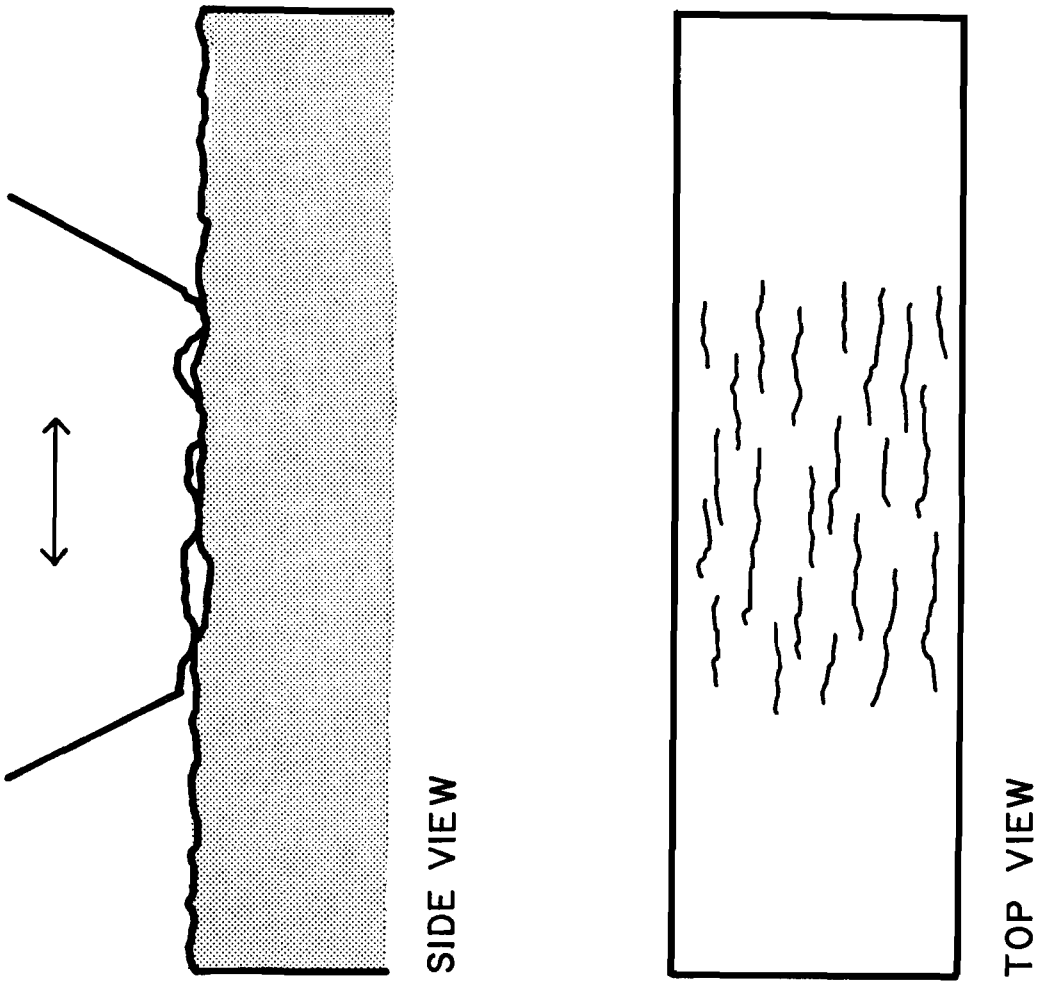

Fig. 3.5 Abrasive pit-digging mechanism

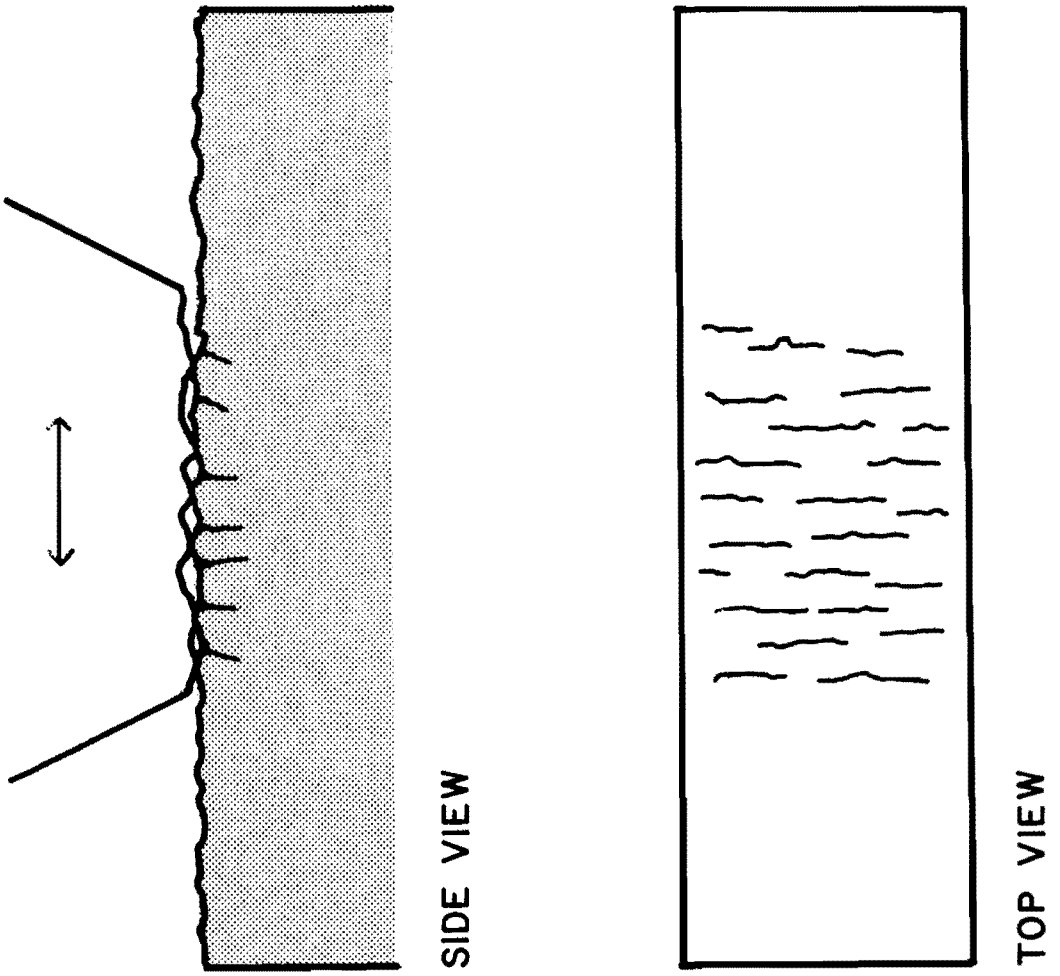

Fig. 3.6 Asperity contact mechanism

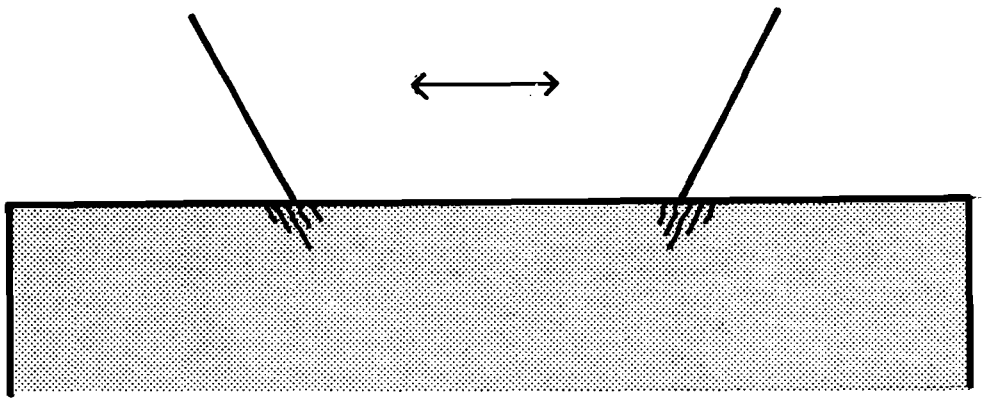

Fig. 3.7 Friction-generated cyclic stress fretting hypothesis

propagate parallel to the surface and finally intersect the surface. As the crack propagates to the surface, it releases a thin film of wear debris. Thereafter the mechanism is quite similar to the three-body abrasive wear mechanism already presented. The delamination mechanism may be more serious however as some of the subsurface microcracks may develop into macrocracks and propagate into the material.

These four mechanisms are not mutually exclusive and could be active simultaneously. The controlling mechanism (if one exists) is highly test dependent. In any case, the fretting process is known to be especially important in the crack initiation stage and of little importance in the crack propagation stage.

Fretting can significantly decrease the fatigue life. Tests performed in which the specimens were first fretted then fatigued showed decreases in the expected fatigue life of approximately 18% [18]. The situation of simultaneous fretting and fatigue would be more critical and the reduction in the fatigue life would be even greater. Over fifty variables have been identified which have an effect during the fretting process. Eight are believed to be of substantial importance. The eight major variables are given [3] as:

(1) The magnitude of relative motion.
(2) The magnitude and distribution of stress at the interface.
(3) The state of stress and its variance with time.
(4) The number of fretting cycles accumulated.
(5) The material from which each of the fretting surfaces is fabricated.
(6) The cyclic frequency.
(7) The temperature in the region of the fretting surfaces.
(8) The environment in which the fretting process is being conducted.

Unfortunately, no quantitative method now exists which gives the relative effects of each of these variables. Only trends will be presented. The eighth variable will not be discussed in this section. A more complete description of the environment will be presented in the next section. In general the reduction in fatigue life increases as the slip amplitude increases. However, it has been found that there is a level of slip amplitude at which no further decrease in life occurs with an increase in slip. The fretting fatigue life tends to decrease with increasing clamping stress. The state of stress is important. However, for complex multi-axial states of stress the effect is difficult to determine. In general, large tensile stresses would be worse than compressive stresses. Fretting damage always increases with increasing number of cycles. The rate of increase is highly test specific however. As in the other forms of wear, the properties of the material pair have an effect. Harder surfaces tend to resist fretting damage better than softer materials. Fracture

toughness should also be considered to have the same affect in the fretting process as in the adhesive wear process. The effects of frequency and temperature on fretting damage have not been determined. The multitude of variables and their complex interaction make the prevention of fretting fatigue failures difficult; however, the trends presented here may serve as an aid.

3.4 Corrosion and Corrosion Fatigue

Unlike wear and fretting discussed above, corrosion can accelerate both the crack initiation and the crack propagation phases of fatigue. The causes and types of corrosion will be presented in this section. Corrosion assisted fatigue or corrosion fatigue will also be discussed.

3.4.1 Forms of Corrosion. Corrosion may be defined as the undesired deterioration of a material through chemical or electrochemical interaction with the environment [3]. Eight different forms of corrosion have been recognized [25] though only the four most significant (for this application) will be discussed. The definitions and mechanisms of uniform attack, galvanic corrosion, crevice corrosion, and pitting corrosion are presented here.

The form of corrosion termed uniform attack is probably the most common form of corrosion. This form of corrosion is typically characterized by a chemical or electrochemical reaction which proceeds uniformly over the entire exposed surface. While uniform attack is responsible for the greatest amount of destruction of metal on a tonnage basis, it is not of the greatest concern from a technical standpoint since laboratory tests can accurately determine the rate of deterioration. The remaining three forms of corrosion are more serious due to their unpredictable rates of deterioration.

Galvanic corrosion is an accelerated electrochemical corrosion that occurs when two dissimilar metals in electrical contact are made part of a circuit completed by a connecting pool or film of electrolyte or corrosive medium. An electrolyte is a solution containing ions. Salt-water is an example of an electrolyte. The mechanism of galvanic corrosion is illustrated in Fig. 3.8. A potential difference usually exists between the two metals which leads to electron flow from the anode (less resistant metal) to the cathode (more resistant metal). The anodic metal would corrode while the cathodic metal would be protected.

Another important factor in determining the rate of corrosion is the ratio of the area of the cathode to the area of the anode. An unfavorable area ratio consists of a large cathode and a small anode. In this case, for a given current, the current density

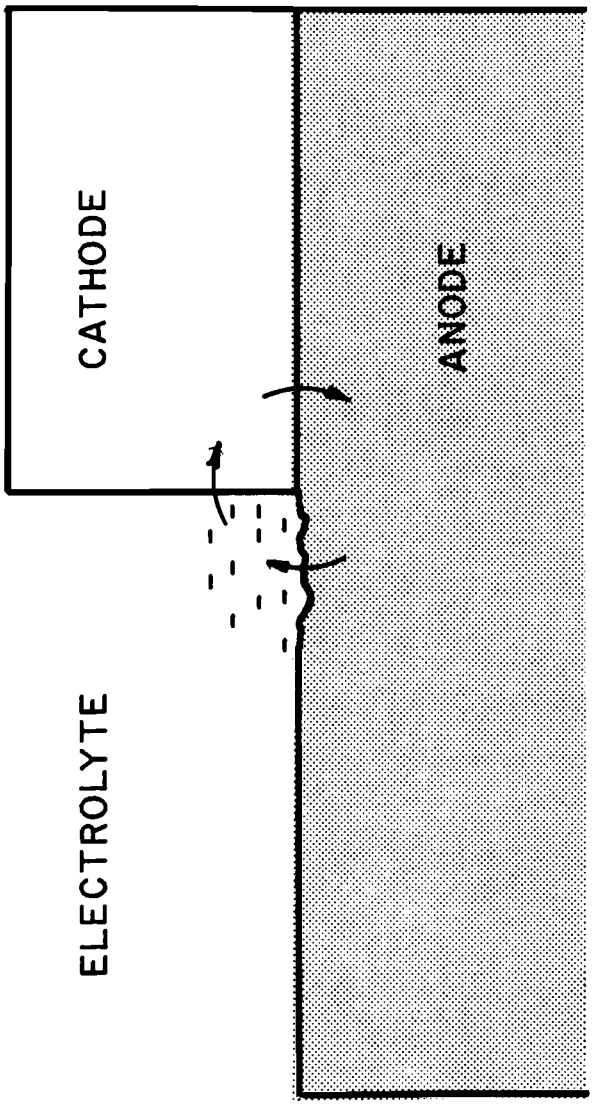

Fig. 3.8 Galvanic corrosion mechanism

would be greater in the anode than in the cathode. The current density determines the rate of corrosion.

Crevice corrosion is the intense localized corrosion that occurs in crevices on metal surfaces exposed to corrosives. For corrosion to develop, a crevice must be large enough to permit liquid entry and small enough (around a few thousands or hundredths of an inch) [25] to maintain a stagnate zone. For this reason, crevice corrosion rarely occurs within wide (about 0.125") grooves or slots. Crevice corrosion is thought to develop as a result of local oxidation and reduction reactions which results in oxygen depletion in the stagnate crevice region. The oxygen depletion leads to an excess positive charge in the crevice due to increased metal ion concentration. Chloride and hydrogen ions flow into the crevice which increases the rate of corrosion. Crevice corrosion requires a long incubation period; however, once begun, corrosion continues at an ever-increasing rate.

Pitting corrosion, like crevice corrosion, is a highly localized form of corrosion. Individual pits, while small, may be so numerous that the entire surface appears to be roughened. Pitting corrosion occurs by the same mechanism as crevice corrosion; however, the pits are typically produced by abrasion or other forms of wear. Pitting is one of the most destructive forms of corrosion and is very difficult to predict through laboratory experiments.

3.4.2 Corrosion Assisted Crack Initiation. The effect of two corrosive environments, gaseous and aqueous, on the crack initiation stage will be presented in this subsection. Not all researchers agree on the effects of the environment on the crack initiation stage [18]. Some contend that the environment plays no role in encouraging crack initiation while others believe the crack initiation stage to be profoundly effected [27] by corrosive environments. The possible effects of gaseous environments will be discussed first.

Those who support the idea of environmentally assisted crack initiation have postulated that cyclically generated slip bands become regions of high oxygen concentration. The dissolved oxygen is believed to prevent the rewelding of nascent cracks and shorten the transition from slip band to microcrack. Other researchers have suggested that metal surfaces are strengthened by an oxide film which, when cyclically stressed, are more susceptible to the formation of cavities and voids. The cavities or voids tend to accelerate the crack initiation stage. These are not widely accepted mechanisms. Many researchers believe that gaseous environments have no effect. In any case, any effect, if one exists, is believed to be small.

While the effect of gaseous environments is debated, the effect of aqueous environments on crack initiation is significant. The

crack initiation stage can be profoundly affected by aggressive aqueous solutions. Theories offered to explain the effect have generally consisted of the following mechanisms: (1) Stress concentrations at the bases of corrosion-produced pits tend to accelerate the crack initiation stage. (2) Stress concentrations produced by electrochemical attack at plastically deformed areas which are anodic to adjacent undeformed metal encourage crack initiation. (3) Crack initiation occurs as a result of stress concentrations produced by electrochemical attack at ruptures in an otherwise protective surface film. (4) Environmental absorption is believed to lower the surface energy of the metal resulting in an increase in the rate of microcrack-to-macrocrack development. Whatever the mechanism, it is known that aqueous environments have much more of an effect than gaseous environments in initiating fatigue cracks.

3.4.3 Corrosion Assisted Crack Propagation. Test data [18] indicates an interaction between the environment and crack growth. Both gaseous and aqueous environments will be discussed in this section. As in crack initiation, crack growth is affected more by corrosive aqueous solutions.

The mechanism proposed to explain the environmental interaction in crack growth rates is based on the influence of oxides at the crack front. When oxygen comes into contact with the freshly created surfaces at the crack tip, oxides form which prevent any rebonding during the reverse cycle. Since rebonding of the material would slow crack growth, the effect of the oxidized surfaces is to accelerate crack propagation. This effect is most pronounced when the mean stress is zero and the crack growth rate is small.

Moisture in the air also affects the crack growth rate. Water vapor is believed to react with the material at the crack tip resulting in a release of hydrogen. The hydrogen can diffuse into the material ahead of the crack tip which, in turn, can have two possible effects on crack propagation: the hydrogen could collect in pockets and recombine to form molecular hydrogen whose pressure would strain the material in tension, or it could embrittle grain boundaries thus providing easy fracture paths. Again, reductions in fatigue lives as influenced by this hydrogen diffusion mechanism, are most noticeable at zero mean stress and low crack growth rates.

The hydrogen diffusion mechanism is also active in aqueous environments. An aqueous solution of salt water is much more corrosively aggressive than is humid air and consequently the effect on the crack growth rate is even more pronounced. Electrochemical reactions also exist which are not present in moist air. Reductions in fatigue lives are, therefore, typically larger in aqueous environments.

It should be noted that the mechanisms presented in this section are not agreed upon by all researchers. However, reductions in fatigue lives of specimens tested in corrosive environments over those tested in a vacuum have been observed. Furthermore, high strength steels are more susceptible to corrosion than lower strength steel. This is significant in light of the fact that prestressing strand is very high strength. Protection of the strand in corrosive environments is very important. In general, the effects of a corrosive environment are much more significant in the crack growth phase than in the crack initiation phase. The effects of corrosive environments in the crack nucleation process are still debated.

3.5 Summary

A variety of failure modes likely to be active in the anchored region of test strands have been presented. It was shown in Section 3.1 that fatigue cracks propagate rapidly in this application and, therefore, any attempt to increase the fatigue life of the anchored region should concentrate on the crack initiation stage. The abrasive and adhesive wear modes were presented and it was shown how they influenced the crack initiation phase of the fatigue process. Fretting fatigue and corrosion fatigue were likewise presented.

The mechanisms by which each of these failure modes leads to premature fatigue failures have been presented. In general, each of the processes may lead to surface damage in the form of pits, scratches, and grooves, and microcracks formed by the breaking of micro-welds. Surface damage leads to stress concentrations and hence offers prime locations for crack nucleation. The mechanisms of wear and fretting are complex and an empirical understanding of them represents the state of the art. Many of the variables involved in these mechanisms are difficult to control or even measure.

CHAPTER 4

EXPERIMENTAL TEST METHODS

The details of the two experimental investigations, the fatigue tests and the load distribution tests are presented in this chapter. The test specimens and equipment are common to both tests and are presented first. The majority of this chapter is devoted to the description of the test equipment and procedures used in determining the fatigue performance and the load distribution characteristics of the anchorages.

4.1 Test Specimens

The test specimens chosen for this research project were Grade 270 0.5 in. and 0.6 in. diameter seven-wire prestressing strands. The decision to test individual strands as opposed to full-scale cables was logical. A greater number of tests could be performed with the smaller specimen size. Another reason for using individual strands was that fatigue data for the 0.5 in. strand used in the tests was available as result of a previous research program [16]. The previous data provided an accurate data base for comparison purposes. The final reason was based on economics. Fabricating enough anchorages for a single, moderate-sized, cable would cost thousands of dollars. The test specimens themselves would be very expensive as well. Ensuring fatigue resistance for the individual strand case is a major step in the development of a fatigue resistant multiple-strand cable stay anchor since the anchorage region of a full-scale cable stay is composed of many individual anchorages. The selection of a single seven-wire, Grade 270 prestressing strand as the test specimen was therefore justified.

4.2 Test Equipment

The test equipment used in this investigation had been used in many fatigue test studies prior to this one. The basic requirement of strand fatigue test equipment is that it be resistant to fatigue, stiff, and the loads applied be axial (i.e. no flexural stresses). The fatigue equipment used satisfied these requirements. The test setup, illustrated in Fig. 4.1, consisted of essentially four main elements: the test frame, flat 60 kip. load cell, servo-controlled center-hole hydraulic ram, and interface discs.

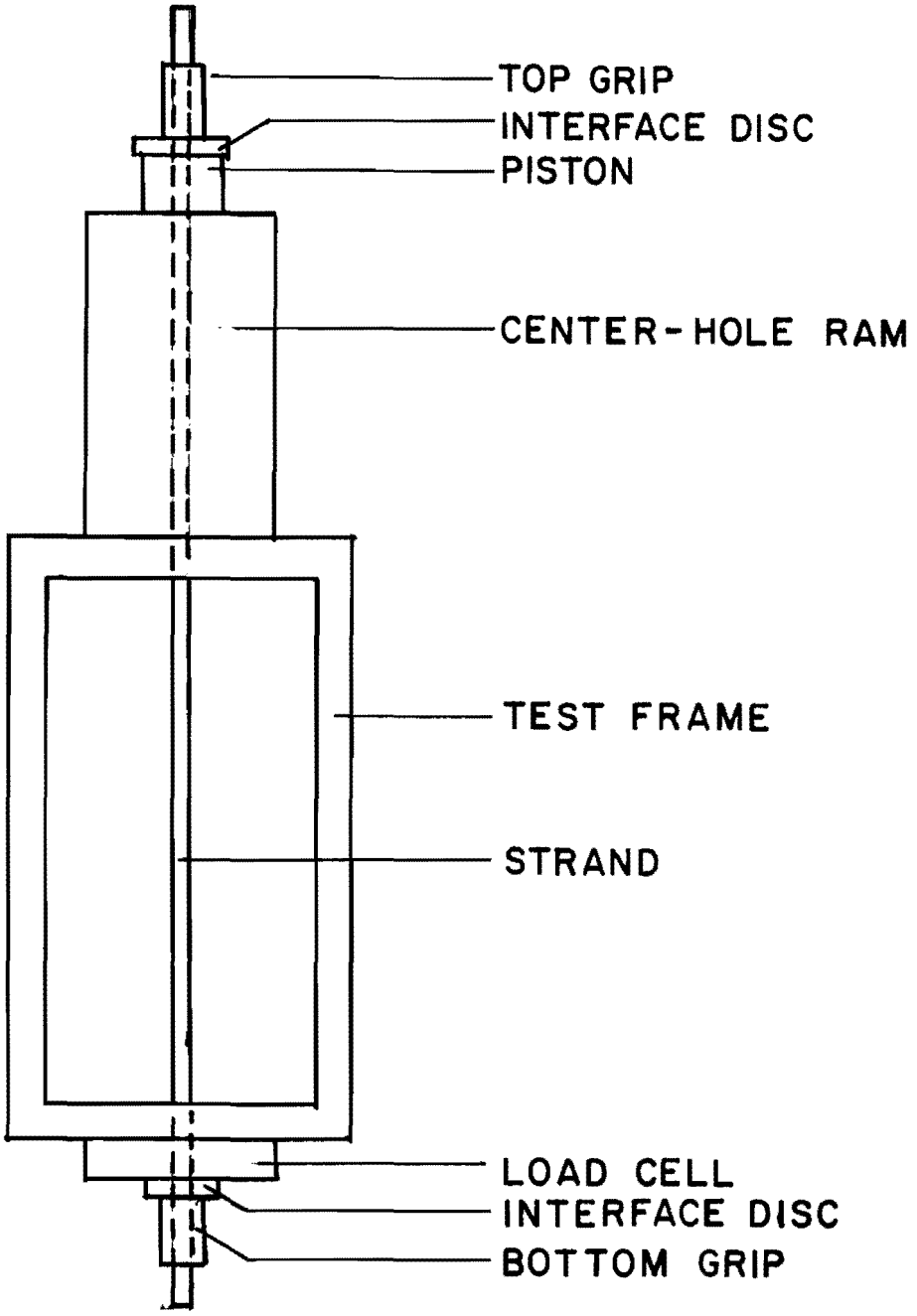

Fig. 4.1 Fatigue test setup

The test frame separated the load cell, which was mounted under the frame, from the hydraulic ram which was mounted on top of the frame. The test frame was fabricated from four two inch tubular steel sections welded to the four corners of a two inch thick steel plate. A similar plate was welded at the top. The load cell was bolted to the lower plate. The hydraulic ram was bolted on top of the upper plate. Holes were drilled through the center of the steel plates to match the hole in the ram's piston and the center hole of the load cell. The holes were drilled such that the strand could easily be placed in the system. As the axis of the strand coincided with the centers of the ram and load cell, only axial forces were introduced into the strand. Two interface discs were fabricated; one, which fit between the top grip and the ram, and the other, which was placed between the bottom grip and the load cell. The interface discs served to insure alignment of the strand with the load cell and the ram. Extension of the piston transferred tensile stress into the strand and compressive stress into the other elements. The length of the test specimens was controlled by the sum of the lengths of the various elements and the extension of the piston. The length between the grips varied between 50 in. and 58 in.

Control over the loads was provided by a closed loop servo-controlled hydraulic system. Prior to testing, the test frame, load cell, servo-controller, and electronics were calibrated in a 60 kip testing machine. The response of the load cell was linear over the its entire range and since all compression elements (except the ram) were included in the calibration process, accuracy of the response during the fatigue testing was insured.

4.3 Test Procedures

4.3.1 Fatigue Tests and Stress Levels. Beginning a fatigue test was a simple process. First, the top grip assembly was attached to the strand. The strand was then slipped into the test setup and allowed to rest on the top interface disc while the bottom grip assembly was attached. The bottom grip assembly was then slid up the strand so that the bottom interface disc almost touched the load cell. A low hydraulic pressure was applied during which time proper seating of the top and bottom grips was checked. After any alignment adjustments were made, the load was increased under low pressure to approximately 10 kips. The remainder of the static load was applied under high pressure. Cycling was begun at low values of frequency and stress range. The stress range (the amplitude of the sinusoidal forcing function) was increased to the desired value after which the frequency was adjusted. The parameters defining the forcing function (mean load, T_{MEAN}, and load range, T_{RANGE}) were monitored with an electronic peak detector. Minor modifications were made as necessary. The cycle counter and signal error detection were provided by the electronic control system. Any significant variation in the forcing

function (brought about by a wire failure for example) would be detected and the system would be shut off. As the entire system was electronically controlled, the system could be shut off in the same cycle as the failure that produced the error resulting in accurate values of fatigue life. A failure of the test specimen is defined as the failure of one or more of the seven wires.

Three values of stress range were selected for testing: 47.2, 33.8, and 27.0 ksi (17.5%, 12.5%, and 10% f_{su} respectively). Tests performed at the 47.2 ksi stress range were cycled at 2 Hz while the tests conducted at the 33.8 and 27.0 ksi levels were cycled at 10 Hz. The low stress range was chosen as it closely resembles the stress levels used in actual bridge stay design (around 20 ksi). The other values were selected so that the performance of the anchorage with respect to stress range could be determined. The minimum stress level was set at 157.7 ksi (58.4% f_{su}) and remained constant throughout the testing program.

4.3.2 Load Distribution Tests. The two-part anchorage used in this research program (described in detail in Chapter 5) allowed for the sharing of the total applied load between the primary and secondary grips. The load distribution tests were performed to determine the extent of load sharing for each of the anchorages tested.

A centerhole load cell was designed to fit between the primary and secondary grips. The load cell was fabricated from 100 ksi steel and was designed to measure loads less than or equal to sixty kips. The load cell was calibrated in a testing machine before any load distribution tests were performed. The response was found to be linear.

Measuring the load distribution was done on one end of the specimen. The top grip assembly was applied as described in the previous section. The bottom grip was applied differently. The load cell was placed behind the primary grip and in front of the secondary grip. Since the load cell did not come into contact with the strand, any load the primary grip could not resist was passed through the load cell and into the secondary grip. The bottom grip assembly including the load cell is shown in Fig. 4.2. The force measured in the load cell was the force carried in the secondary grip. The primary grip carried the difference between the total applied load and the load measured in the centerhole load cell.

The load distribution tests were performed by applying tensile load to the strand in three kip increments and recording the amplified load cell output with a voltmeter. In general, the strand was loaded to some maximum load and unloaded back to the zero-stress level. The tests were performed for a variety of maximum loads. Since load cell readings were taken during the loading as well as the

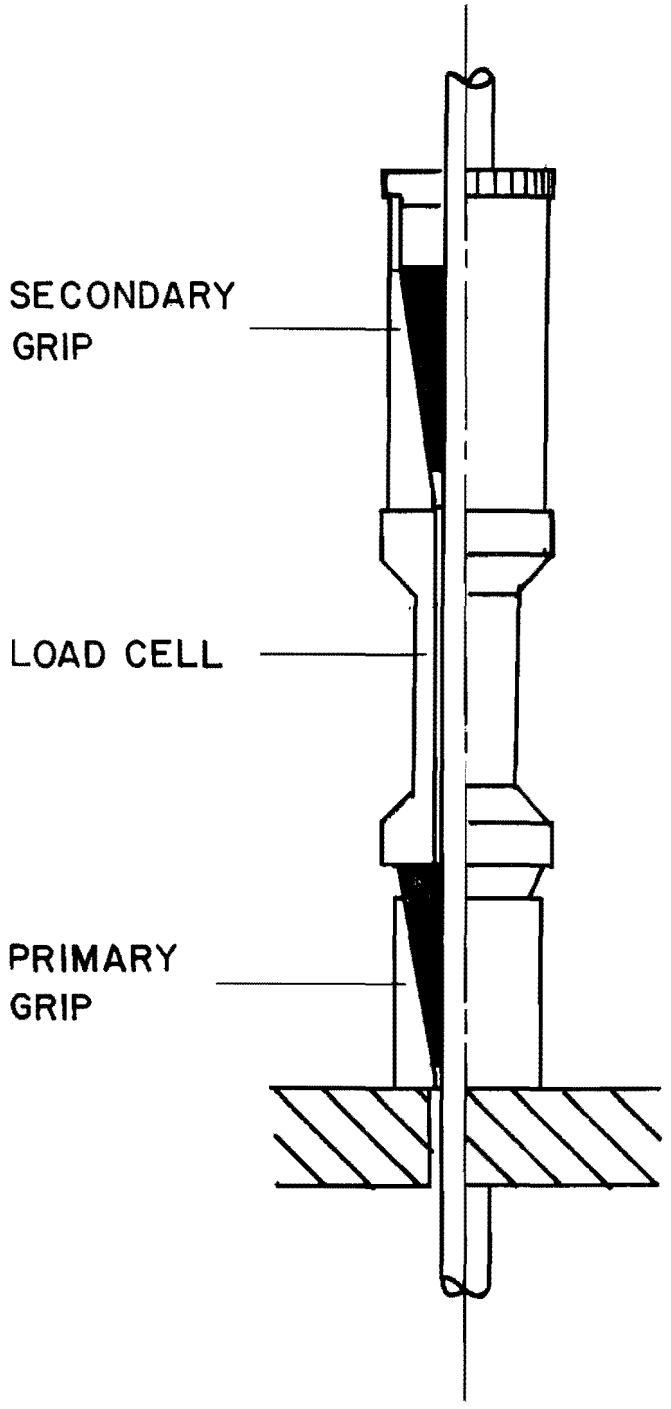

Fig. 4.2 Grip assembly with 60 kip load cell

unloading phase, a complete description of the load distribution during fatigue testing is obtained. The results of this study are presented in Chapter 5.

CHAPTER 5

GRIP BEHAVIOR

The purpose of this chapter is to explicitly define and characterize the method of anchoring the strands tested in this research program as well as the behavior of the gripping technique. The materials used in the fabrication of the two-stage grip will be presented as well as the physical dimensions of the anchorages. Load distribution tests were performed to evaluate the load sharing characteristics of each of the anchorages. Finally, a finite element stress analysis was performed to evaluate the stress distribution along the gripped area. The finite element stress analysis also allowed for the examination of various geometric variables not tested in the experimental program. These results will be presented as well.

5.1 Anchorage Details: Materials and Dimensions

Two general approaches to gripping the strand were considered. One method grips the strand through the use of a clamp as shown in Fig. 5.1. The clamp would have to be tightened prior to tensioning the strand. The other method that is widely used by the prestressing industry is the conical wedge (illustrated in Fig. 5.2). Here, clamping force and the tensile force are coupled. Application of a tensile force in the strand produces an immediate transverse force due to wedging action. The conical wedge is typically divided into three separate wedges. Conical wedges are also available in two sections. While independent control over the clamping force is possible in the clamp system, the wedge anchorage is more practical as it allows for easy adjustment and placement. Some control over the clamping force is possible by varying the material and geometric properties of the wedge. The wedge method of anchoring the strand was selected for use in this test program.

The wedges themselves could be designed in a variety of ways. There are three main geometric variables in the design of the conical wedge as shown in Fig. 5.3. The overall bearing length, the angle of taper of the outside surface (interference angle), and the depth, measured from the inside surface to the point where the taper begins. The interior surface of the wedge will be defined as the surface which makes contact with the strand. The outside or exterior surface is defined as being the surface in contact with the restraining collar. Each of these variables has an effect on the stress distribution along the strand. A complete stress analysis study is presented in this chapter. The various geometric variables were not

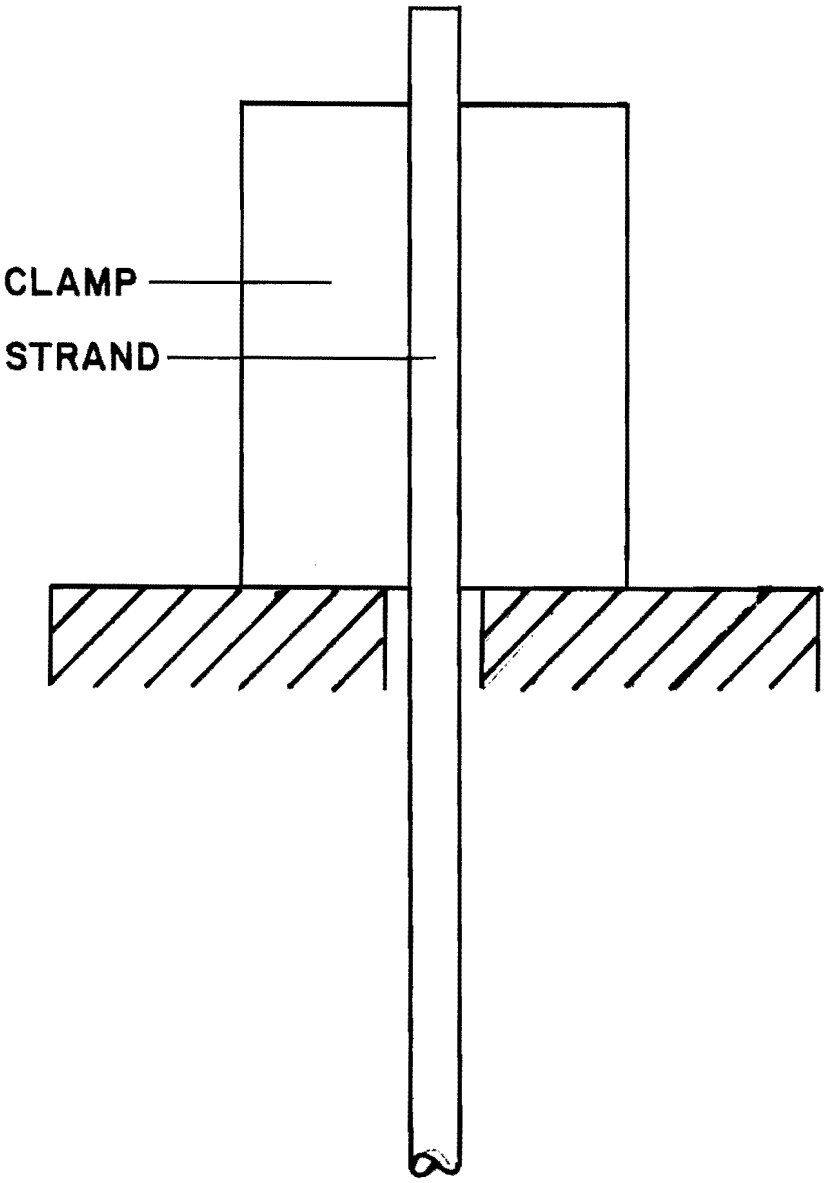

Fig. 5.1 Clamp method for gripping strand

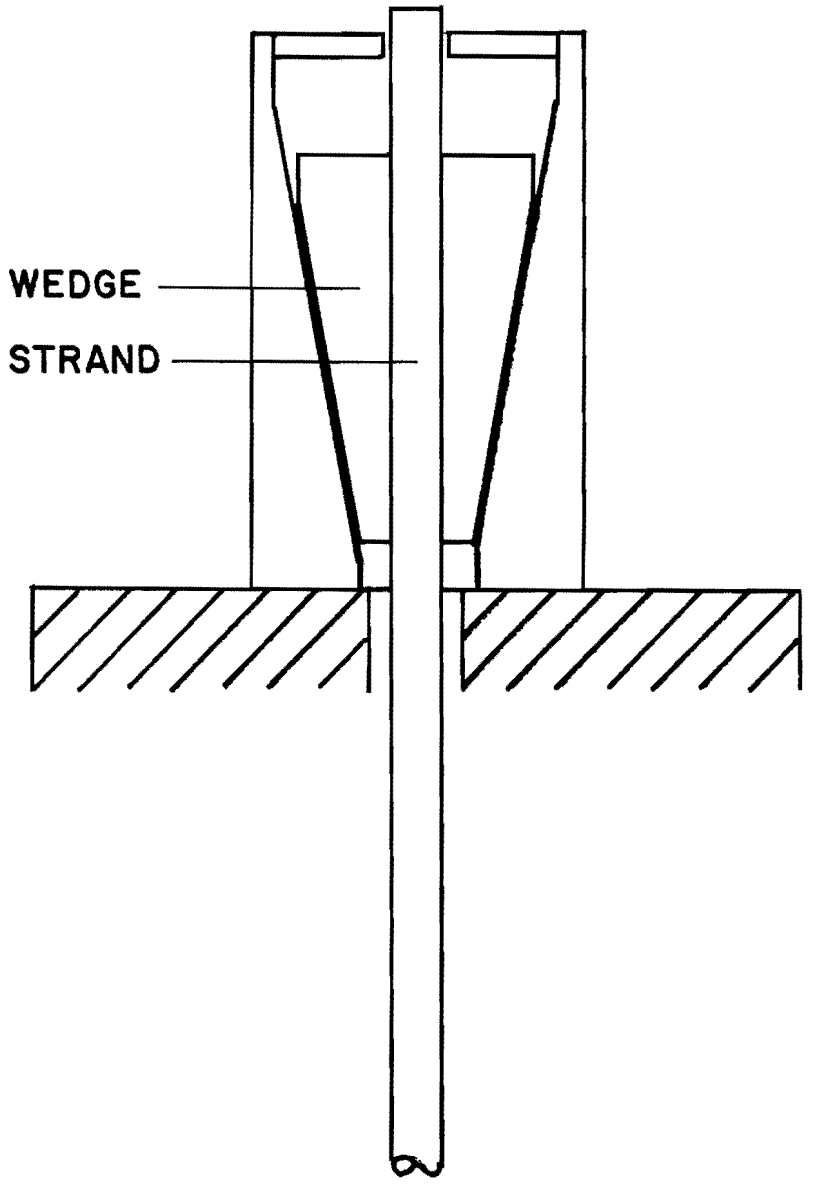

Fig. 5.2 Conical wedge method for gripping strand

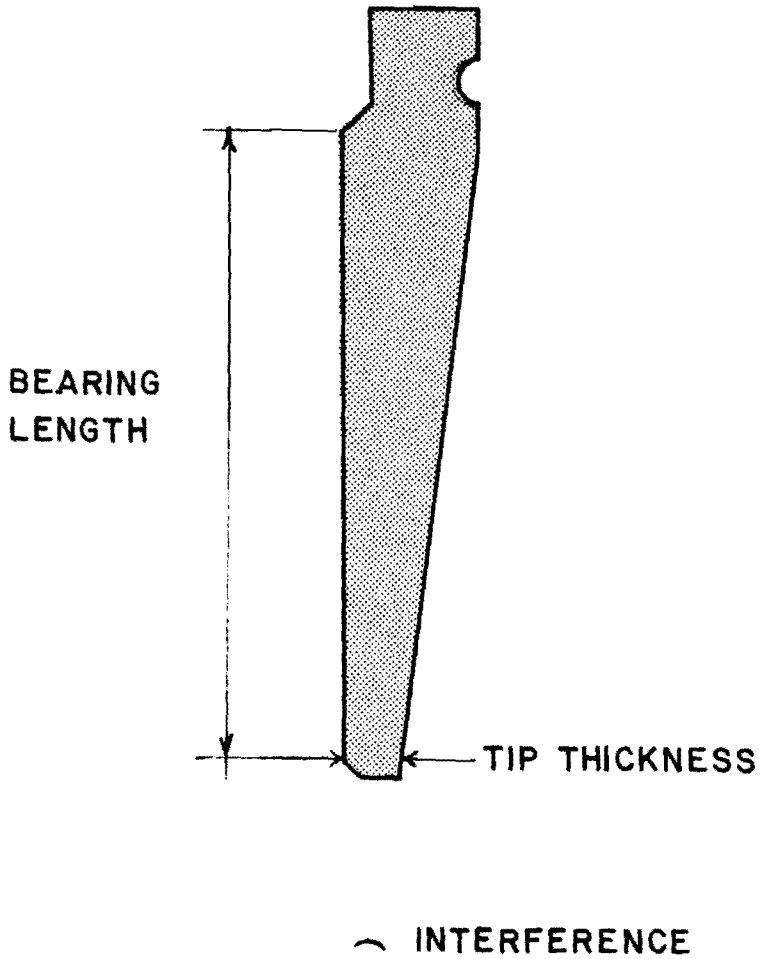

Fig. 5.3 Geometric parameters for conical wedges

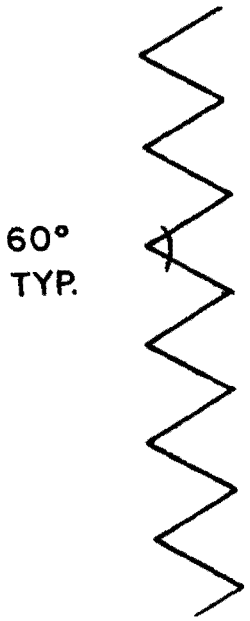

Fig. 5.4 Typical serration detail

tested experimentally. The general configuration of a wedge (Jaw no. 638) manufactured by Supreme Products was selected as a model for the wedges fabricated for this research program. The values of the geometric properties presented above were therefore predefined. These values are given below for the 0.5 in. diameter strand tests:

Bearing Length = 1.625 inches
Taper = 7.00 degrees
Depth = 0.15" (approx.)

The aspect of the wedge chosen as a variable was the material. Obviously, by changing to a different material, all of the material properties described in Chapter 3 change as well. The wedge materials chosen for the 0.5 in. diameter strand were aluminum (2024 alloy), copper, and steel (4340 alloy). The surface hardness and "inferred" tensile strength for these wedges are given in Table 5.1. The "inferred" tensile strength is determined from reference [27] and will allow comparison between materials evaluated on different Rockwell hardness scales in future discussion.

TABLE 5.1 MATERIAL PROPERTIES

Material	Hardness	Inferred F_u
Copper	34.9 B-scale	40.0 ksi
Aluminum	82.1 B-scale	77.0 ksi
Steel	48.0 C-scale	230.0 ksi

Wedge materials tested for the 0.6 in. diameter strand tests were mild steel, hardened (heat-treated) steel, and tungsten carbide-coated steel. In addition to wedges fabricated from these materials, the standard commercial wedges were used for both strand types to provide a standard for comparison. The fatigue tests performed for the earlier research program [16] were performed with a composite wedge. Soft iron wires (0.1 in. diameter) were pre-deformed to match the grooves between the outer wires of the strand. After the wires were placed in the six grooves, aluminum foil was wrapped around them. Commercial wedges were placed around the composite interface. These composite wedges were used in an attempt to force the failure zone out of the grip area and had limited success.

The design for the aluminum, copper, and steel wedges was based on the principle that plastic deformation should be allowed to occur so as to provide a larger area of contact. With this as the

goal, the wedges were designed with serrations on the interior surface so that large contact stresses would form at the tips upon application of tensile stress in the strand. The locally large contact stress would lead to plastic flow of the wedge material along and around the exterior wires of the prestressing strand resulting in a better distribution of stress along the strand. Tests were also performed with wedges which had been previously used. Since the serration pattern for these wedges had already been deformed (through a previous test), these wedges are defined as "predeformed" wedges. Untested wedges are defined as "undeformed" wedges.

The three different wedges (aluminum, copper, and steel) deformed around the outer wires of the strand in varying amounts. The individual outer wires of the strand became discolored through contact with the wedges. It was then possible to measure, directly, the ratio of the actual area of wedge/strand contact to the total outer surface area of the strand in the grip region. This ratio will be defined as the "Contact Ratio" (CR). The values of the contact ratio and the "inferred" tensile strength are given for each material in Table 5.2. The contact ratio is seen to increase with decreasing inferred tensile strength (hardness).

TABLE 5.2 CONTACT RATIOS

Material	Inferred F_u	CR
Copper	40.4 ksi	0.60
Aluminum	77.0 ksi	0.41
Steel	230.0 ksi	0.30

Three levels of serration were used for the aluminum wedges: 24, 20, and 14 serrations per inch (spi). The copper and steel wedges were designed with only one (16 spi.) serration pattern. The commercial wedge uses serrations at 30 per inch. The leading teeth of the commercial wedges are smaller, however, and do not allow complete biting. The serrations were produced by a thread cutting tool and, as a result, wound gradually about the inner surface of the wedge in a helix. A typical serration detail is illustrated in Fig. 5.4. Cross sections of each of the wedges used in 0.5 in. diameter strand tests are shown in Fig. 5.5.

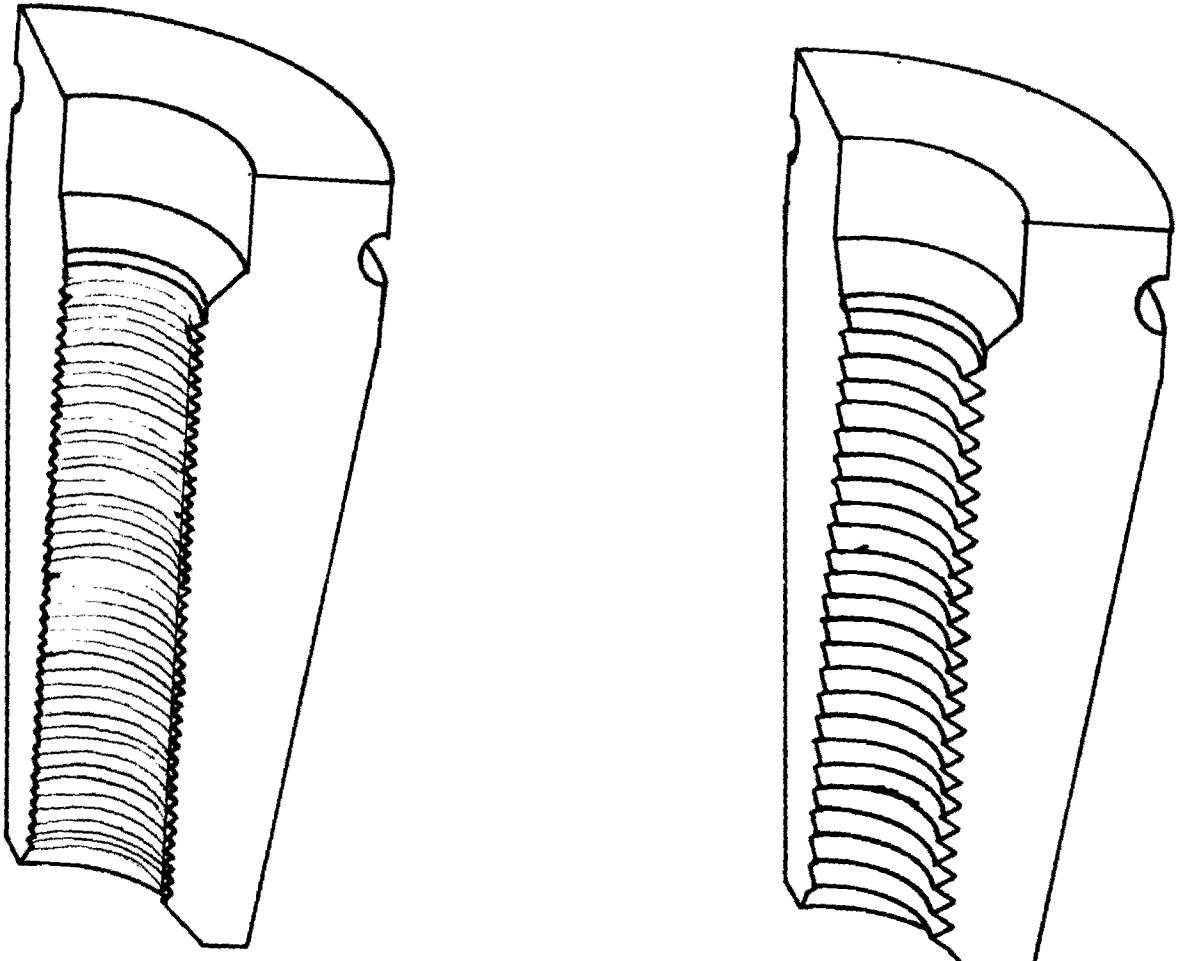

Fig. 5.5 Isometric representation of each of the wedges used in 0.5" diameter strand tests

The three wedges used in the 0.6 in. diameter tests were not serrated. The design of the wedges were different from those used in the 0.5 in. diameter tests in that they were divided into two parts as opposed to the three-part wedges used in the 0.5 in. diameter tests. A wide range of material property combinations was provided with this selection of wedges.

With the exception of tests performed with the commercial grip, all anchor assemblies were composed of a primary and a secondary grip. The primary grip is defined as the grip into which the strand first enters and is composed of the wedges described above. The commercial wedges performed the function of the secondary grip in all dual-grip anchorages. The secondary grip is placed behind and in contact with the primary grip and serves to prevent slippage of the primary grip during the seating process and testing. The dual anchorage is illustrated in Fig. 5.6. This dual grip assembly also allows for the axial stress transfer from the strand to occur over a greater distance.

5.2 Load Distribution Tests

This series of tests was performed to characterize the load distribution between the primary and secondary grips. The load cell specifically designed for these tests and the test procedure were described in Chapter 4. The results of these tests will be presented in two sections. The first section will contain the results obtained by the procedure of Chapter 4. These tests are the "static" load tests. Since the basic purpose of the load distribution tests was to determine the load distribution between the the two grips during cycling, the second section will contain the "fatigue" load distribution results.

5.2.1 Static Load Distribution Results. These tests were conducted for each of the wedge types tested in the fatigue study. The results of the undeformed and predeformed copper wedges will be presented first. Load distribution test results are also presented for the undeformed and predeformed steel wedges. No load distribution tests were performed on the undeformed aluminum wedges. The predeformed test results will be given. Tests were also performed on the wedges used in the 0.6 in. diameter strand fatigue tests. Only the undeformed heat-treated and mild steel load distribution test results will be presented. Load distribution tests were not performed on the pre-deformed heat-treated or mild steel wedges. Tests were also not conducted on the tungsten carbide-coated wedges. The results from the copper wedge tests will be discussed first and will be used to present the general characteristics of the load distribution curves.

Both the undeformed and the predeformed copper wedges were subjected to load distribution tests. The maximum load applied to the

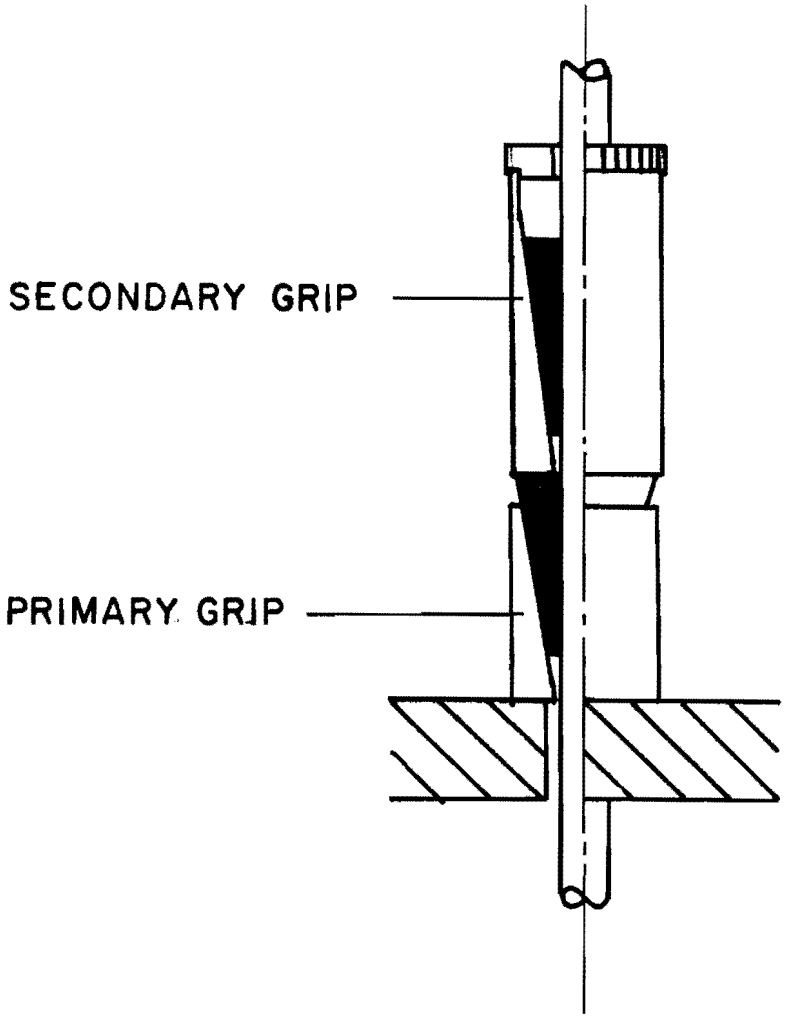

Fig. 5.6 Dual grip anchorage

strand in each of the cases was thirty kips (196.0 ksi). The load was then reduced to zero. The load carried by the secondary grip (T_S) at various values of tension in the strand (T) are presented in the trilinear curve of Fig. 5.7. The primary grip used for this test was the undeformed copper wedge. The three legs are labeled A, B, and C. The leg labeled "A" corresponds to the loading phase of the test while the two other legs (B and C) were obtained during the unloading phase. The load carried by the primary grip (T_P) can be obtained by subtracting the load in the secondary grip from the total load applied to the strand ($T_P = T - T_S$). The load transferred by the primary grip as a function of the tension applied to the strand is presented in Fig. 5.8. The form is, again, essentially trilinear. The three legs are labeled A', B', and C'. The leg labeled A' corresponds to the data obtained in the loading phase while the legs labeled B' and C' were obtained during the unloading phase. The dotted line in both Figs. 5.7 and 5.8 (and subsequent load distribution curves) represents the hypothetical case of $T = T_S$ (or $T = T_P$) and is plotted for reference. Similar load distribution curves for the predeformed copper wedges are given in Figs. 5.9 and 5.10. Each of the three legs will be discussed in a general sense before any other results are given.

The discussion will concentrate on three common characteristics of the load distribution curves. These characteristics are: (1) the nonlinearity of the A (loading) leg resulting from the use of the undeformed (previously untested) wedges, (2) the constant-load segment (B leg) found in the load distribution curves of secondary grips, and (3) the "negative" load transfer found in primary grip load distribution curves.

Nonlinearity of the A leg is a result of the nonconservative work done during the seating process of the primary and secondary grips. The nonlinearity resulting from the primary grip dominates while the nonlinearity resulting from the secondary grip is negligible.

During the initial loading phase, the serrations of an untested wedge deform, plastically around the six outer wires of the strand. The work done during this process is not conserved since the plastic deformation is not recoverable once the load is removed. One would therefore expect the degree of nonlinearity of the loading leg to be a function of the yield stress (and hardness) of the wedge material and the geometry.

A second source of nonlinearity is that resulting from the seating process of the secondary grip. As load is transferred into the secondary grip, wedging action forces the serrations of the commercial wedge to dig into the surface of the six outer wires of the strand. The notches formed by the digging are another form of plastic deformation which, in turn, is nonconservative. This source of nonlinearity is negligible, however, when compared to that resulting

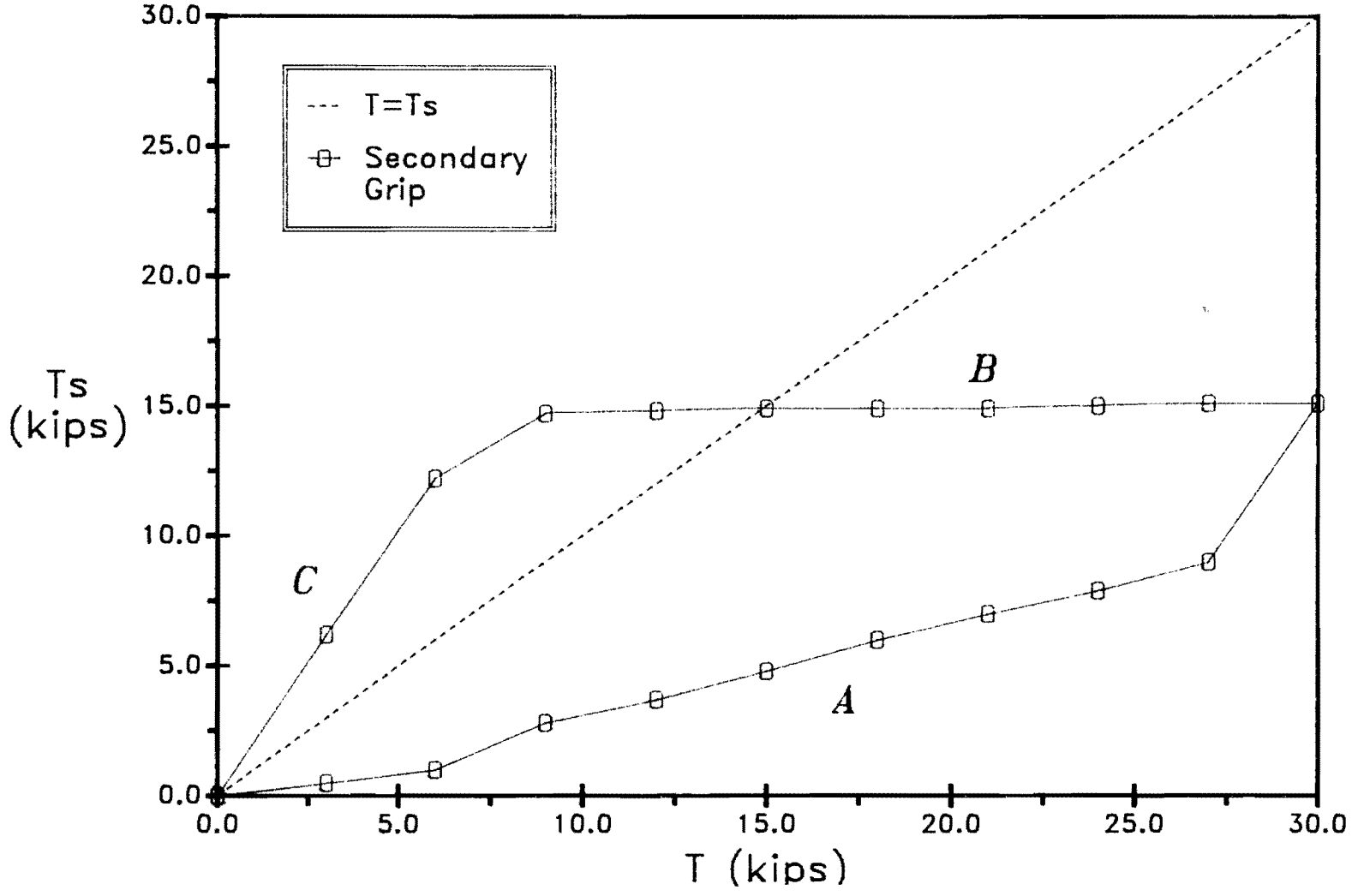

Fig. 5.7 Secondary grip load distribution curve for undeformed copper wedges

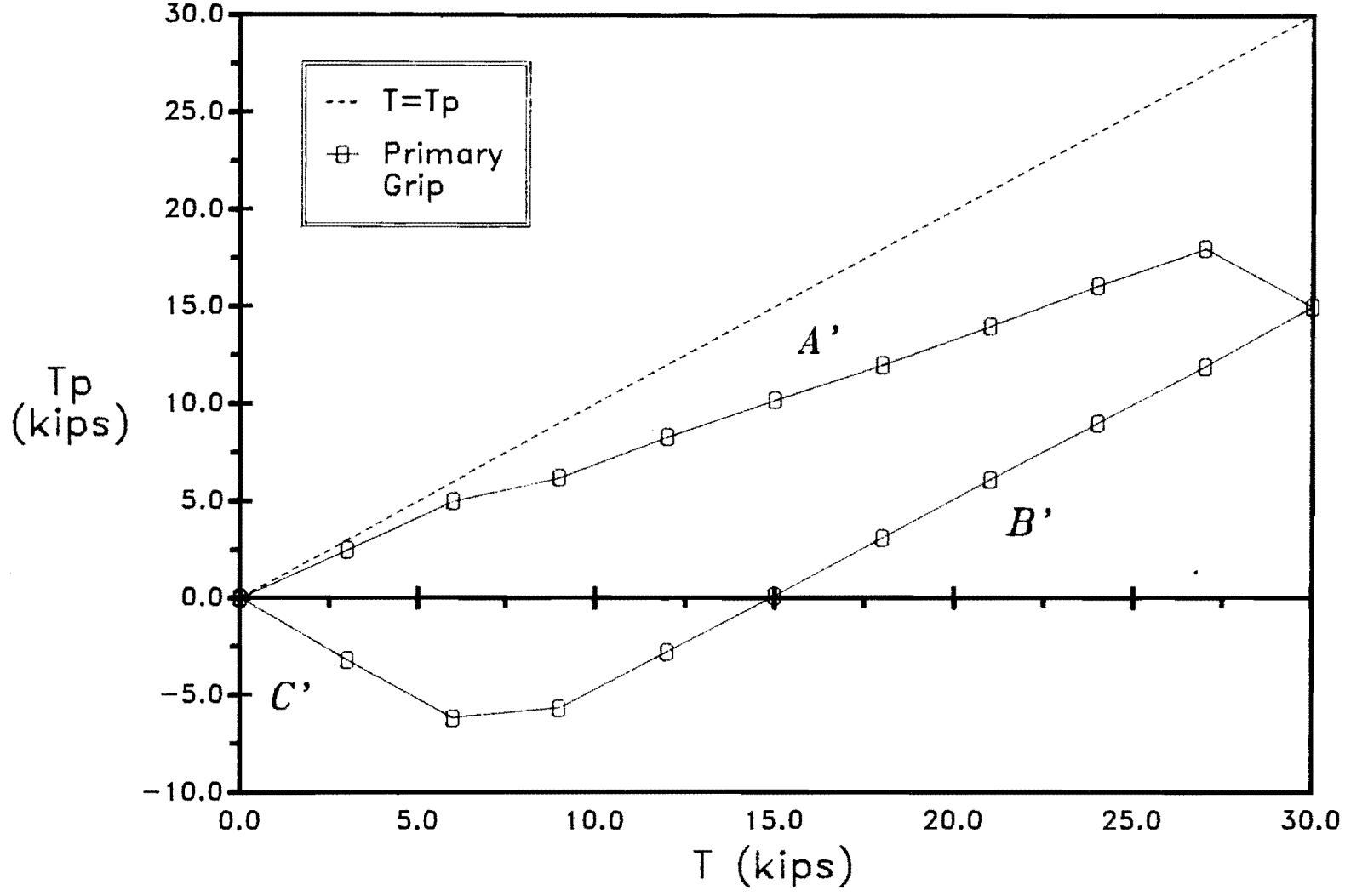

Fig. 5.8 Primary grip load distribution curve for undeformed copper wedges

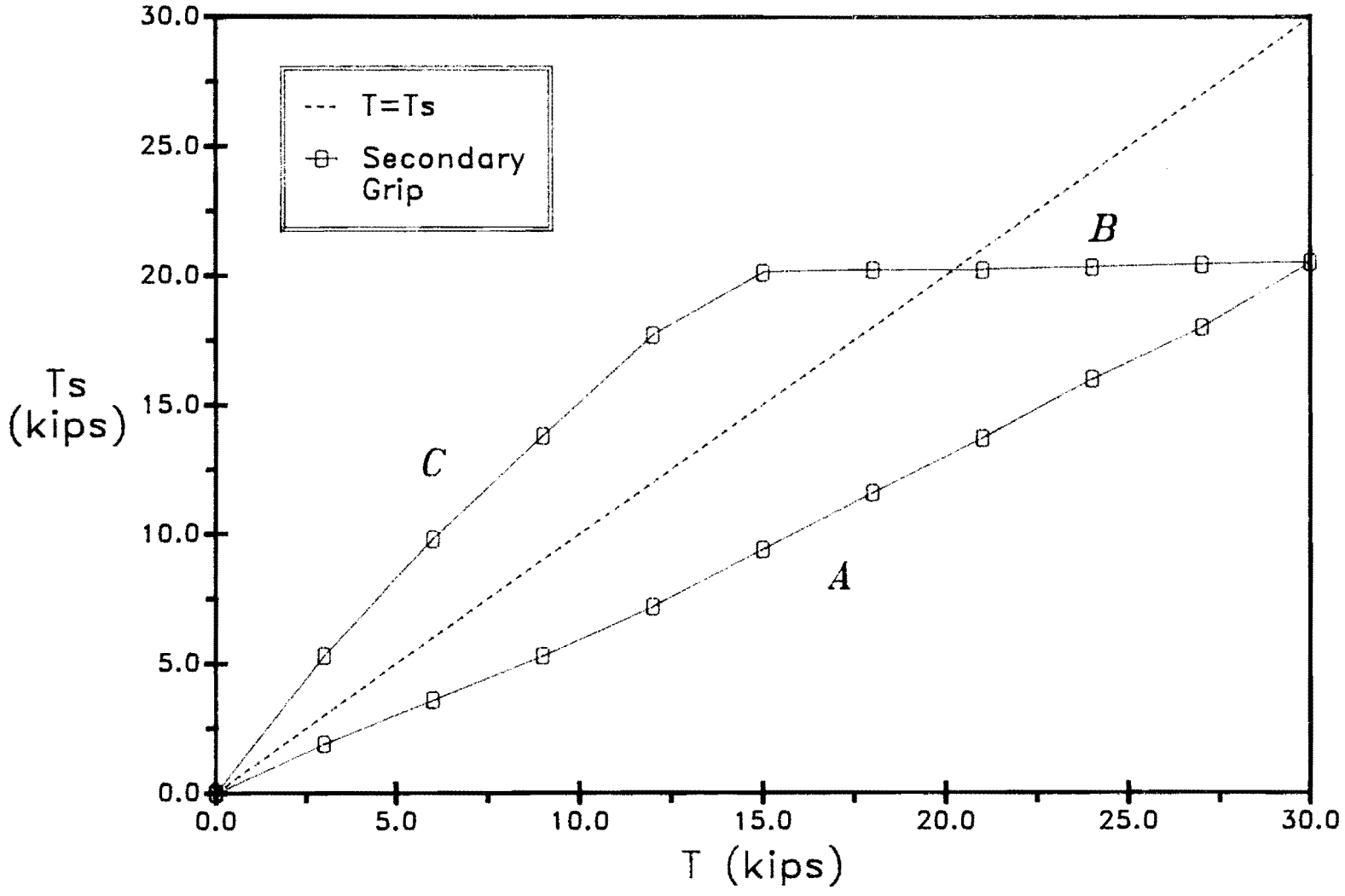

Fig. 5.9 Secondary grip load distribution curve for predeformed copper wedges

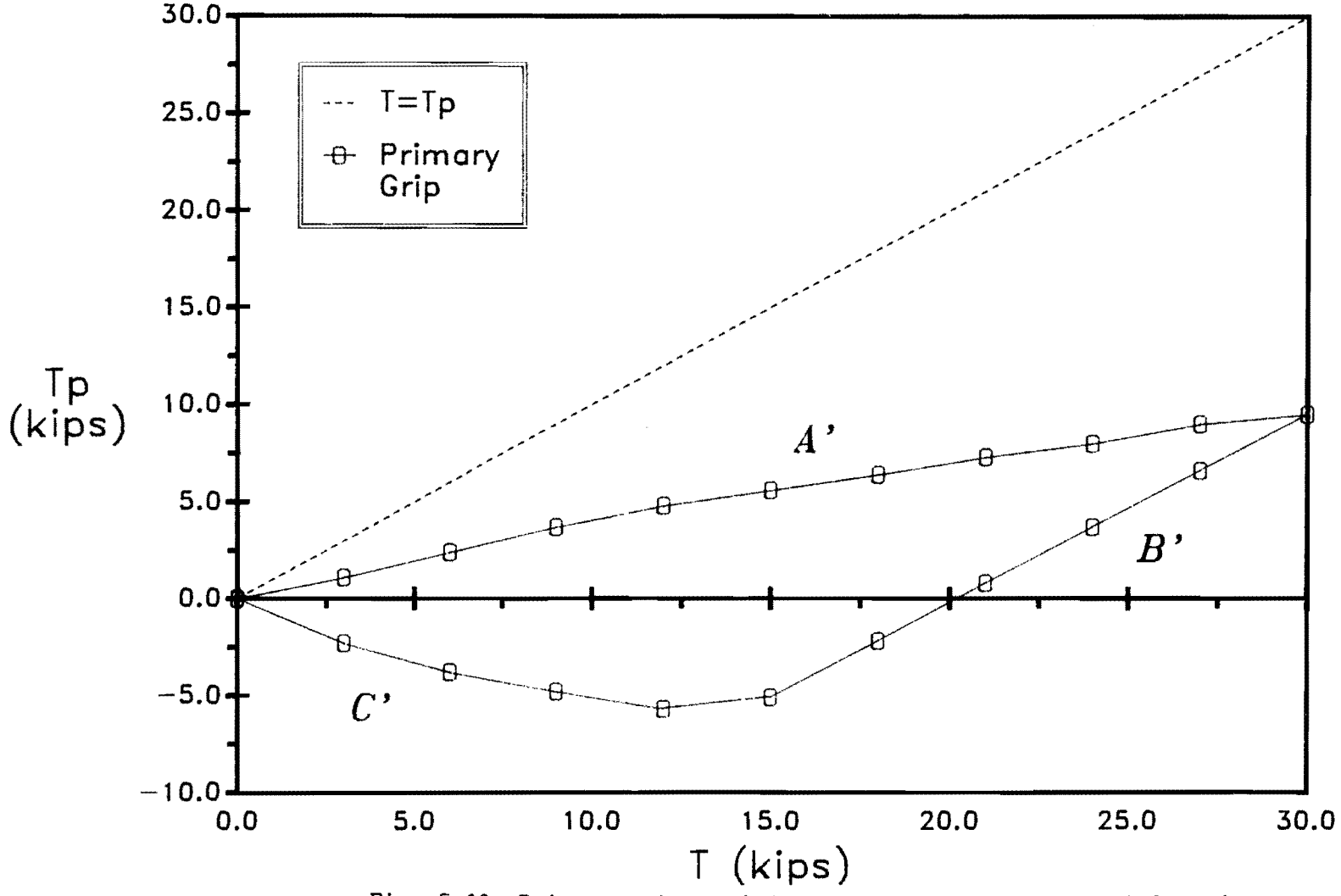

Fig. 5.10 Primary grip load distribution curve for predeformed copper wedges

from primary grip seating. This can be observed in the load distribution curves obtained with predeformed wedges. In the case of predeformed wedges, plastic deformation of the primary grip does not occur. However, the secondary wedge group does cause notching in the strand. Despite the seating of the secondary grip, the A leg is quite linear. It can, thus, be concluded that the seating of the secondary grip has little effect on the nonlinearity of the loading leg.

The constant-load, or B, leg is also of interest. The B leg of the secondary grip of a load distribution diagram is termed the "constant-load leg" since the load in the secondary grip remains constant as the load in the strand is decreased. As long as any cyclic load is applied within the range of the constant-load leg, no fatigue loading will reach the secondary grip (a detailed discussion of fatigue loading and the load distribution curves is presented in Section 5.2.2.). This is important as the secondary grip will be shown (Chapter 6) to be fatigue sensitive but well-suited for static loads. The flat plateau is a common characteristic of the secondary grip load distribution curves. Because of the fundamental importance of the constant-load leg an explanation for its development will be offered.

The constant-load leg can best be explained from a diagram of the idealized strain distribution in the strand as it enters the anchorage region. The strain diagram presented in Fig. 5.11 shows the distribution of strain at the time of maximum load in the strand. Illustrated below the diagram is a cross section of the anchorage region. The horizontal axis of the strain diagram corresponds to the axis of the strand in the drawing below it. The effect of the various elements of the anchorage on the strain distribution can easily be seen.

For the purposes of this discussion, the decrease in strand tension is assumed to be such that the resulting tension in the strand is always greater than or equal to the constant load in the load cell. The case of the load cell force being greater than the tension in the strand will be discussed later. Since the load in the secondary grip is known to remain constant upon reduction of the tensile load in the strand, the strain in the intermediate load cell must also remain constant during the decrease in strand tension. Were the entire length of strand free from contact, the change in strain would be uniform over the length. In this case, however, the wedges resist any change in strain. A change in strain implies a change in length between any two points on the strand. Changes in length occurring within the primary grip are resisted through friction between the wedge material and the surface of the strand. As long as the primary grip has enough frictional capacity to resist movement, all of the change in strain brought about by a change in strand tension will be distributed within the primary grip. The two important factors controlling the frictional resistance are the normal load and the coefficient of friction between the wedge and the strand. If either is increased, the frictional

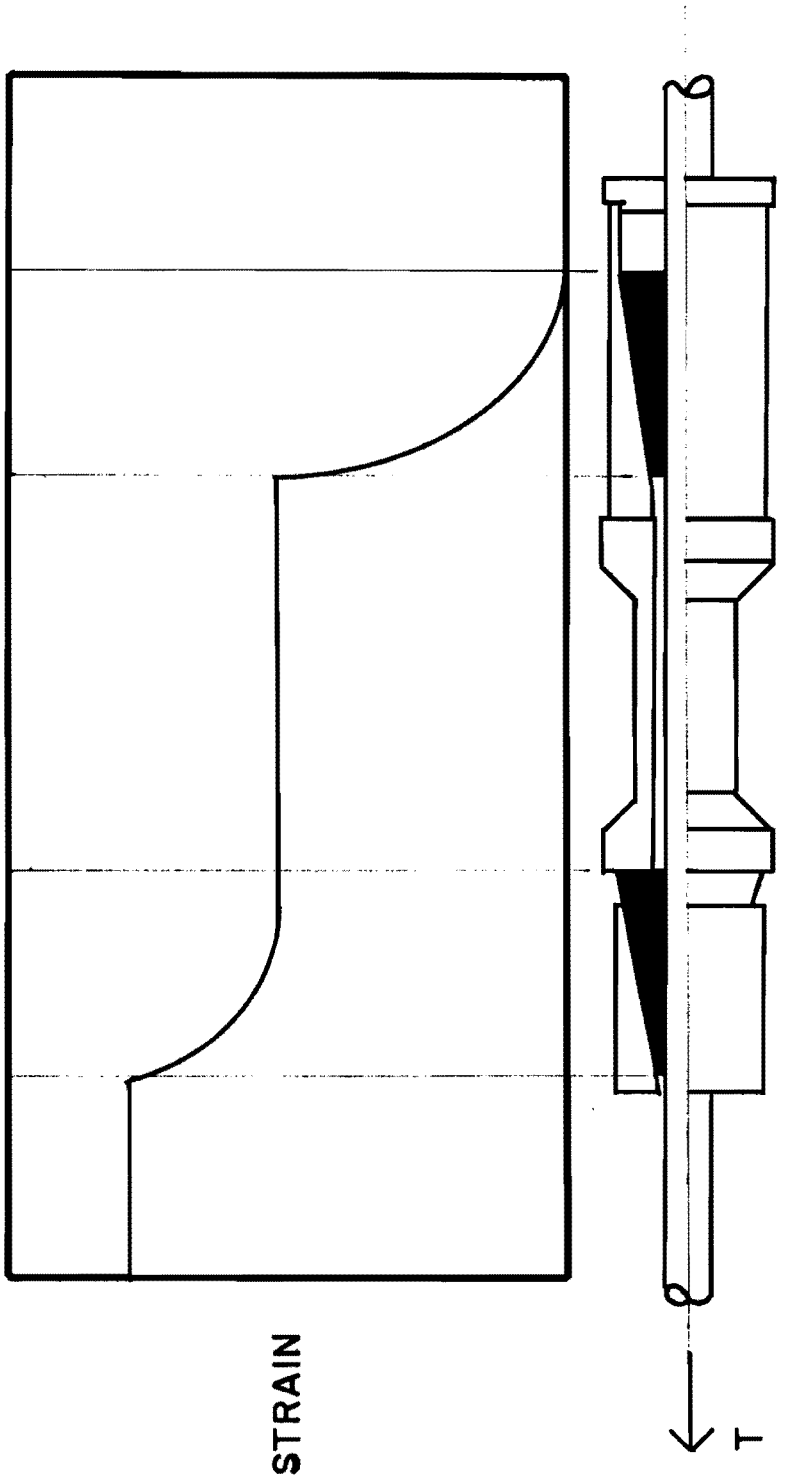

Fig. 5.11 Hypothetical strain diagram

resistance is increased. A larger frictional resistance in the primary grip results in a longer constant-load leg for the secondary grip.

The discussion presented on the constant-load leg of the secondary grip load distribution triangle was based on the assumption that the load in the strand was greater than the load carried by the secondary grip. It can be seen from any secondary grip load distribution triangle that a portion of the constant-load leg lies to the left of the intersection of the $T = T_S$ line and the constant-load leg. The previous discussion concentrated on that portion lying to the right of the intersection. The remainder of the discussion will concentrate on the part of the constant-load leg to the left of the intersection and the C leg. For this section of the secondary grip load distribution diagram, the load in the secondary grip is greater than the load in the strand resulting in a change in direction of the frictional stresses in the primary grip. This change in direction of the primary frictional stresses is shown in the primary grip load distribution diagrams as negative load transfer.

The friction mechanism described above is responsible for the reversal of frictional stresses in the primary grip as well. The strain diagram presented in Fig. 5.12 illustrates the distribution of strain in the anchorage region. The line labeled with a "1" represents the distribution of strain at the time of maximum tension in the strand. Reducing the tension to a level such that that the load in the strand is equal to that in the load cell produces the strain diagram labeled with a "2". This load level corresponds to the point on a secondary grip load distribution diagram where the $T = T$ line crosses the B leg. It can be seen from the diagram that the strain in the strand is equal to the strain in the primary grip region. Reducing the strain to this level has relieved the strain (i.e. frictional stresses) in the primary grip.

Decreasing the stress in the strand further leads to the strain diagram labeled with a "3". It is known from the results of the intermediate load cell that the strain in that section of strand remains constant. The strain differential must be resisted within the primary grip. Since the load transferred by the primary grip passed the zero-load mark, the resistance to the strain differential is translated into "negative" stress transfer. Further reductions of tension in the strand cause greater and greater strain differentials. Eventually, the imposed strain compatibility cannot be satisfied and the strain over the entire anchorage length decreases. The strain distribution for this case is labeled in Fig. 5.12 with a "4". The corresponding reduction in load transfer is shown on the load distribution diagrams as the C leg.

To investigate the effect of the maximum tensile load on the shape of the load distribution curves a series of tests were performed using the predeformed copper wedges with different values of maximum

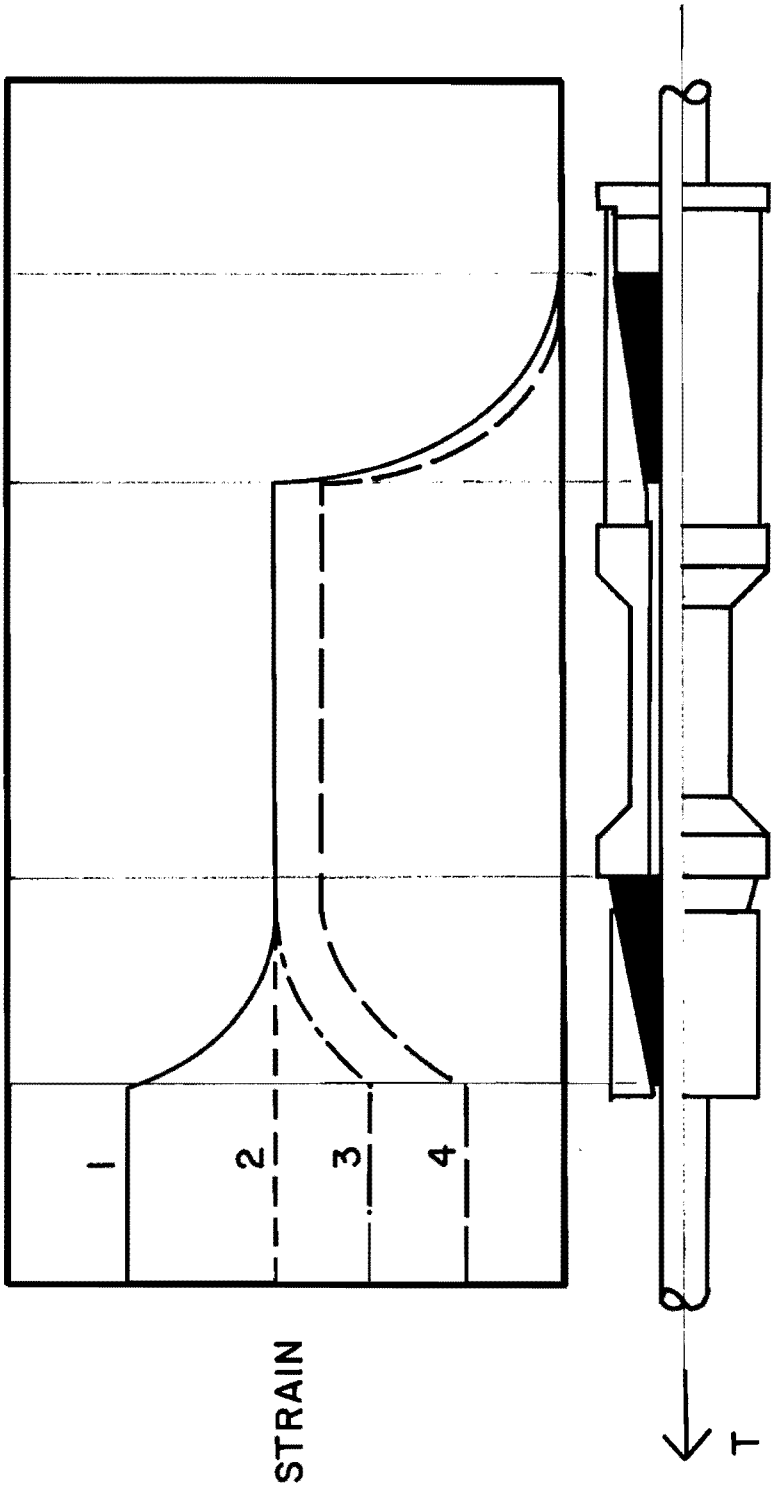

Fig. 5.12 Hypothetical strain diagram

load. Tests were performed with maximum loads of 12, 18, and 24 kips (78.4, 117.6, and 156.9 ksi, respectively). The load carried in the secondary grip is plotted in Fig. 5.13 for each of these maximum loads. The trilinearity is retained. Indeed, as all of the interior angles of the "load triangle" are equal, it can be seen that each of the "load triangles" are similar triangles. It is therefore possible to represent the load transfer behavior of the primary and secondary grips in a nondimensional fashion. When each of the four data series of Fig. 5.13 are divided by their respective maximum loads, the nondimensional trilinear curve of Fig. 5.14 is obtained. The corresponding graph for the primary grip is given in Fig. 5.15. These curves are general and therefore independent of the maximum load. Completely generalized nondimensional curves for the undeformed wedge are not possible due to the nonlinearity of the "A" leg.

Load distribution tests were also performed with the undeformed and predeformed steel wedges. These curves are similar in form to those obtained with the copper wedges and will not be presented separately. The results for the steel and aluminum are summarized instead. All of the load distribution curves for the 0.5" diameter strand have a similar form. Each of the curves is trilinear. Furthermore, each of the curves for the secondary grip has a constant load plateau. To allow for further comparison it will be convenient to summarize the characteristics of the load distribution curves in tabular form. Two parameters are required to uniquely describe the load distribution characteristics of a particular anchorage. The two parameters will be defined as the "Load Distribution Ratio" (LDR) and the "Constant Load Ratio" (CLR). The LDR is defined as the maximum load transferred by the primary grip divided by the maximum load applied to the strand.

$$LDR = T_{P\ max} / T_{max}$$

A small value of the load distribution ratio indicates little load transfer is occurring within the primary grip. An LDR equal to zero would imply all load transfer is occurring in the secondary grip region. On the other hand, an LDR equal to one would indicate that all of the load transfer is occurring within the primary grip.

The CLR is the normalized length of the constant-load leg of the secondary grip load distribution diagrams and is calculated by dividing the value of the tension in the strand corresponding at the intersection of the B and C legs by the maximum tension in the strand (30 kips for the 0.5 in. diameter strand tests) and subtracting that value from 1.0.

$$CLR = 1.0 - T_{BC}/T_{max}$$

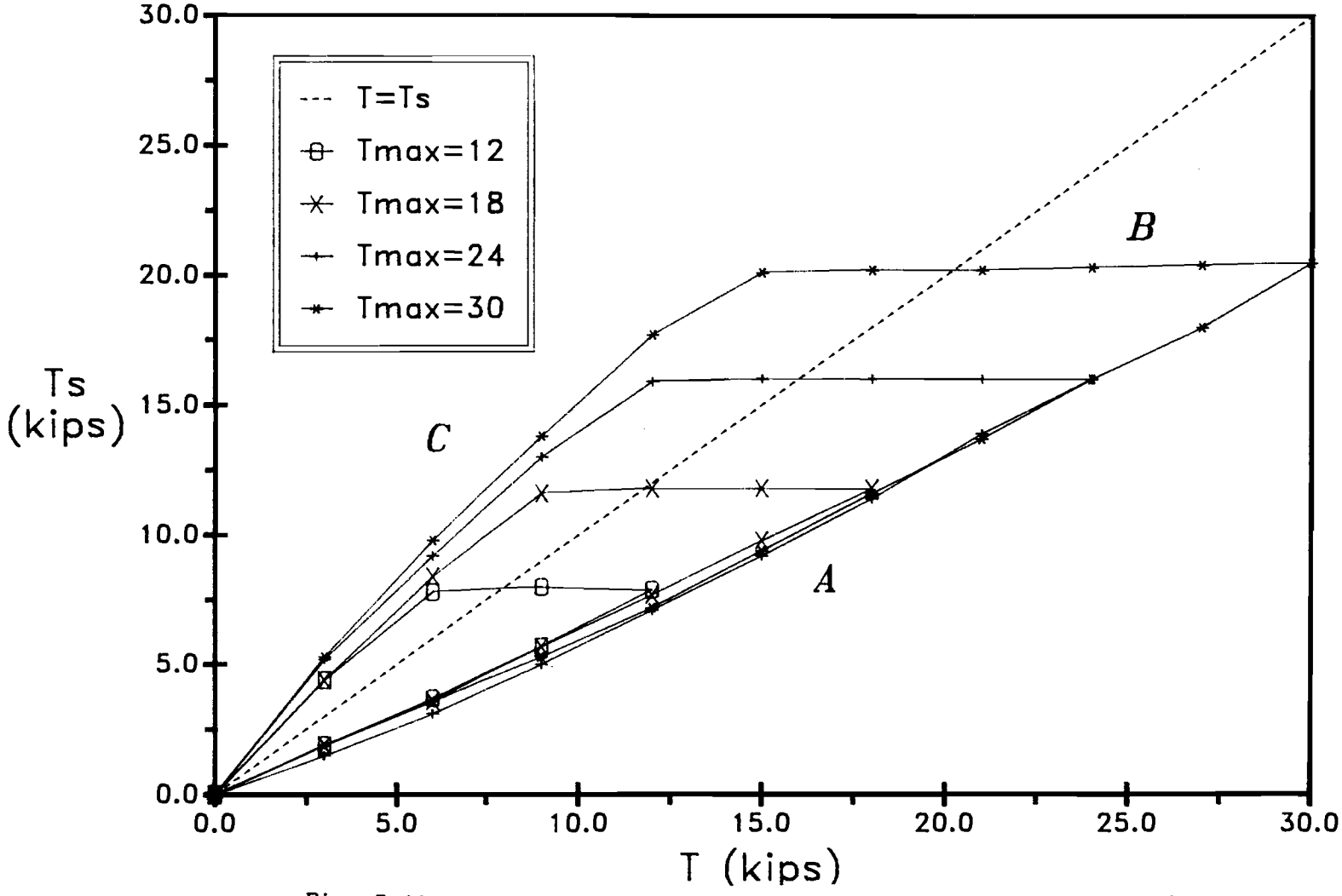

Fig. 5.13 Secondary grip load distribution curves for different maximum loads (predeformed copper wedges)

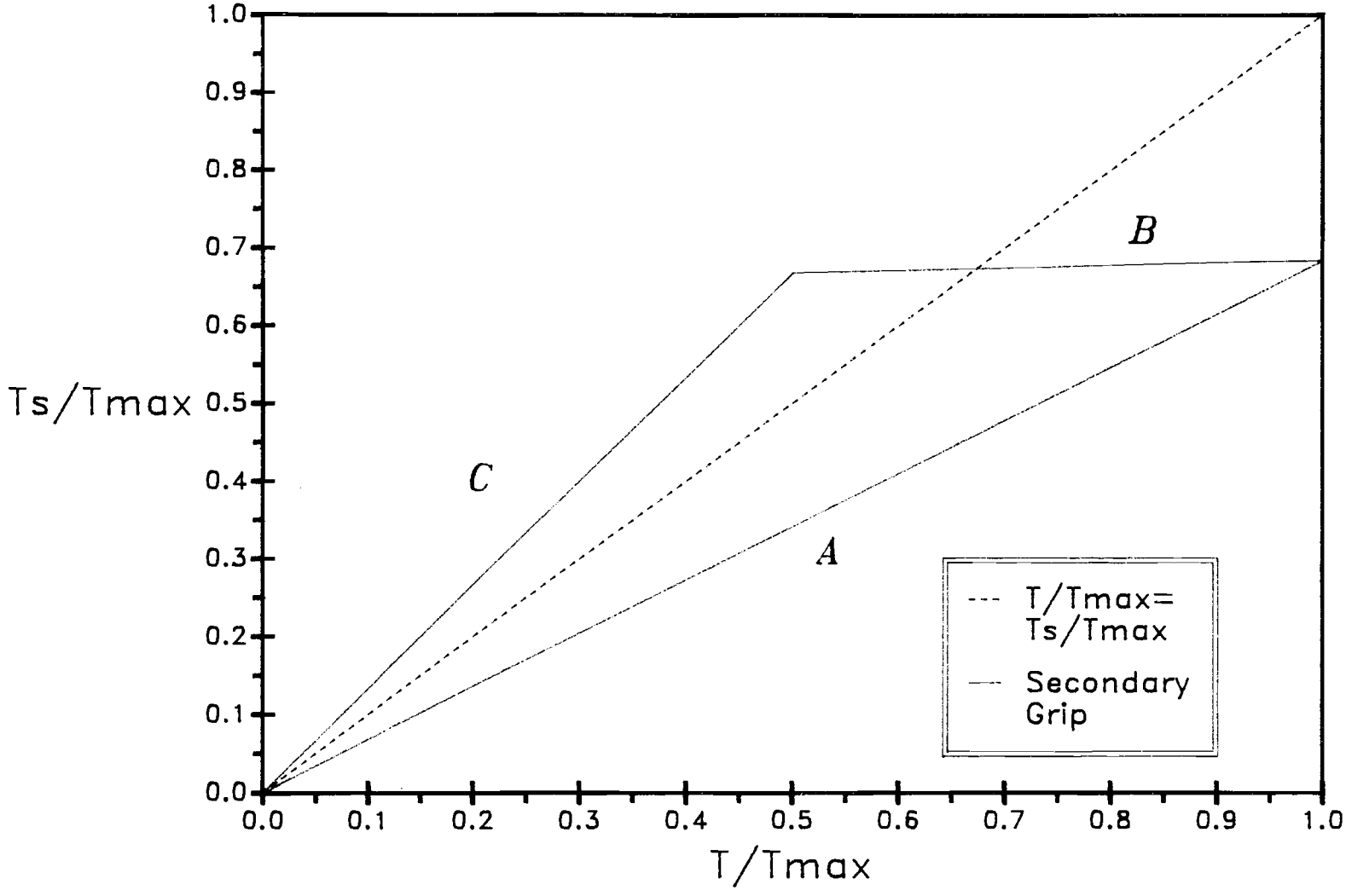

Fig. 5.14 Secondary grip nondimensionalized load distribution diagram for copper wedges

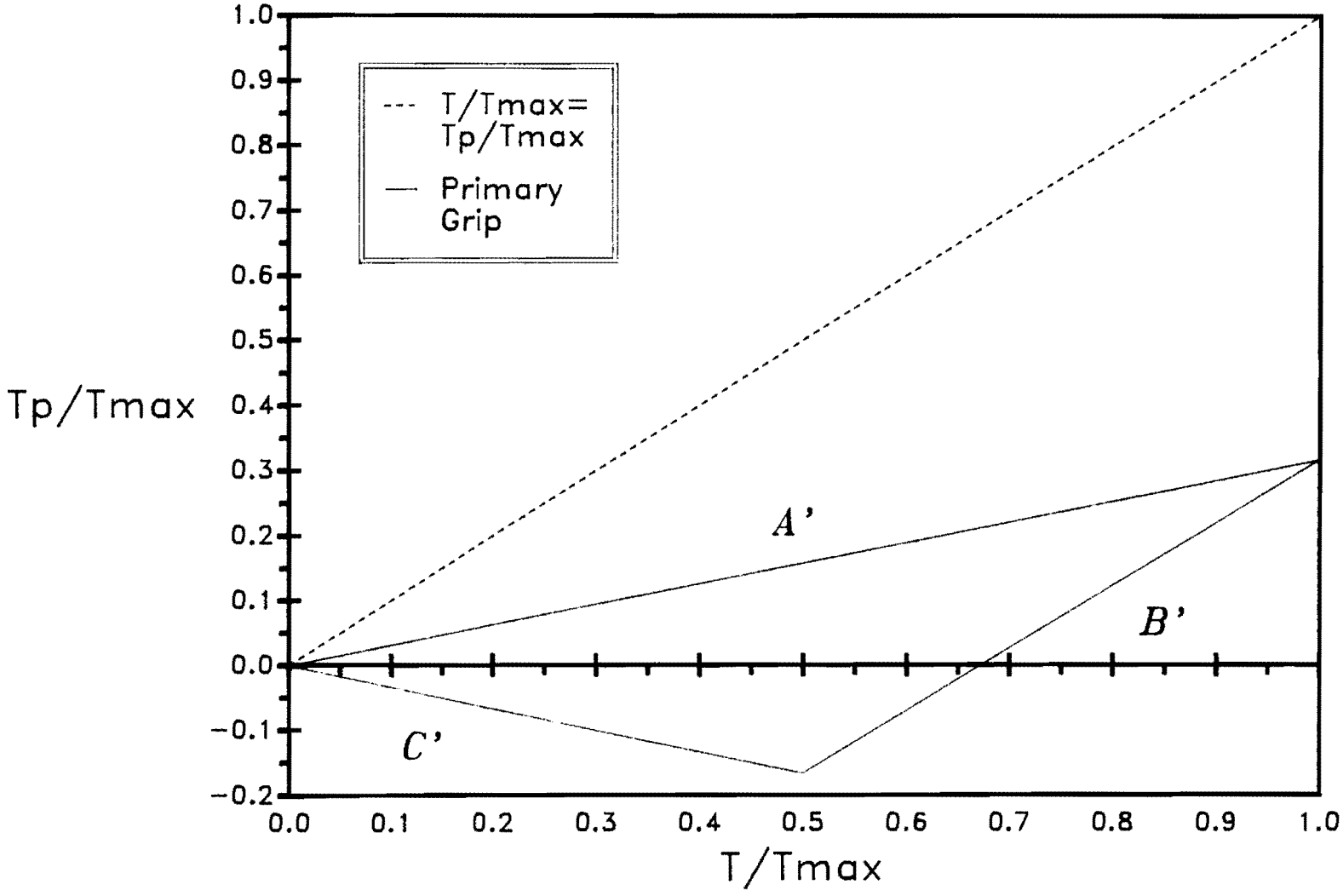

Fig. 5.15 Primary grip nondimensionalized load distribution diagram for copper wedges

The LDR and CLR are given for each of the anchorages in Table 5.3. It should be noted that the values of LDR and CLR for the undeformed wedges are only valid for values of T_{max} equal to thirty kips. The values of the LDR are plotted along the vertical axis of the bar graph of Fig. 5.16. The horizontal axis is labeled with the primary grip material and the corresponding inferred tensile strength. Two important observations can be made from this graph. First, the load distribution ratio tends to increase as the inferred tensile strength (and hardness) increases. This fact is true for both the undeformed and predeformed wedges. The second important point is that the load distribution ratio for a given material is consistently larger in the case of the undeformed wedge when compared to the predeformed type. This difference is due to the difference in the initiaal surface geometry between the undeformed and predeformed wedges. The undeformed wedges are initially effective in resisting the tension applied to the strand because of the locally high contact stresses under the tips of the serrations. High contact stresses imply high, localized, contact forces and therefore high frictional forces. The predeformed wedges, on the other hand, have smooth surfaces and are thus less effective in resisting the applied tension.

TABLE 5.3 SUMMARY OF LOAD DISTRIBUTION CHARACTERISTICS FOR 0.5" DIAMETER STRAND WEDGES

Material	Wedge	LDR	CLR
Copper	Undeformed	0.53	0.80
	Predeformed	0.27	0.43
Aluminum	Undeformed	---	---
	Predeformed	0.43	0.65
Steel	Undeformed	0.63	0.77
	Predeformed	0.57	0.70

Another material dependent characteristic is the difference between the load distribution ratios of the undeformed and predeformed wedges of the same material. It was shown in Fig. 5.16 that a primary grip composed of predeformed wedges carries less of the total strand tension than does a primary grip composed of undeformed wedges of the same material. The ratio of the predeformed load transfer to the undeformed load transfer is always less than one for the primary grip and greater than one for the secondary grip. Data are available for the predeformed and undeformed copper and steel wedges. The ratio of the predeformed load transfer to the undeformed load transfer will be

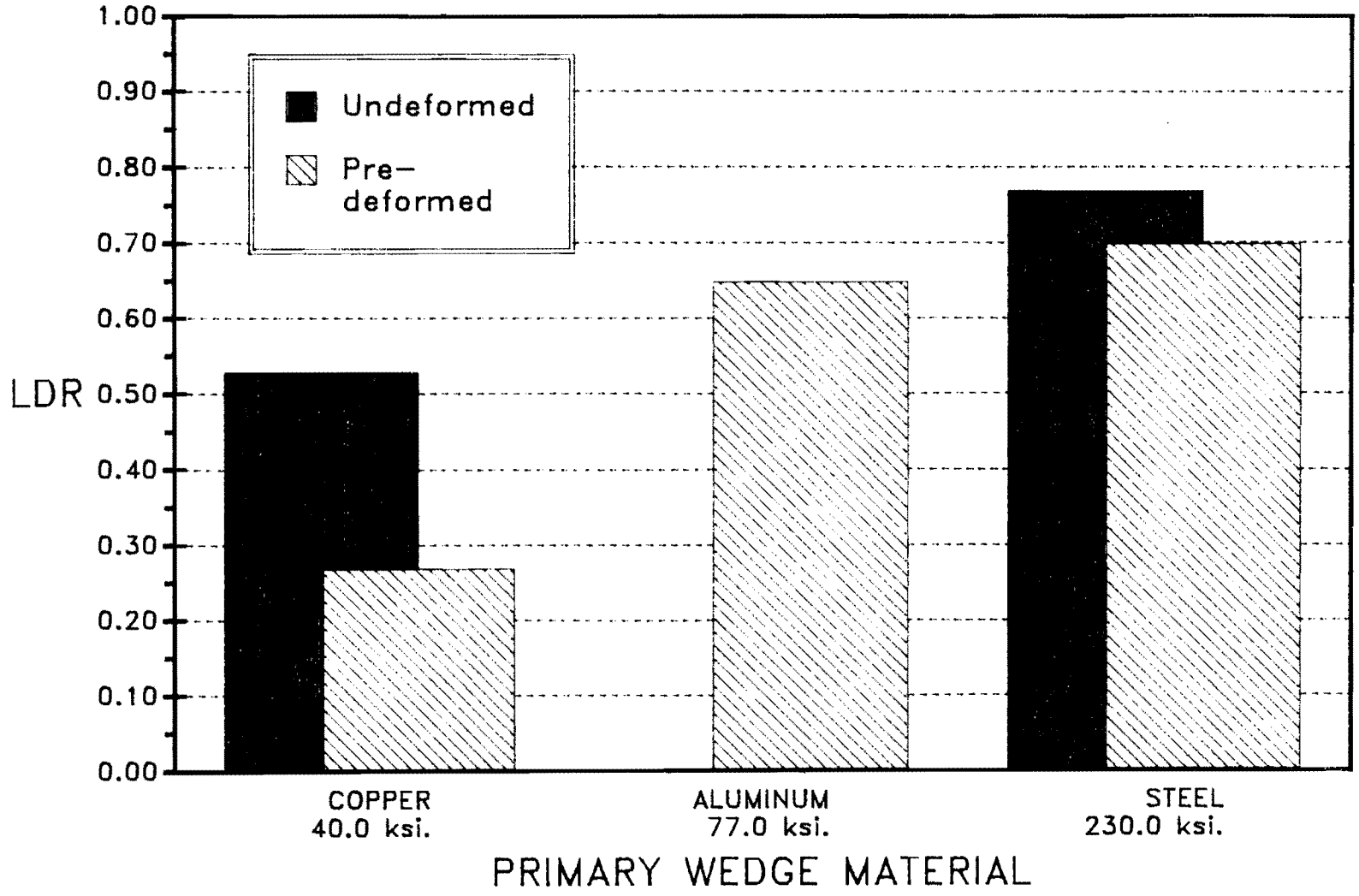

Fig. 5.16 Load distribution ratio (LDR) vs primary wedge material

defined as the "Load Transfer Ratio" (LTR). The load transfer ratios for the steel and copper are compared in the bar graph of Fig. 5.17.

Two important observations can be made from Fig. 5.17. First, the load transfer ratio is very close to one for the steel wedges. A load transfer ratio equal to one indicates no difference in the load transfer characteristics of the primary grip wedges. This is true only if the primary grip wedges do not change (i.e. plastically deform) from their undeformed configuration during loading. In this limit case, an undeformed wedge is the same as a predeformed wedge.

The second observation, is the decrease in the load transfer ratio from the steel to the copper. The difference in load transfer ratios implies a relationship between the hardness and the load transfer ratio. The contact ratio defined and measured earlier in this chapter provides a convenient base for comparison as the variables of hardness and deformability are implicitly included. The load transfer ratios for the steel and copper are plotted as a function of the contact ratio in Fig. 5.18. The dotted line connects the two data points. The line shown in Fig. 5.18 is intended to illustrate the trend. The actual variation in the load transfer ratio between the two measured points is not known. In general, those materials with low hardness (i.e. low yield stress and stiffness) show a greater difference between the undeformed and pre-deformed load distribution ratios. This will be particularly important when the fatigue strength is considered in the next chapter.

In addition to the load distribution tests performed on the anchorages used in the 0.5 in. diameter strand fatigue tests, tests were also conducted on those anchorages used in the 0.6 in. diameter strand fatigue tests. The strand in these tests was loaded to a maximum of forty-two kips (194.0 ksi.) which corresponded to the maximum load achieved during the fatigue tests. The load carried by the secondary and primary grips as a function of the load in the strand is plotted for the undeformed heat-treated steel wedges in Figs. 5.19 and 5.20 respectively. Similar curves are presented for the undeformed mild steel wedges in Figs. 5.21 and 5.22. These curves are similar in form to those discussed earlier. Both wedges exhibit a trilinear form and both have a constant-load leg in the secondary grip load distribution diagrams. The mild steel produced a lower LDR than the heat-treated steel (0.51 as compared to 0.67 for the hardened steel). This is constsent with the findings of the 0.5 in. strand wedges which indicated a lower load distribution ratio for wedges of lower hardness. Load distribution tests were not performed using the pre-deformed wedges of either the heat-treated or the mild steel type since fatigue tests were not performed with these wedges.

The results of the load distribution tests have been presented and discussed in this subsection. Each of the anchorages was shown to possess specific load distribution characteristics (LDR, CLR,

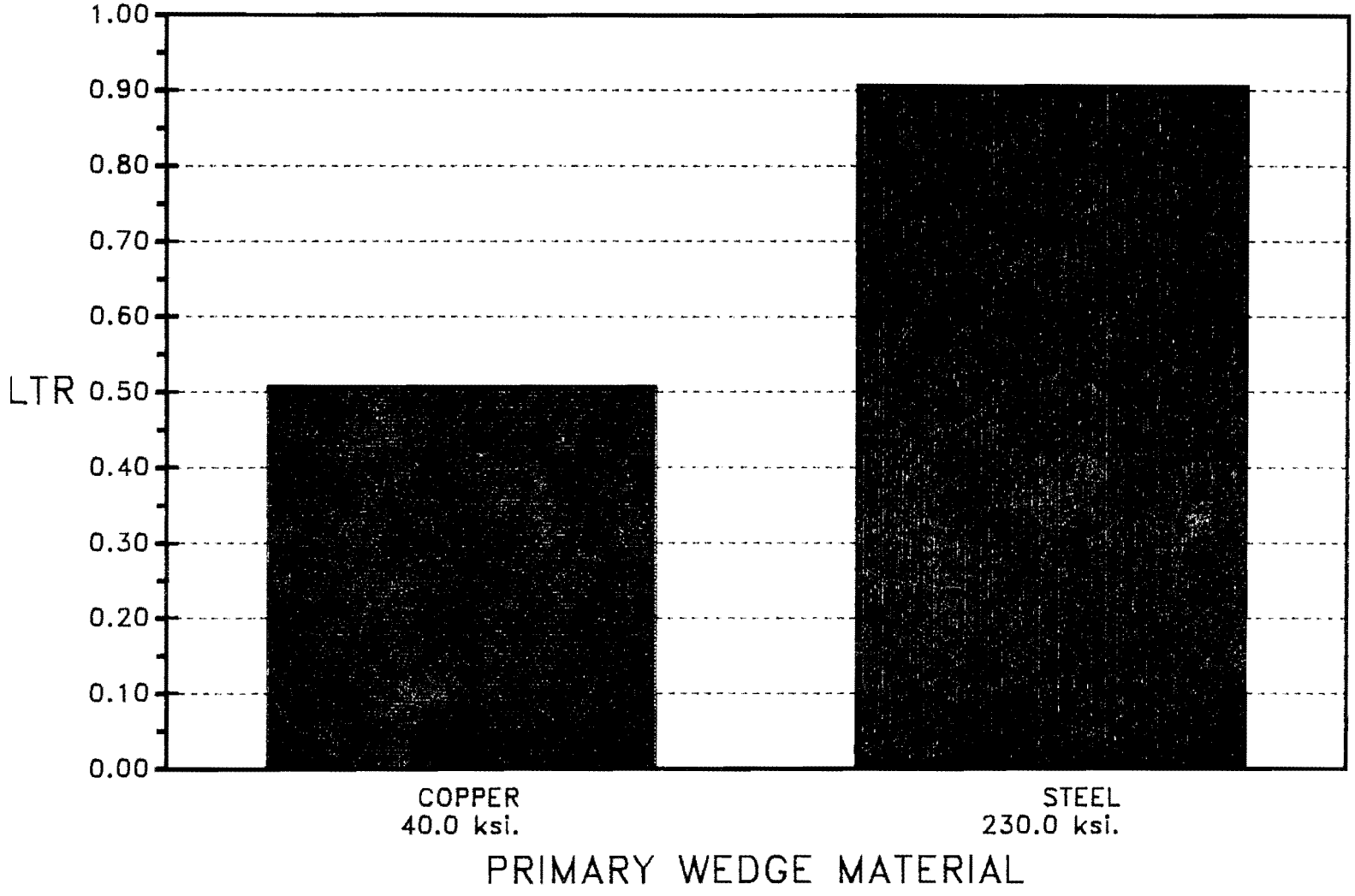

Fig. 5.17 Load transfer ratio (LTR) vs primary wedge material

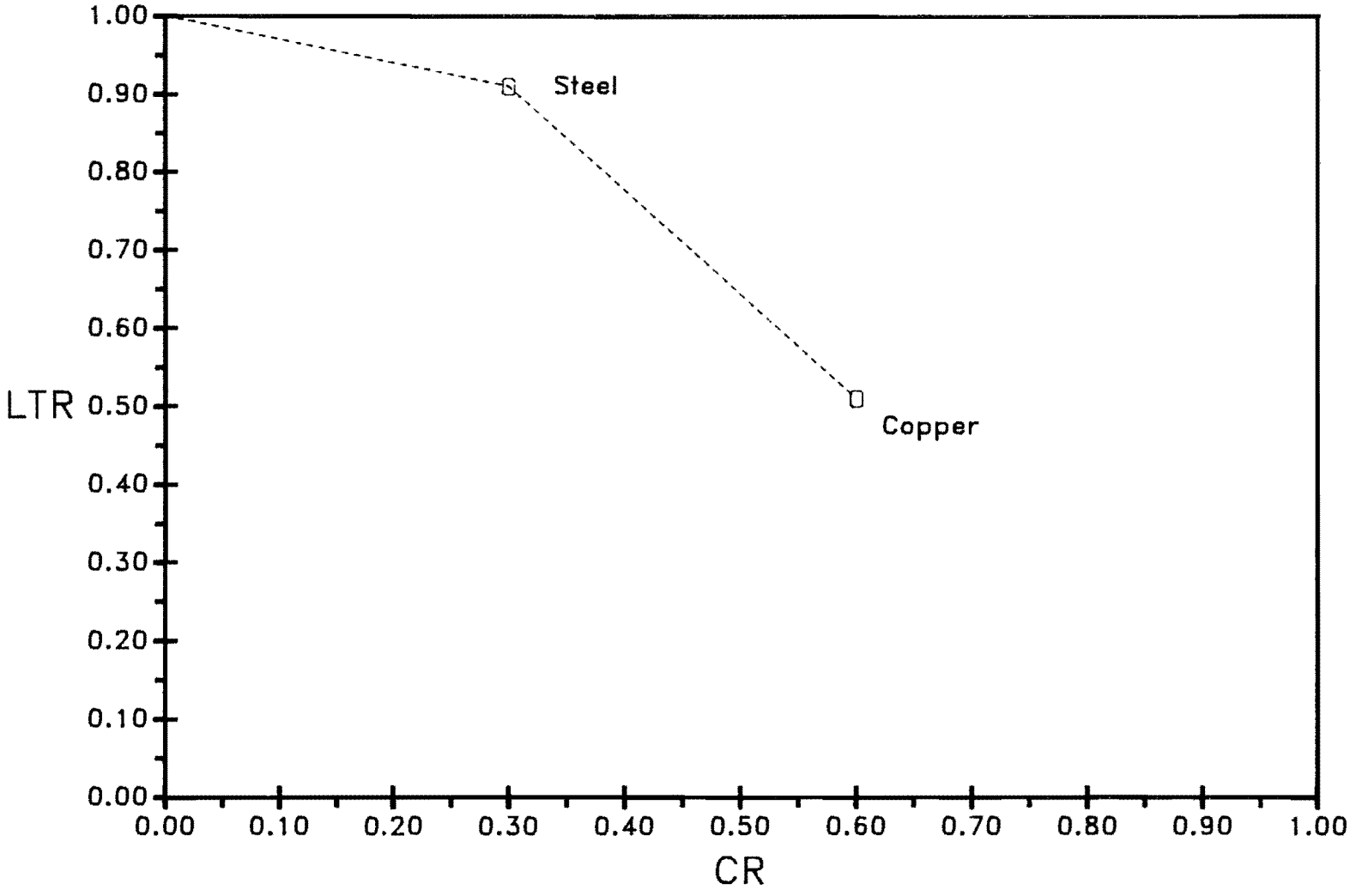

Fig. 5.18 Load transfer ratio (LTR) vs contact ratio (CR)

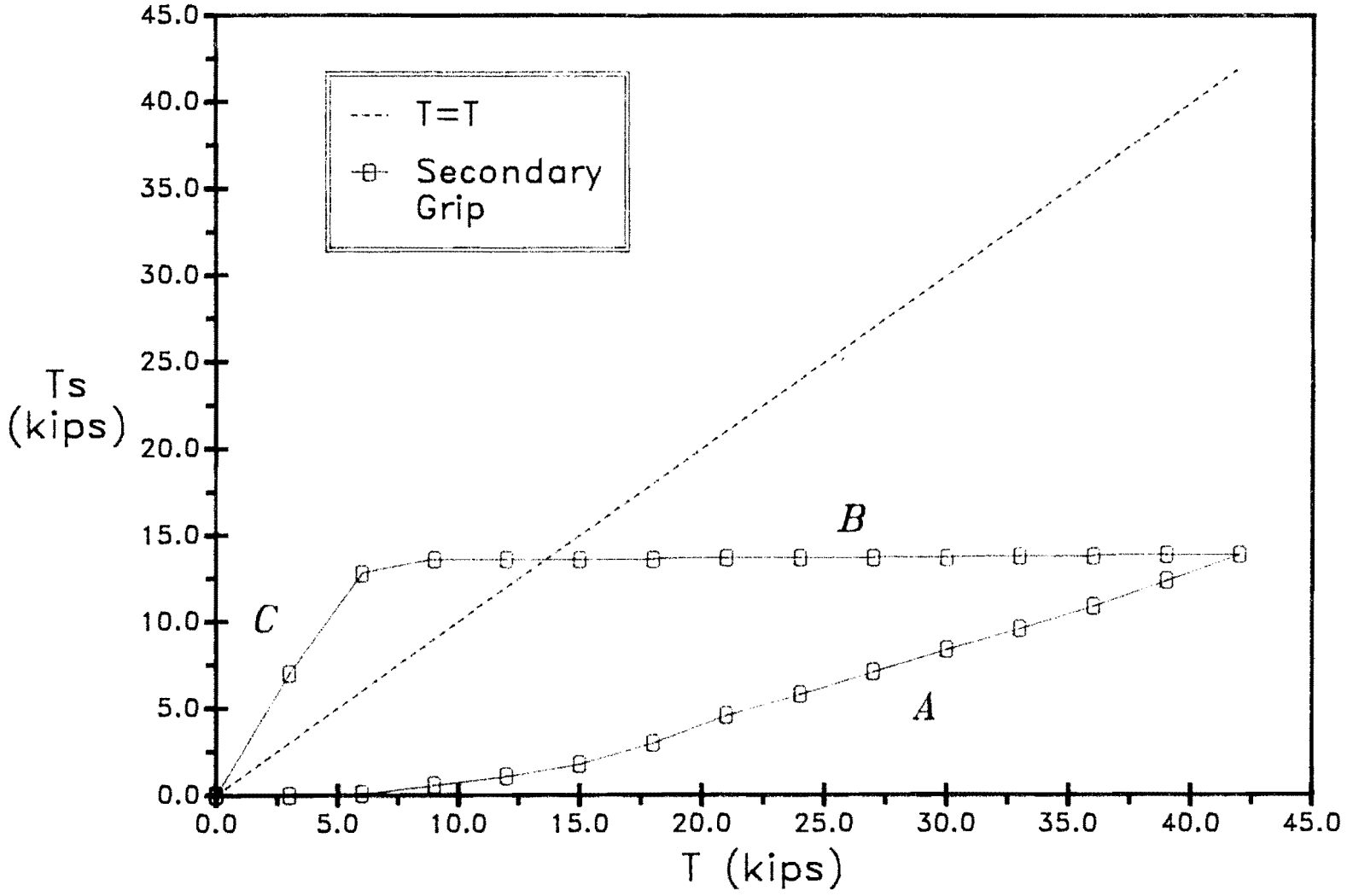

Fig. 5.19 Secondary grip load distribution curve for heat-treated steel wedges (0.6" ϕ)

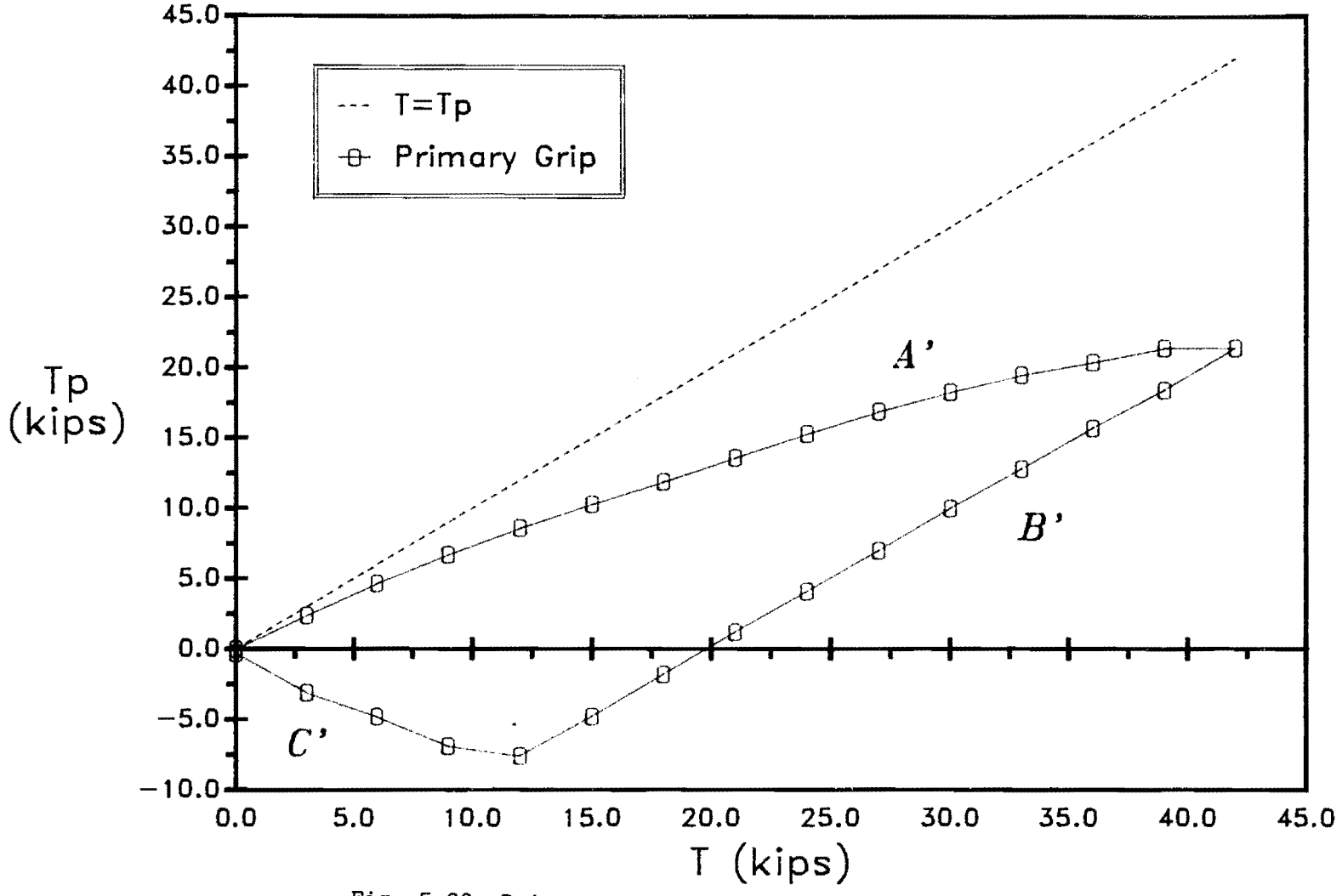

Fig. 5.20 Primary grip load distribution curve for heat-treated steel wedges (0.6" ∅)

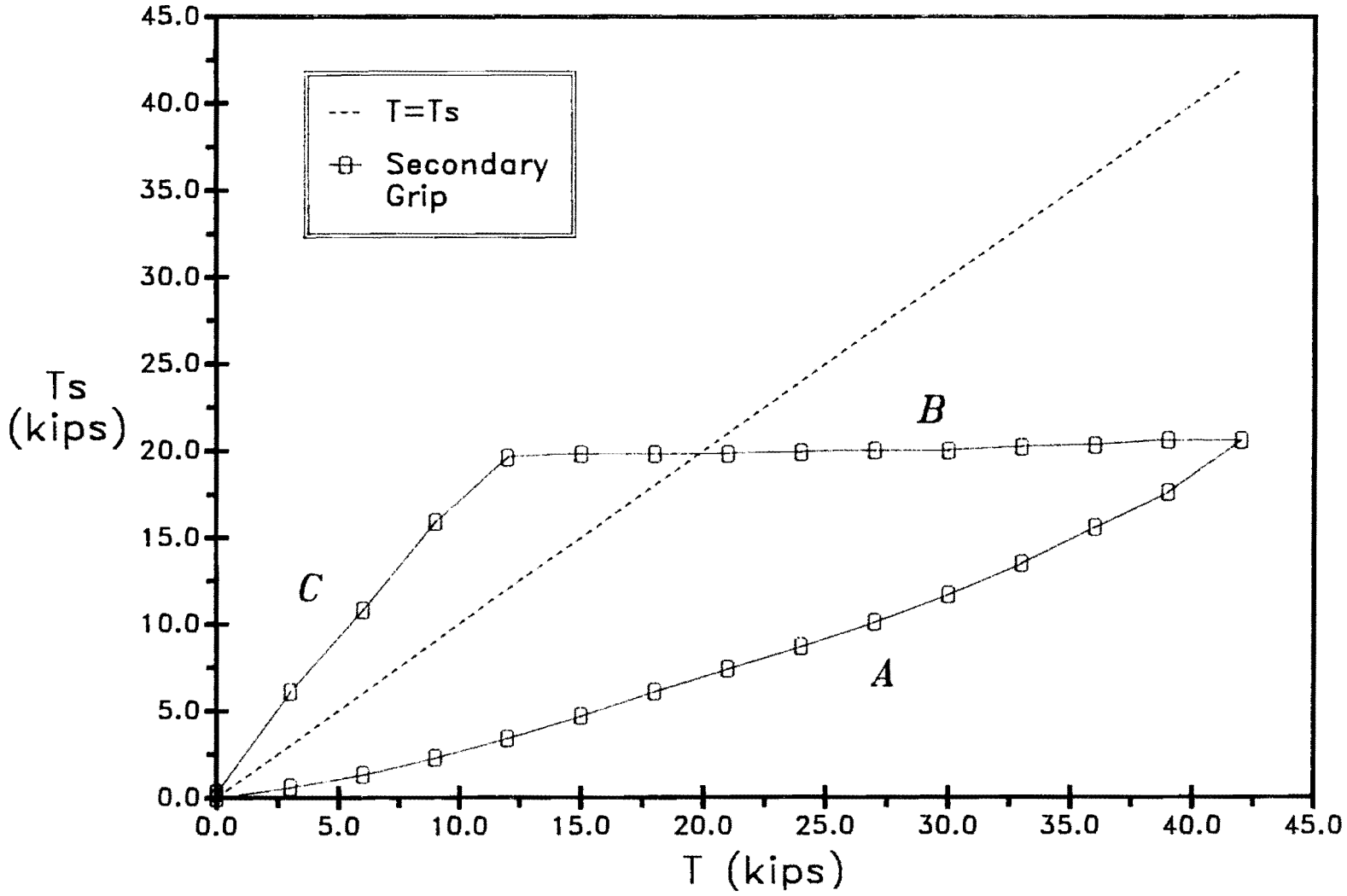

Fig. 5.21 Secondary grip load distribution curve for mild steel wedges (0.6" ∅)

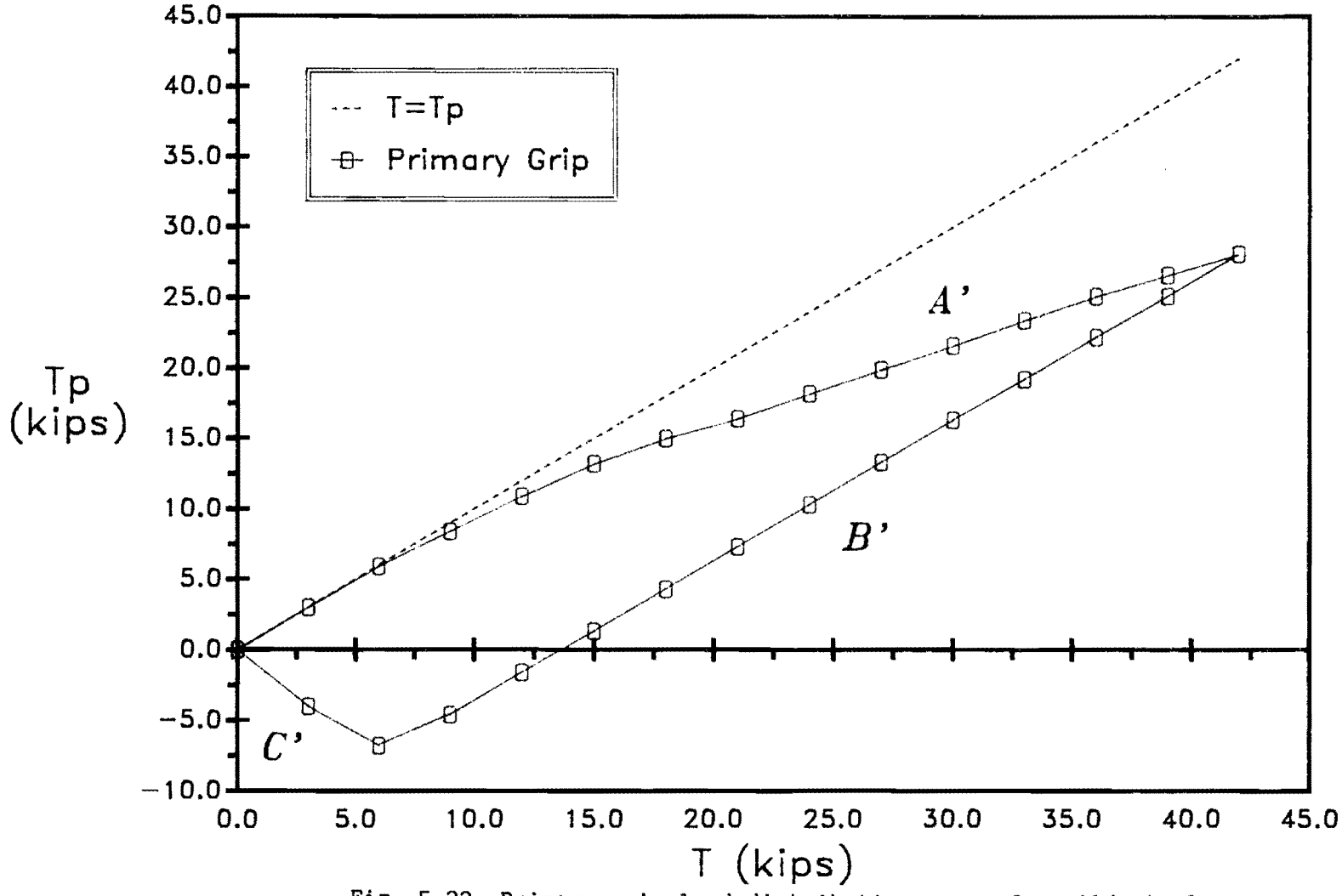

Fig. 5.22 Primary grip load distribution curve for mild steel wedges (0.6" ϕ)

and LTR). The material hardness (and related properties) were shown to be responsible for the different load distribution characteristics. An increase in hardness leads to a greater amount of the applied tension being transferred by the primary grip. An increase in the primary wedge hardness also reduces the difference in the load distribution ratio between the undeformed and predeformed wedges. This relationship was illustrated with the aid of the load transfer ratio.

5.2.2 Fatigue Load Distribution Tests. The test results presented in previous subsection were, in general, performed by loading the strand up to the maximum tensile load seen by the strand in fatigue tests and then unloading back to zero load. As such, these tests do not explicitly predict the load distribution characteristics resulting from a strand tension of the form:

$$T = T_{MEAN} + (0.5)(T_{RANGE})[SIN(\omega t)].$$

where T_{MEAN} in the equation is the mean tension in the strand, T_{RANGE} is the load range, ω is test frequency, and t is the varying time parameter. The load is seen to vary with time between a maximum and minimum tensile load given by:

$$T_{MAX} = T_{MEAN} + (0.5)(T_{RANGE})$$

$$T_{MIN} = T_{MEAN} - (0.5)(T_{RANGE})$$

In terms of the load distribution curves presented in the previous subsection, the load in the strand is increased to T_{MEAN}. Just before cycling is begun about T_{MEAN} the magnitude of the load carried by the secondary grip (T_S) can be read at the intersection of the line $T = T_{MEAN}$ and the "A" leg of the typical secondary load diagram given in Fig. 5.23. This point is labeled with a "1". Once cycling is begun, the tensile load increases to T_{MAX} (the intersection of the A and B legs labeled as point 2) in the first quarter of the load cycle. After reaching the peak load of T_{MAX}, the load in the strand decreases to T_{MIN} or point "3" in the figure. Note that the load in the secondary grip remains constant during the decrease in strand tension.

The load does not decrease below T_{MIN} in fatigue tests, but rather, increases back to T_{MAX} and continues to cycle between T_{MIN} and T_{MAX} until a failure is obtained. The load in the load distribution load cell was monitored during cycling. The load transferred by the secondary grip (T_S) was found to remain constant over time for the life of all specimens. No dynamic load reaches the secondary grip. A schematic of the load distribution between the primary and secondary

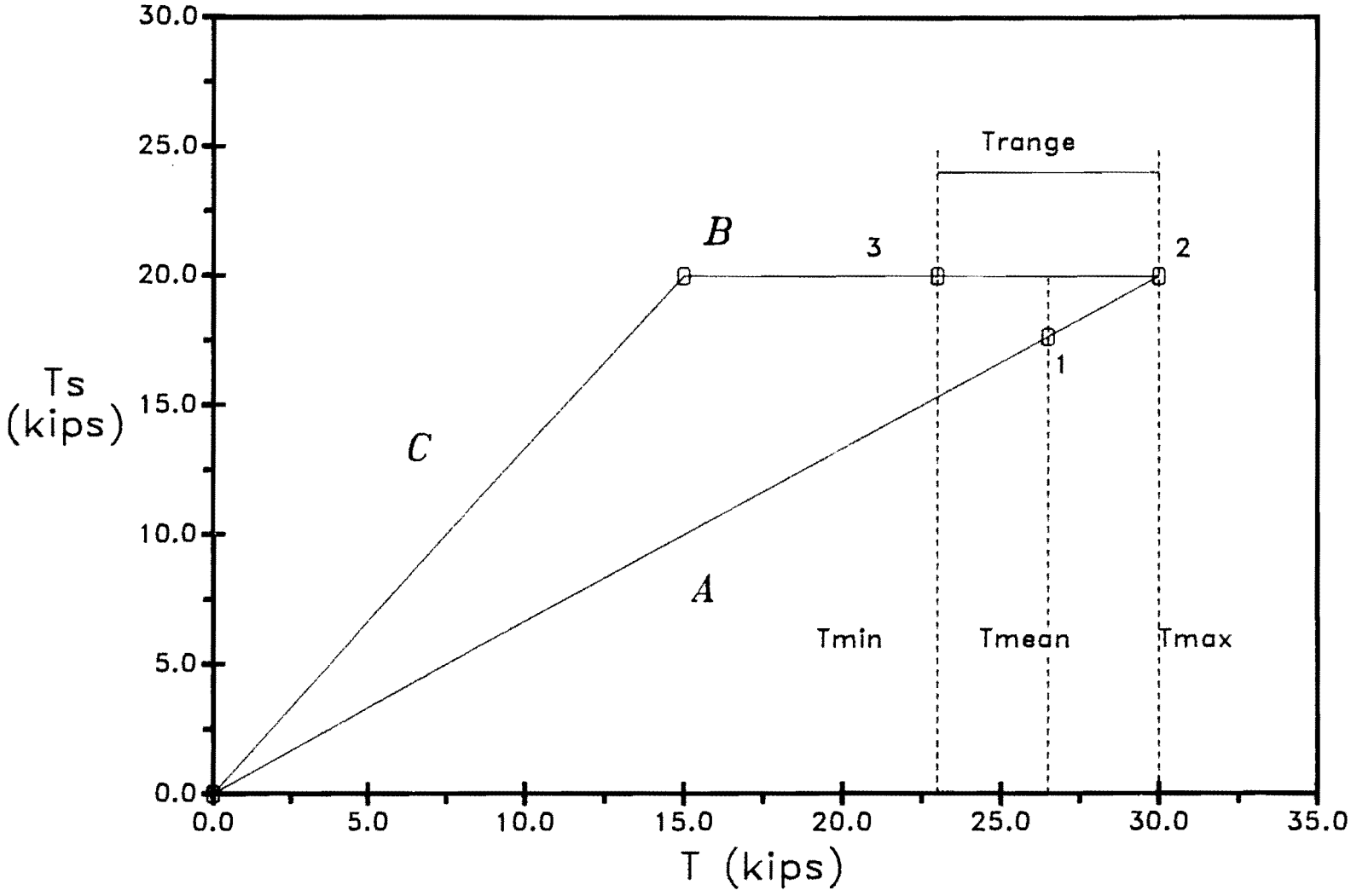

Fig. 5.23 Typical secondary grip load distribution curve showing fatigue test parameter

grips during cycling is illustrated in Fig. 5.24 for a few representative cycles. The variation in the strand tension over time is generalized as a "saw-tooth" function rather than the actual sinusoidal function. The various points ("1", "2", and "3") discussed in Fig. 5.23 are shown in Fig. 5.24 for reference. The secondary grip is not subjected to any dynamic load.

The similarities between the load distribution curves for each of the wedge types has allowed a general presentation of the load distribution behavior during fatigue testing. The variation of load during cycling was shown to occur only within the primary wedge. The portion of the strand contained within the secondary grip is not fatigued at all, but, rather held under a constant static load equal to the maximum value of T_S occurring during the initial loading phase. Since cyclic load never reaches the fatigue-sensitive secondary grip, it is necessary to concentrate efforts in improving the fatigue life only on the primary grip.

5.3 Finite Element Stress Analysis

The finite element stress analysis described in this section was performed using a general-purpose finite element program [28] which was donated to the University of Texas for research purposes. The purpose of the stress analysis was two-fold. The first goal was to obtain an idea of how the normal and frictional stresses were distributed along the strand within the gripped region. The "normal" stress will be defined as that component of the contact stress oriented perpendicular to the axis of the strand. The load distribution study presented in the previous section gave only the total frictional load transferred in the two grips. The results of those tests do not, therefore, offer any information as to how the that load is distributed along the strand.

The second goal of the finite element study was to study, analytically, geometric variables not tested experimentally. By comparing the experimentally obtained fatigue results with the results from the stress analysis and the other supporting tests, it should be possible to intelligently deduce the probable fatigue performance of anchorages composed of wedges of different geometries. The geometric variables studied were the interference angle of the exterior face of the wedge, and the thickness of the wedge material between the inner and outer surfaces. The thickness was characterized by the thickness at the narrow end of the wedge. The length of the wedge could also be varied, but, as will be shown, its effect would be minimal.

5.3.1 The Finite Element Model. The finite element model used in this analysis was composed of 110 axisymmetric elements. These element were divided into seven different sets. The element sets and the location of all of the elements are illustrated in Figs. 5.25 and

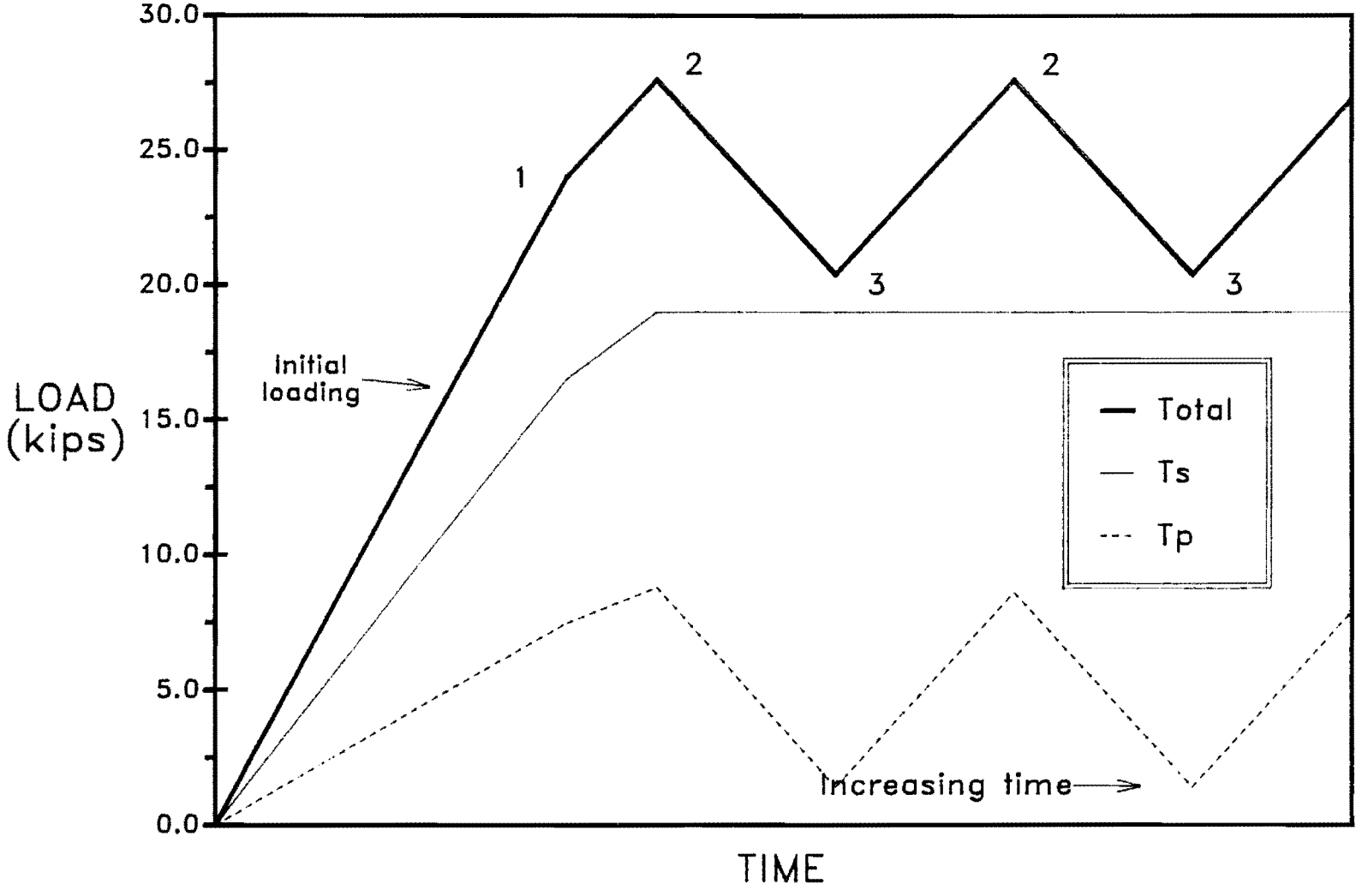

Fig. 5.24 Primary and secondary load distribution during fatigue testing (general case)

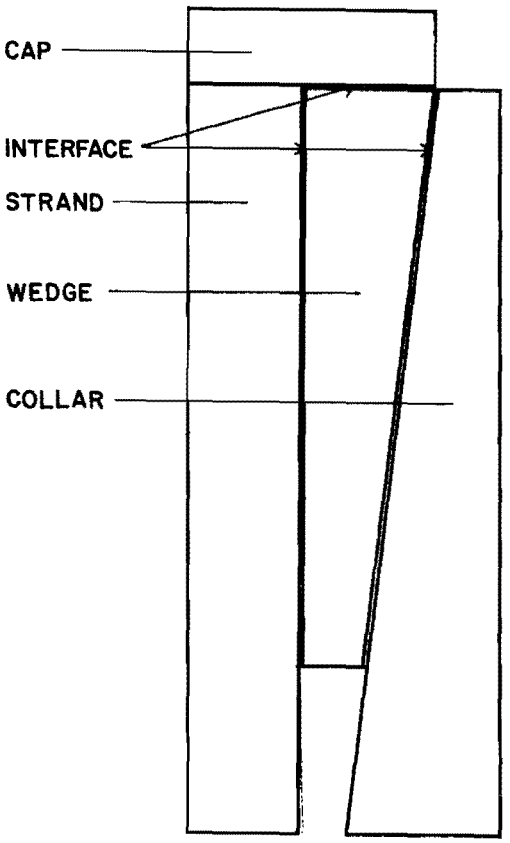

Fig. 5.25 Location of element sets in finite element model

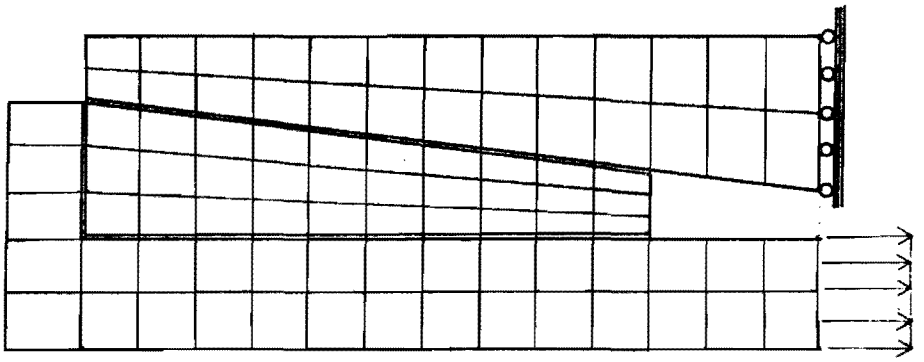

Fig. 5.26 Location of elements in finite element model

5.26. The first set was composed of twenty-six, eight-noded elements and was intended to model the behavior of the strand. Rather than modeling the seven individual wires and the helical twisting of the outer six wires, the strand was idealized as a "bar" with a constant radius of 0.5 in. The modulus of elasticity was specified as 29,000 ksi. and the bar was assumed to behave, in all respects, as linear-elastic.

The second element set modeled the wedge and was composed of thirty, eight-noded elements. The modulus of elasticity was set at 10,000 ksi for those analyses in which the geometry varied. Two other analyses were made in which the modulus of elasticity was specified as 30,000 ksi and 50,000 ksi. These two studies were intended to study the effect of the material stiffness on the stress distribution. The wedge geometry was similar to that tested experimentally. The surface of the wedge was assumed to be smooth. Again, the behavior of the wedge was assumed to be linear-elastic.

The collar or restraining tension ring was simulated with twenty-six eight-noded elements. The modulus of elasticity was specified as 29,000 ksi and remained constant throughout the various analyses. Linear-elastic behavior was assumed. It was necessary to modify the geometry in some of the analyses due to the increased diameter of the wedge (resulting from changes in the interference angle and the tip thickness).

A "cap" was modeled with five eight-noded elements and was attached to the top of the strand. The cap simulated, in effect, the existence of the secondary grip. The purpose of the cap, like the secondary grip, was to push the primary wedge group into the collar, thus inducing wedging action, upon application of tension in the strand. The modulus of the cap elements was set at 290,000 ksi to produce a high flexural rigidity to simulate the secondary grip. Linear-elastic behavior was assumed.

The final three element sets were not composed of the typical eight-noded elements employed in the other four sets. "Interface" elements were used to model the three interfaces existing in the model. The first interface was that lying between the strand and the wedge elements. As interface elements are not of the stress-displacement type and, consequently, do not have stiffness properties, no modulus of elasticity is given for this set or the other two interface sets. The contact stresses are output at locations lying between corresponding nodes on either surface. The interface elements themselves, are defined with six nodes- three from each of the contacting surfaces.

The remaining two sets of interface elements are between the collar and wedge, and the cap and wedge. The wedge is, thus, surrounded on all three sides with interface elements. A stress of

159.4 ksi was applied to the lower strand elements, which simulated the effect of a uniform tensile stress in the strand. The magnitude of the stress was chosen so that the total tensile force in the analytical model was equal to that found in the experimental tests.

5.3.2 Results of Stress Analysis. The two finite element studies conducted for this research program included a study designed to determine the effect of the modulus of elasticity of the wedge material on the stress distribution. The wedge in that study was modeled with geometric properties similar to those of the wedges tested experimentally. The second study was designed to investigate the effect of two of the geometric variables, thickness of the wedge at the narrow end and the angle between the outer surface and the inner surface.

To study the effect of the modulus of elasticity, three separate stress analyses were performed, each with a different modulus for the wedge elements. The three values of modulus tested were: E_1 = 10,000, E_2 = 30,000, and E_3 = 50,000 ksi. All other factors remained constant. The distribution of the normal stress along the length of the strand is given in Fig. 5.27. In all three cases the magnitude of the contact stress and, therefore, the frictional stress is greatest at a value of X equal to zero which corresponds to the location where the strand enters the primary wedge group. This peak stress is seen to increase with increasing modulus.

The second series of stress analyses was performed with a constant wedge modulus of 10,000 ksi. To study the effect of geometry, nine separate analyses were conducted. For each of three different values of the angle parameter, three different values of thickness were tested. The angle between the interior and exterior surfaces was given values of three, seven, and ten degrees. The angle between the interior and exterior surfaces of the wedges actually tested in the laboratory was seven degrees. For each of these values of the angle, three values of tip thickness were tested: t_1 = 0.15 in., t_2 = 0.30 in., and t_3 = 0.50 in. The wedges tested experimentally were fabricated with a tip thickness of 0.15 in.

The graphs showing the various stress distributions will be presented twice. Each of the three graphs of the first series are labeled with the value of the angle and contain the stress distributions resulting from a combination of that angle and the three values of tip thickness. These three graphs are presented in Figs. 5.28, 5.29, and 5.30. The general form of the stress distribution in each of these graphs is similar to those presented earlier. The peak stress occurs at the entrance of the primary wedge group. It can also be seen that for any value of the angle, the stress tends to increase with decreasing tip thickness.

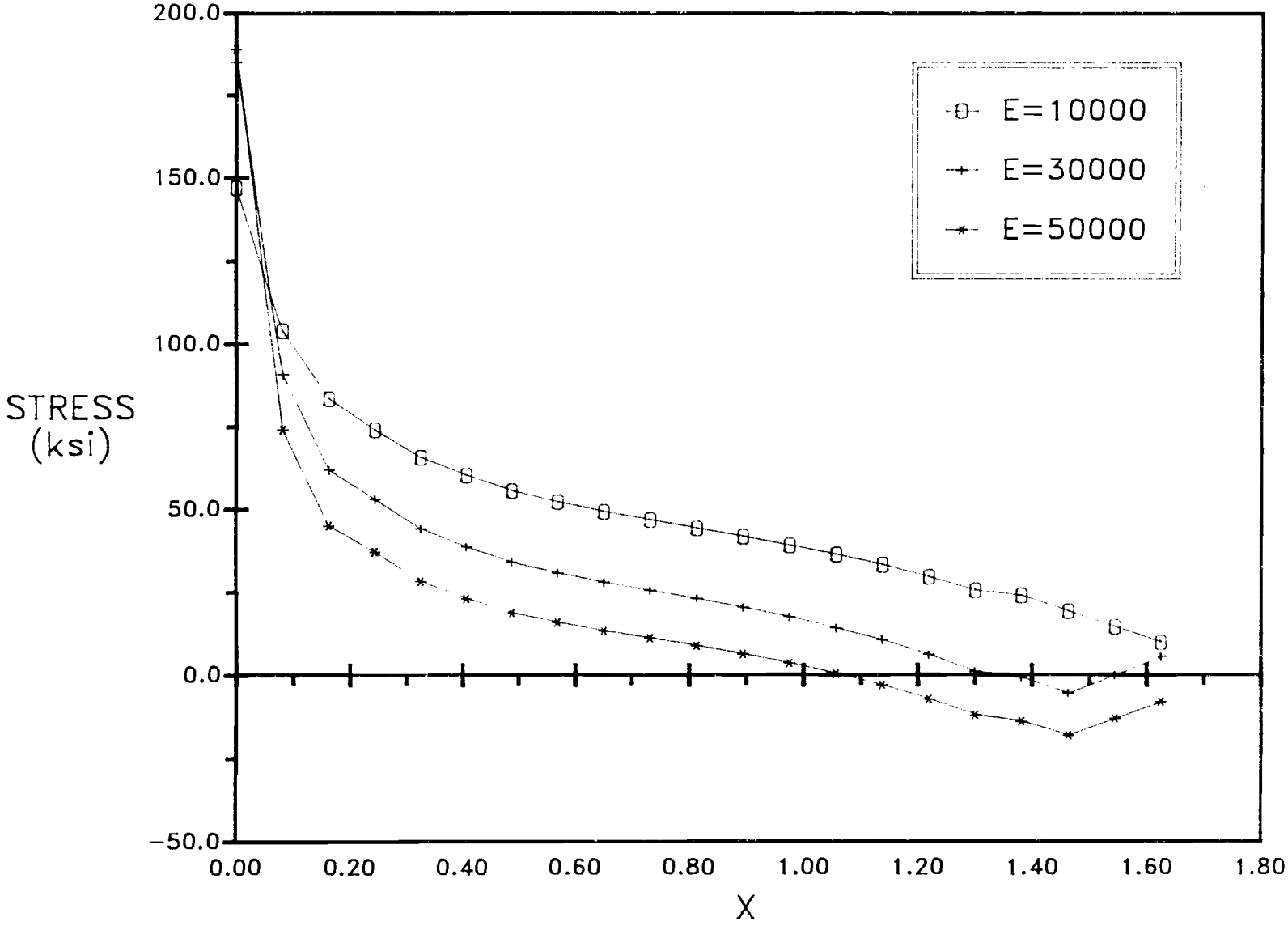

Fig. 5.27 Effect of primary wedge modulus on normal contact stress distribution

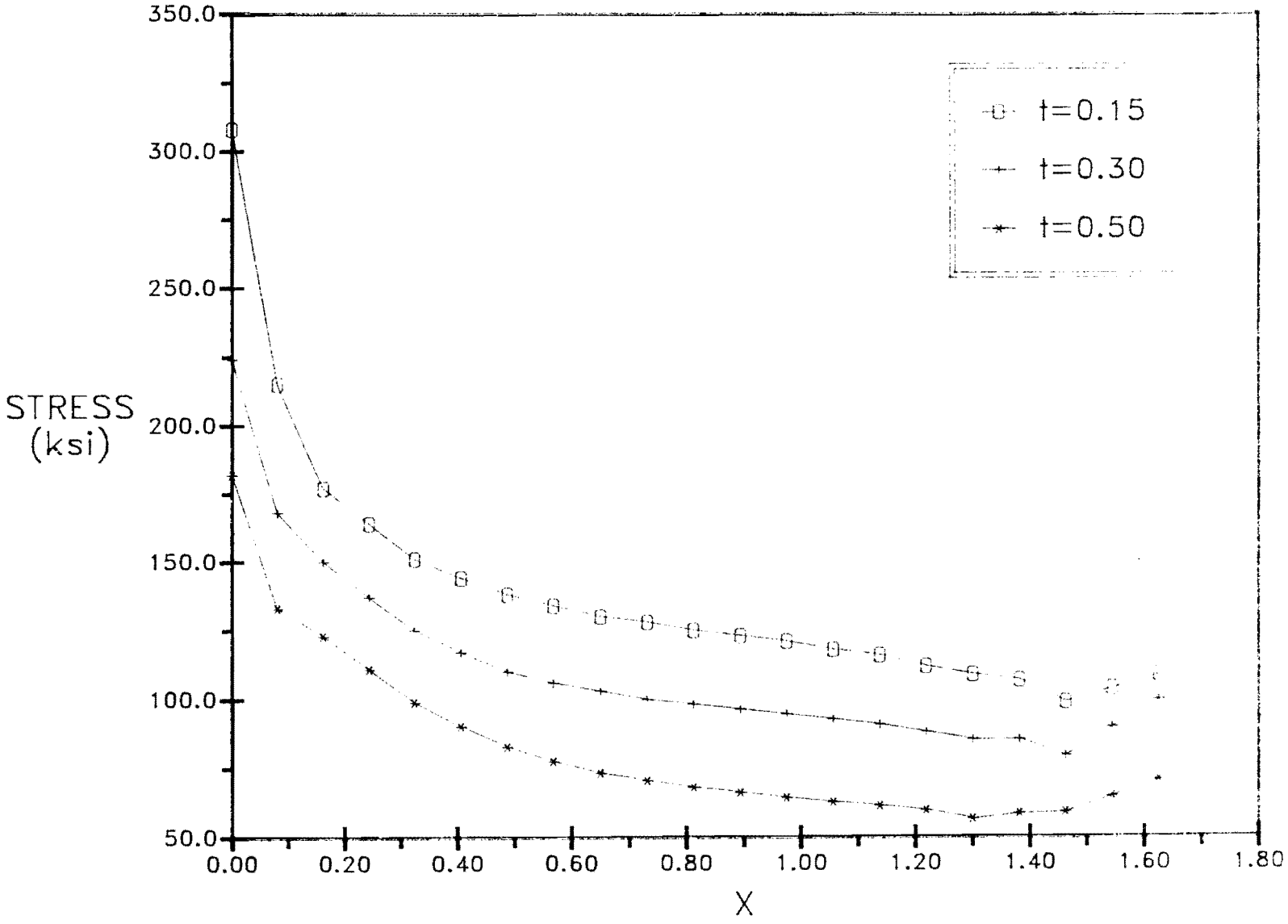

Fig. 5.28 Effect of variation in tip thickness for interference angle = 3^{o}

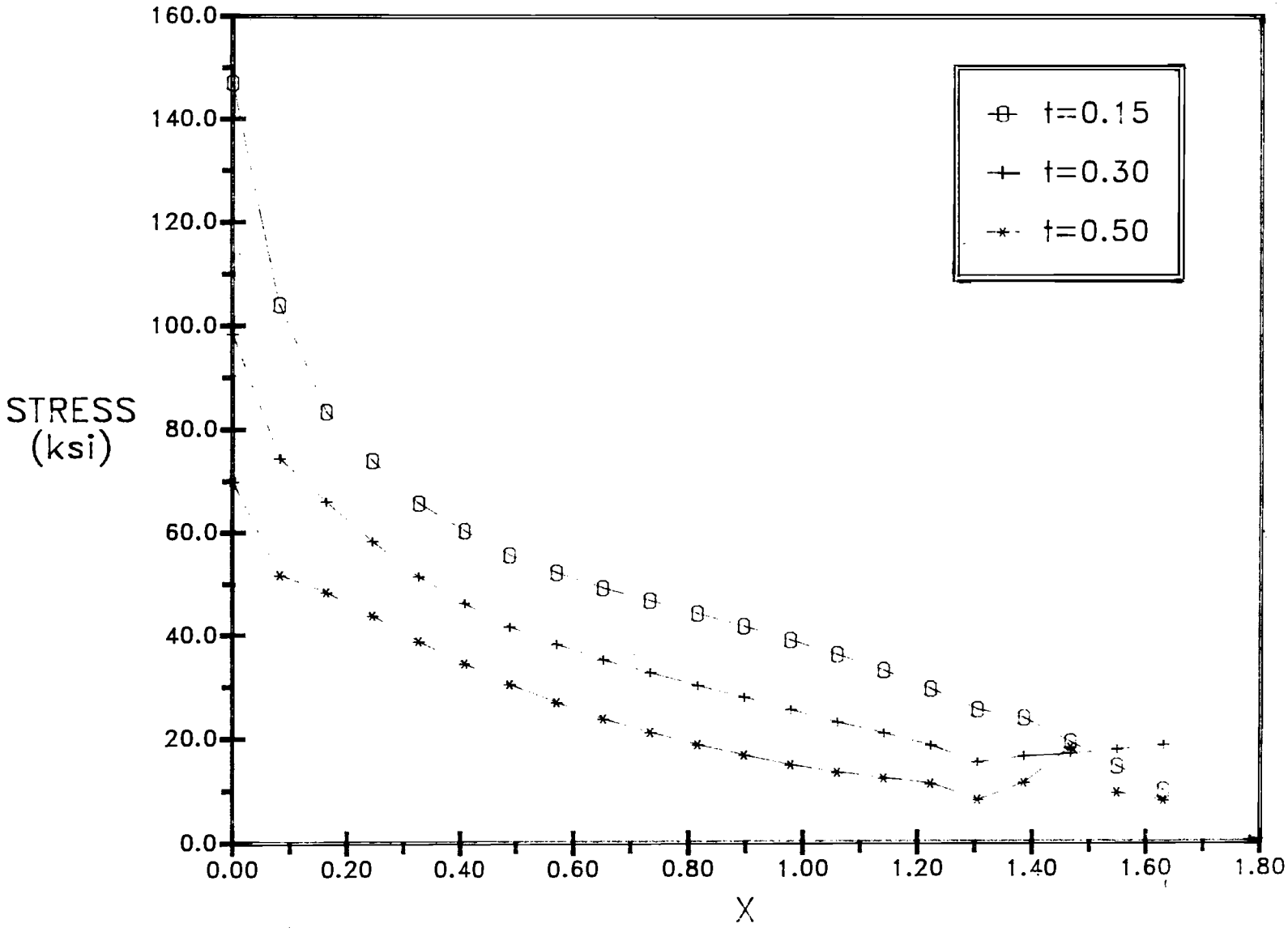

Fig. 5.29 Effect of variation in tip thickness for interference angle = 7^{o}

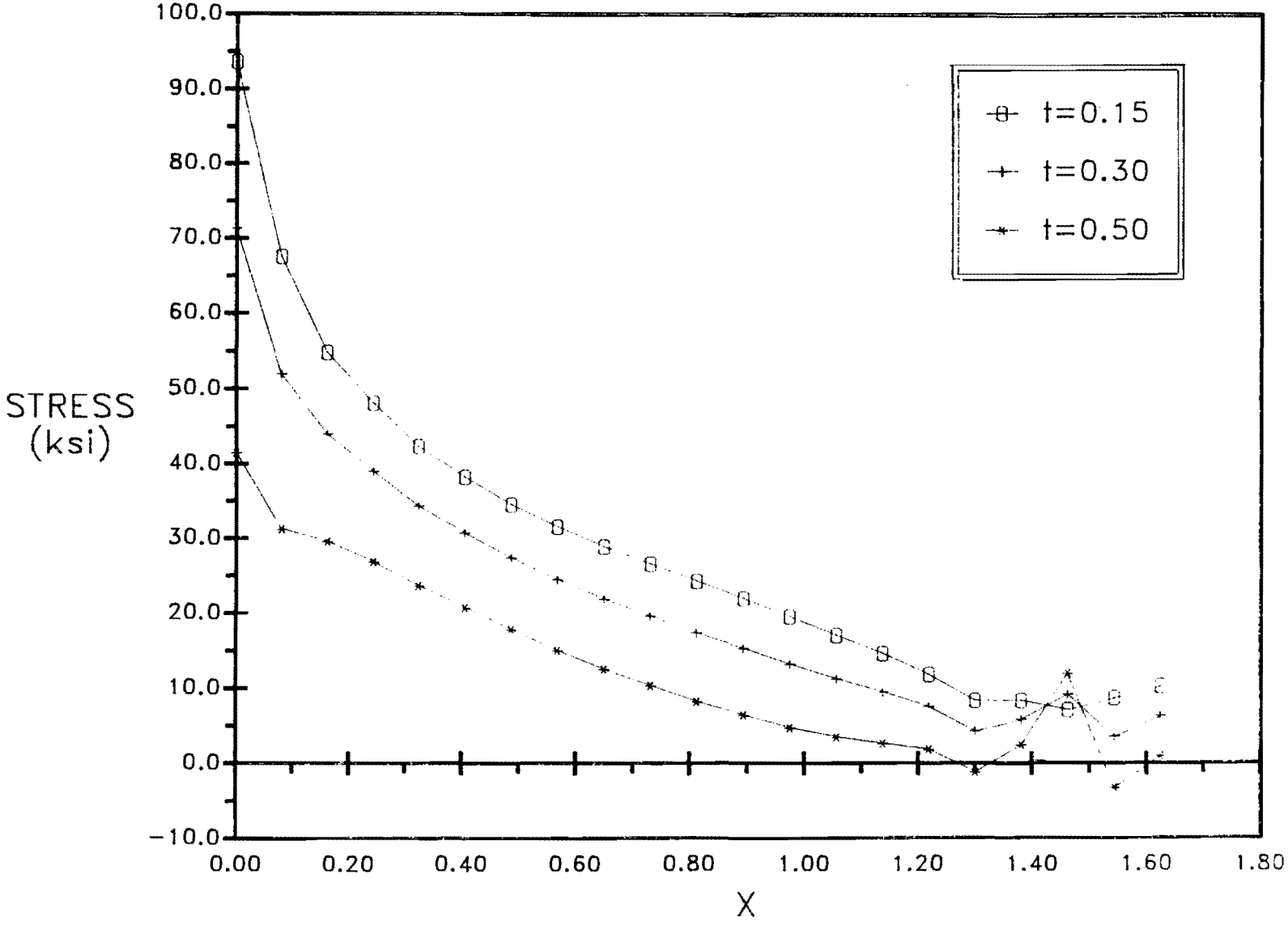

Fig. 5.30 Effect of variation in tip thickness for interference angle = 10^{o}

These graphs are presented again in Figs. 5.31, 5.32, and 5.33. This series of presentations is based upon a constant value of tip thickness. The stress distributions resulting from different values of the angle are plotted in each of the three graphs. In general, the peak stress is shown to decrease with increasing values of the angle.

The finite element model and resulting stress distributions have been presented in this section. Large peak stresses were shown to develop at the entrance into the primary wedge group. The location of the peak stress was also shown to be independent of the material and geometric variables selected for this analysis. While the location remained constant, the magnitude of the peak stress was shown to vary with different material and geometric variables. The stress distributions were presented twice to simplify visual comparisons between the two different geometric variables. The significance and implications of these analyses are presented in the next subsection.

5.3.3 Effect of Geometric and Material Variables. Since fatigue failures in the anchorage region consistently occur at the base of the primary wedge group, the resulting contact stresses resulting from the geometric and material variables presented earlier will be discussed only at that location.

The effect of wedge material stiffness will be discussed first. The modulus of elasticity was varied from 10,000 to 50,000 ksi. The effect of this variation on the peak stress is illustrated in Fig. 5.34 and tabulated in Table 5.4.

TABLE 5.4 PEAK STRESS VS. MODULUS

Modulus (ksi)	Peak Stress (ksi)
50,000	189.0
30,000	185.0
10,000	147.0

It can be seen from the graph that the modulus of elasticity can have a significant effect on the maximum stress. The effect is less pronounced for changes in the wedge modulus above that of the surrounding strand and collar (29,000 ksi).

The geometric variables can also have a significant effect on the peak stress. The peak stress results are given in Table 5.5 for each of the combinations of tip thickness and angle tested.

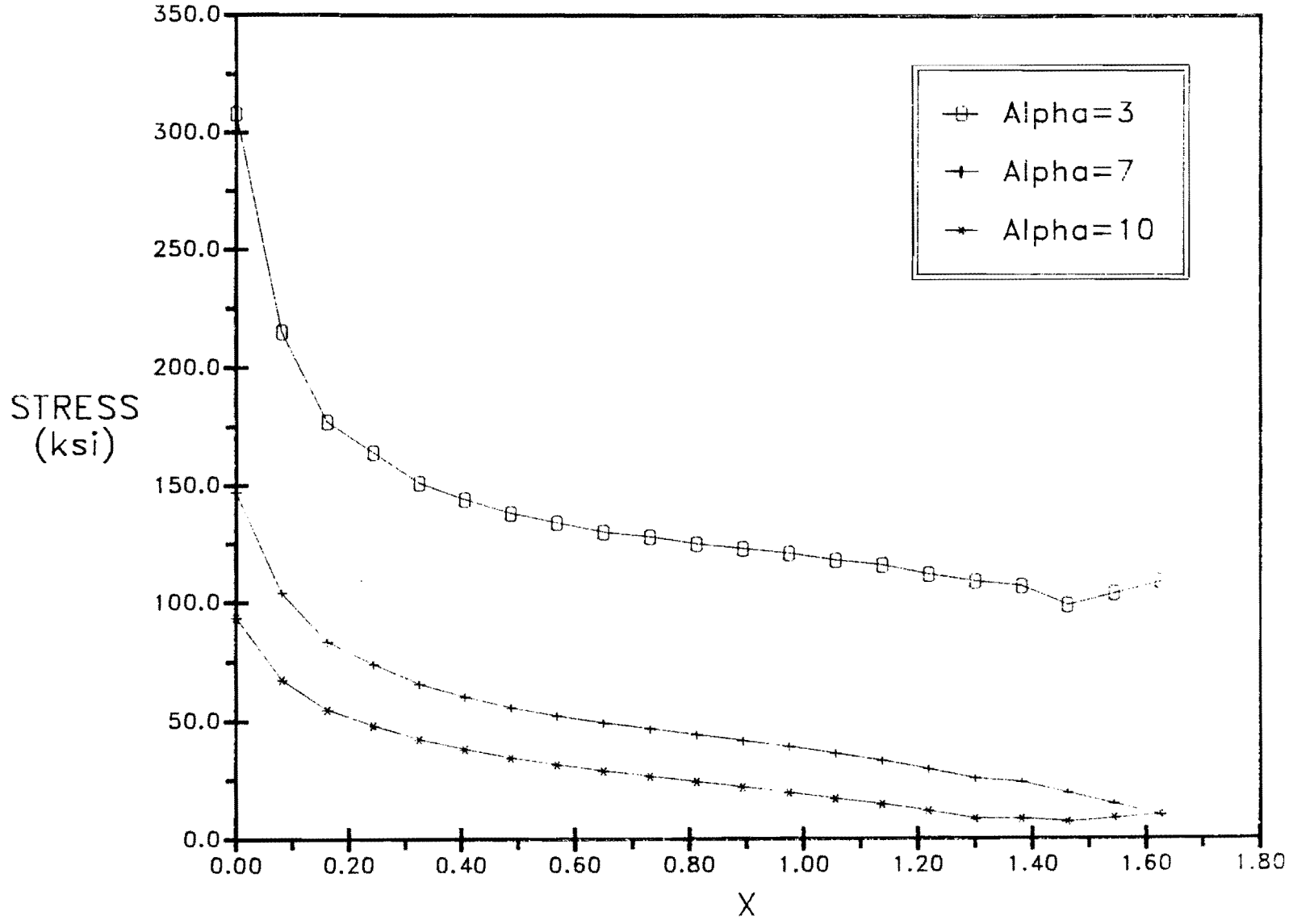

Fig. 5.31 Effect of variation in interference angle for tip thickness = 0.15"

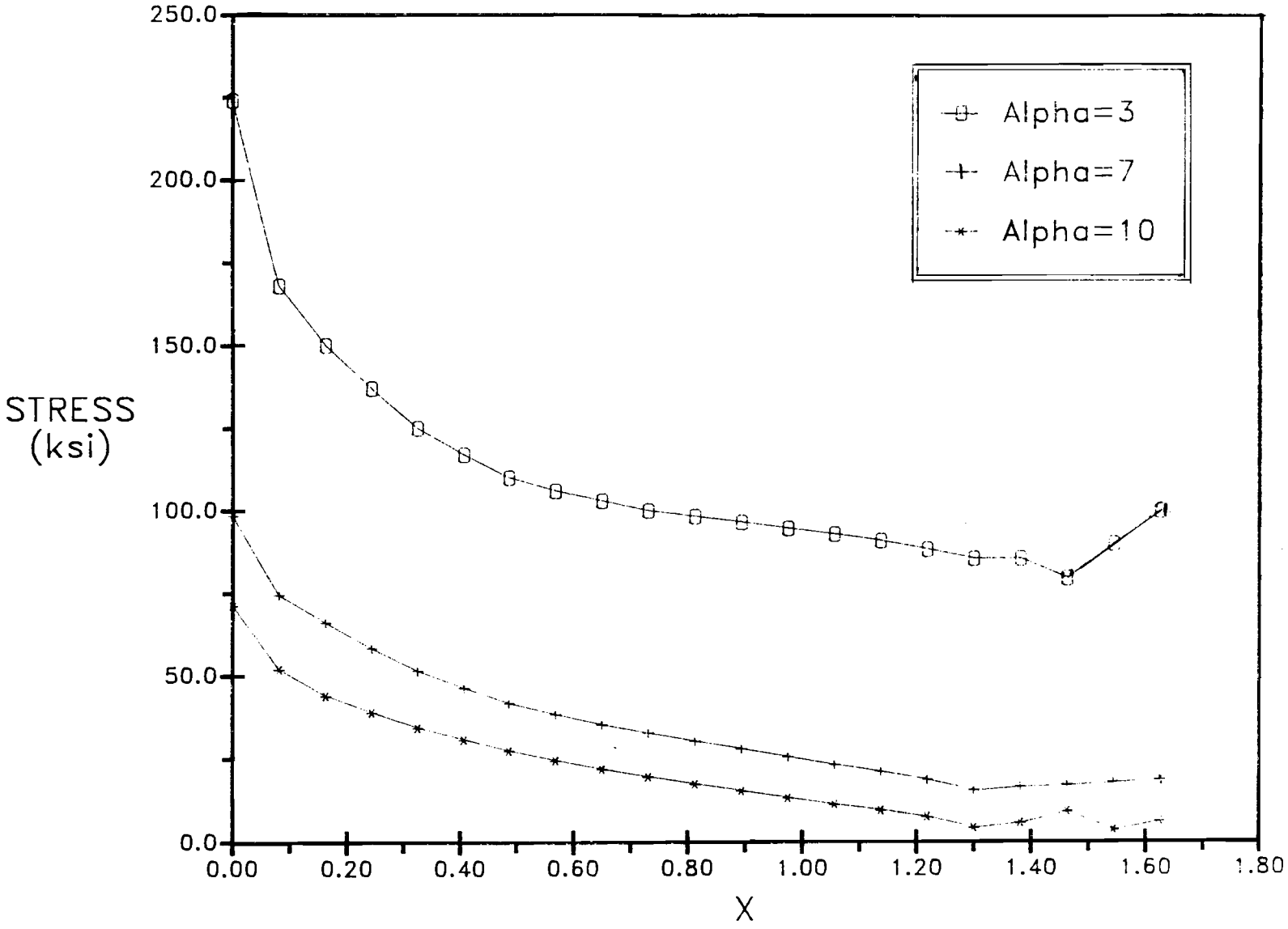

Fig. 5.32 Effect of variation in interference angle for tip thickness = 0.30"

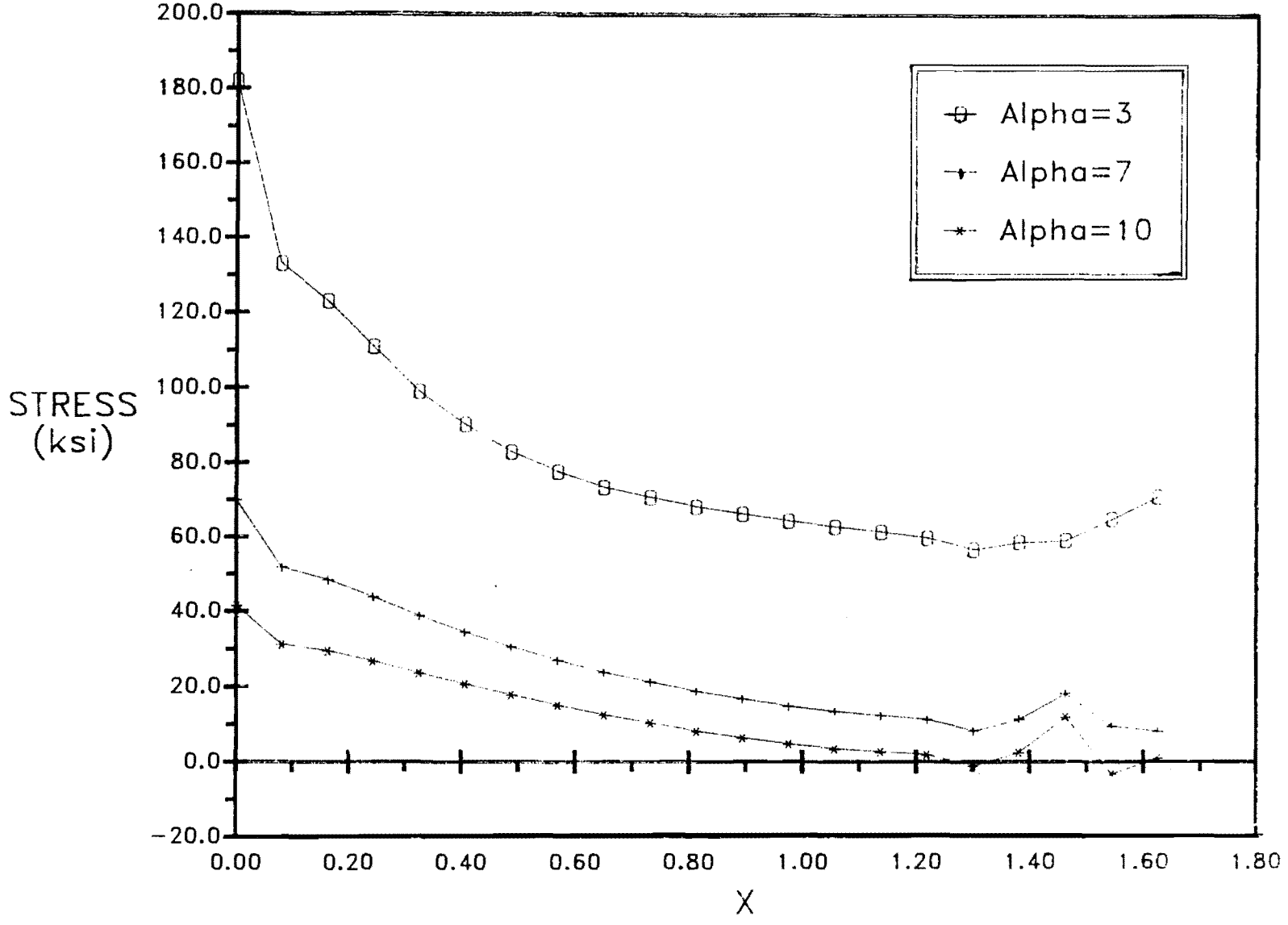

Fig. 5.33 Effect of variation in interference angle for tip thickness = 0.50"

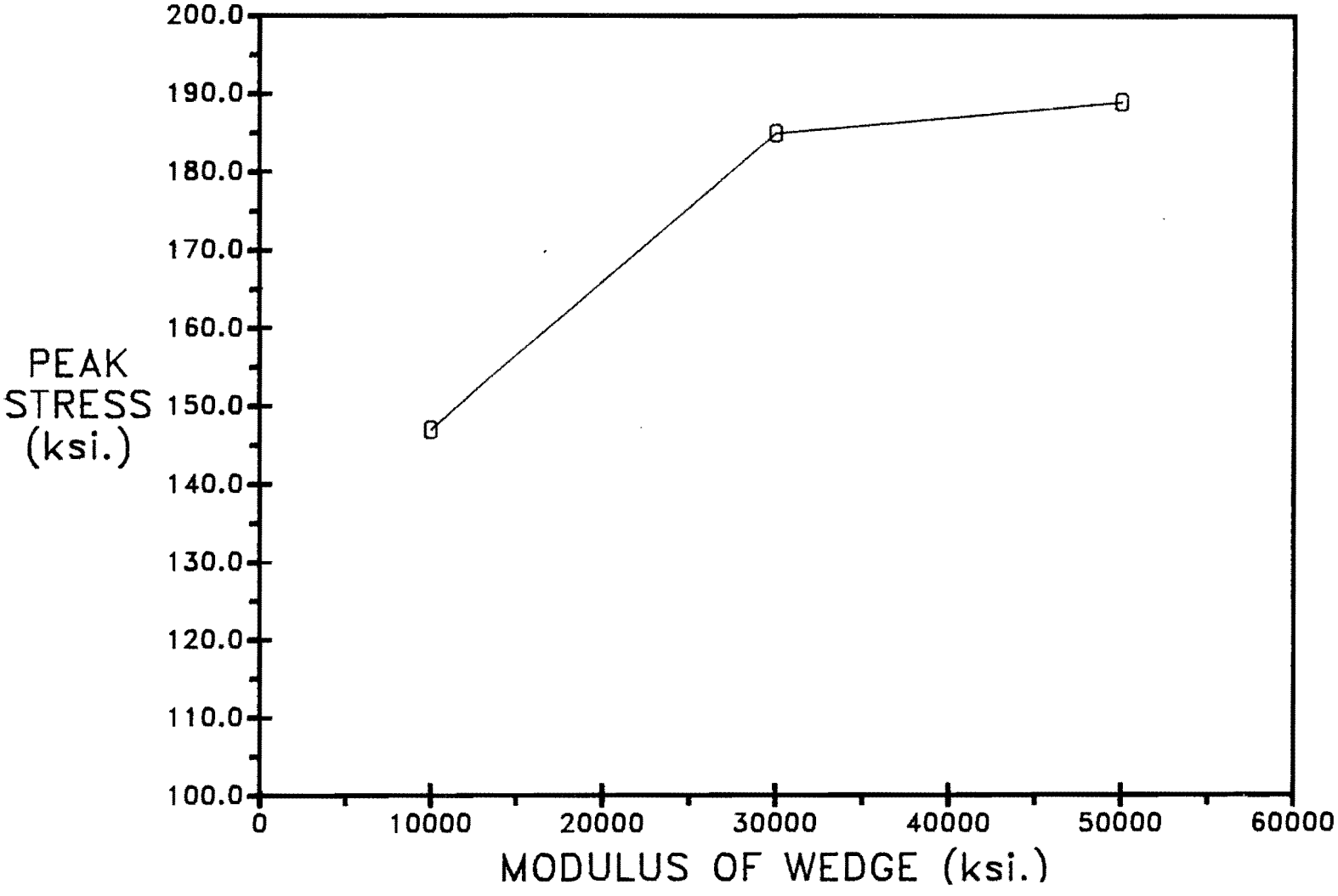

Fig. 5.34 Effect of primary wedge modulus on peak stress

TABLE 5.5 PEAK STRESS VS. GEOMETRY

Thickness	Angle (Deg.)	Peak Stress
0.15"	3.0	308.0
	7.0	147.0
	10.0	94.0
0.30"	3.0	224.0
	7.0	98.0
	10.0	71.0
0.50"	3.0	182.0
	7.0	70.0
	10.0	42.0

The effect of changes in the tip thickness is shown in Fig. 5.35. The three lines in the graph represent results from the different angles. For any given angle between the outer and inner surfaces any increase in the tip thickness produces a decrease in the maximum contact stress. Furthermore, the variation in stress with tip thickness is essentially linear.

The results of Fig. 5.35 are presented again in Fig. 5.36. This time however, the angle is varied while lines of constant tip thickness are shown in the graph. In general, for a given tip thickness, the contact stress is shown to decrease with increasing angles. The difference in peak stress is less significant for increases in the angle above seven degrees.

The length of the wedge group was not considered as a variable since the anchorage fatigue failures consistently occurred at the lead-in section. Also, the contact stress distribution is essentially constant along the length of the primary wedge after the first eighth of the wedge/strand contact region. Any change in length would thus have no effect.

An increase in tip thickness or a decrease in modulus of the wedge material results in a lower stiffness wedge. Any change in geometry or material resulting in an increased wedge stiffness was shown to lead to an increase in the peak stress at the lead-in section of the primary wedge group. Changes in the wedge modulus above the modulus of the surrounding strand and collar produced little change in the peak stress. The change in peak stress was also shown to be small for angles greater than seven degrees.

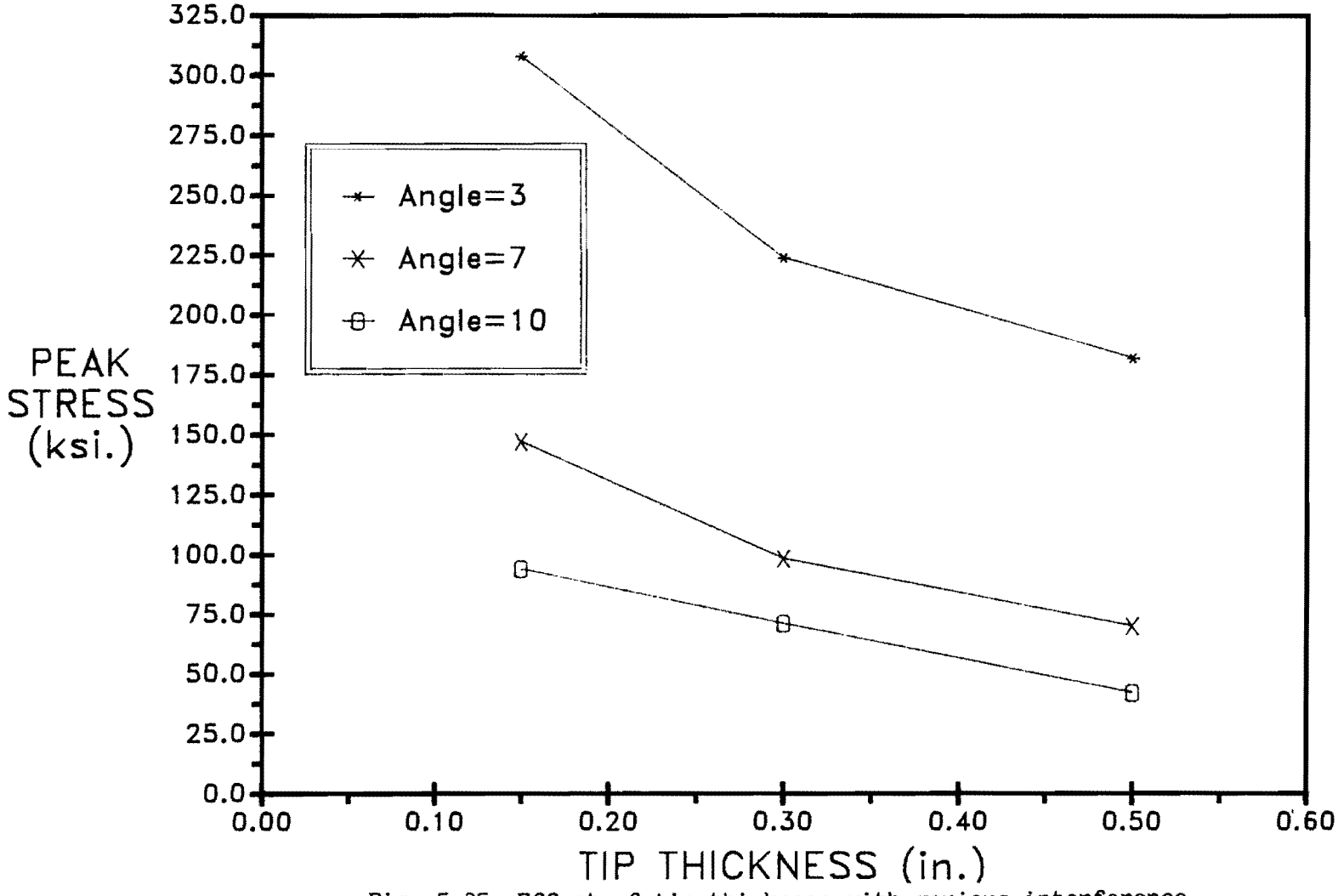

Fig. 5.35 Effect of tip thickness with various interference angles on peak stress

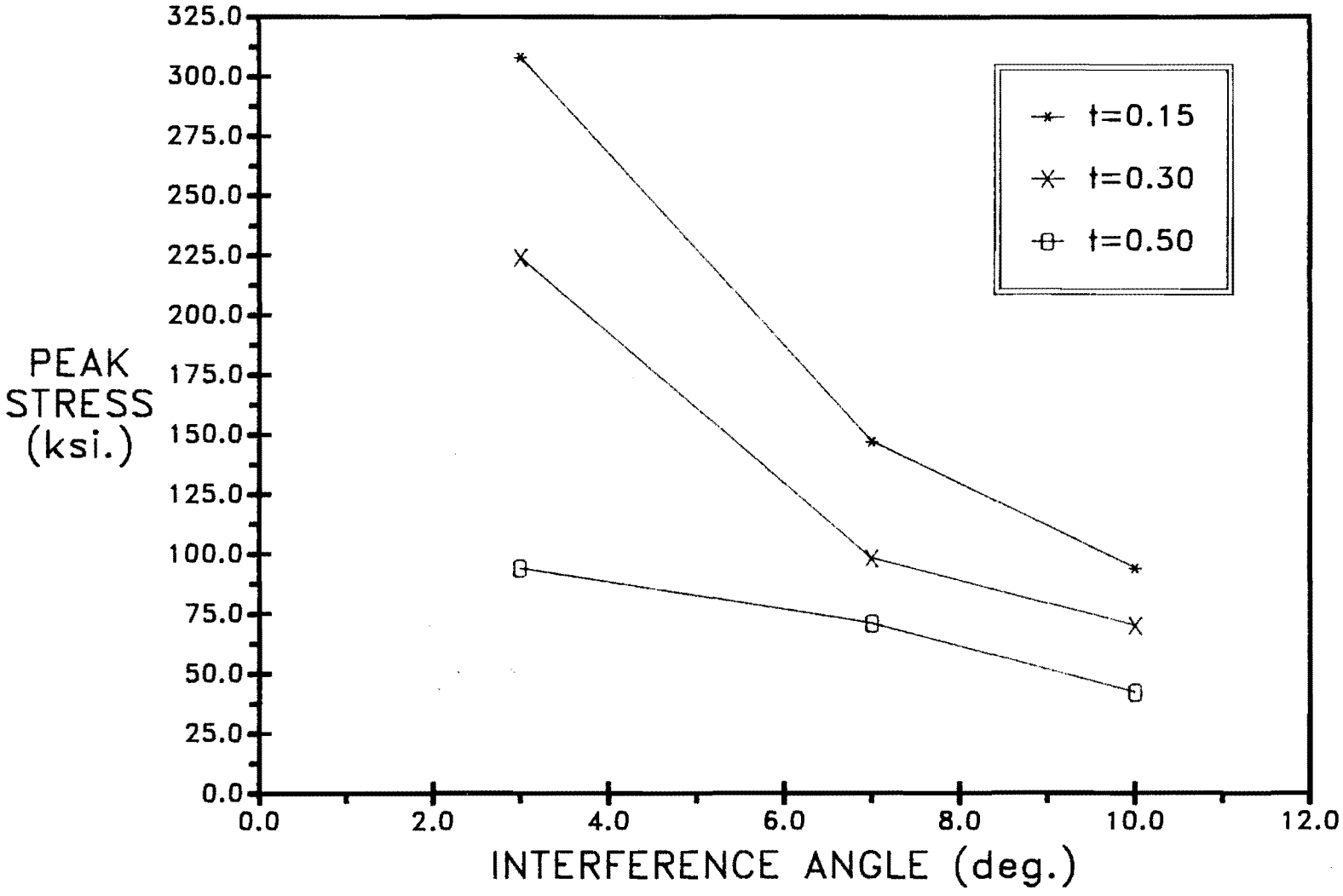

Fig. 5.36 Effect of interference angle with various tip thicknesses on peak stress

5.3.4 Effect of Load Distribution. Another relationship not discussed in the previous subsection is that between the load distribution and the stress distribution within the primary grip. The tensile load applied to the strand elements in the finite element model was constant throughout the study and set equal to a load of 30 kips. Since no frictional stresses developed during the application of the load none of the tensile load was transferred by the primary grip. This situation corresponds to a load distribution ratio of zero. All of the load distribution ratios measured in the laboratory were found to be greater than zero however. Increases in the load distribution ratio above zero affect both the normal and the frictional stress distributions. The effect of the load distribution ratio on the latter is most obvious and will be discussed first.

An increase in the load distribution ratio is defined as an increase in the load transferred by the primary grip for a given total tension in the strand. An increase in the load distribution ratio therefore implies an increase in the magnitude of the frictional stresses along the length of contact between the strand and the primary wedge group.

The effect of the load distribution ratio on the normal stress distribution is not as clear since no measurements directly illustrate the relationship. An increase in the load distribution ratio of an anchorage and the resulting increase in the frictional stress distribution would require an increase in the normal stress along the length of contact as well. Load distribution ratios greater than zero would lead to a frictional stress distribution of the same form as that of the normal contact stress. As the primary grip carries more of the applied load (large LDR), the frictional and normal stresses would increase to provide the required resistance.

5.3.5 Effect of Assumptions in F.E. Model. The actual grip assembly is very complex. It was beyond the scope of the finite element study performed for this research program to attempt to model the exact behavior of the grip assembly. A broad understanding of the stress distribution along the surface of that part of the strand in contact with the primary grip was the goal. Several assumptions were necessary to achieve a simple and workable model. Assumptions were made in modeling the geometry and the material behavior. Some assumptions are also required in the analysis of the results. These assumptions and their effect are described in this subsection.

The strand itself was modeled as a smooth "bar" with a radius of 0.25 in. The actual strand has a complex geometry consisting of seven individual wires six of which are wrapped helically around a center wire. This assumption would tend to underestimate the actual contact stresses as the area of contact is larger in the finite element model.

Some approximations were also required for the wedge. First, the inner surfaces of the wedges were assumed to be smooth in the finite element model. The actual surface was initially serrated. Modeling the surface as smooth would tend to underestimate the stress at the interface. High local stress would develop at the tips of the serrations. This approximation in conjunction with that made in modeling the strand would tend to result in low values of contact stress.

In addition to the approximations made in modeling the inner surface of the wedges, the three-part wedge group was modeled as a single axisymmetric unit. This assumption would also tend to underestimate the contact stresses. Modeling the wedges as an axisymmetric unit creates artificial tangential stiffness which does not exist in the actual three-part wedges. Application of compressive normal stresses on the outer surface of the wedge group in the finite element model is reacted in part by compressive hoop stress in the axisymmetric wedge. The remainder of the applied compressive normal stress is resisted through normal contact stress on the inner surface of the wedge. The actual wedges, on the other hand, do not come into contact with one another and, hence, do not have any tangential stiffness. The absence of tangential stiffness forces any compressive stress applied to the outer surface to be fully reacted through normal contact stress on the inner surface.

An approximation in material behavior was also required to simplify the analysis. Each of the materials was assumed to behave elastically throughout the loading process. While this assumption is reasonable for the collar and strand elements since no plastic deformation was observed in practice, it is obviously incorrect for the wedge elements. The inaccuracy increases with decreasing yield stress. The effect of this assumption is difficult to judge. Were plasticity modeled in the study, redistribution of peak stresses would initially lead to a more uniform stress distribution along the strand. However, upon further application of normal stress, confinement of the wedge material would not allow for further redistribution and the contact stress would tend to increase above the plastic limit. It is reasonable to assume any beneficial effects of stress redistribution to be negligible when compared to the sum of the detrimental effects of the other assumptions. For the purposes of this discussion a "beneficial" effect would lead to an actual contact stress distribution of lower magnitude than that predicted by the model. A "detrimental" effect would produce actual magnitudes of contact stress higher than those calculated.

The actual magnitudes of contact stress are as important as the distribution of stress along the strand. The assumptions described above would not significantly affect the general distribution of the contact stress. It is reasonable to assume that large peak stresses

forming at the base of the primary grip result naturally from this configuration.

Much has been written concerning the contact stresses while little discussion has been devoted to the frictional stresses known to exist (from load distribution tests) along the strand. It will be assumed that the friction shear stresses developed during the loading process are linearly related to the contact stresses by a constant (the coefficient of friction). If this assumption is made, the resulting friction stress distribution is similar in form to the contact stress distribution. The largest surface shear stresses from the friction form at base of the primary grip and decrease along the strand.

The effects of the various assumptions on the stress distribution were that the calculated normal stresses are expected to be less than those actually existing along the strand. The maximum normal and friction shear stresses will occur at the location where the strand enters into the primary wedge group. This is important in light of the fact that all of the fatigue failures occurring in the anchorage zone also occurred at the point where the strand enters the primary wedge group (Chapter 6).

CHAPTER 6

INFLUENCE OF GRIP BEHAVIOR ON FATIGUE LIFE

The dependency of the fatigue life of the test specimens on the grip characteristics presented in the previous chapter will be presented. It will be shown that the fatigue life of the individual prestressing strands is influenced to a great extent by the anchorage used in the test.

The fatigue test results will be presented and discussed first. The location of grip failures will be shown to be very consistent from one specimen to another. A discussion of the scanning electron fractography will be presented to allow a more detailed study of the failure zone. Finally a complete synthesis of all of the independent investigations will be presented including the controlling crack initiation mechanism.

6.1 Presentation And Discussion of Fatigue Test Result

The results of the various fatigue tests will be presented and discussed in this section. The first subsection will be devoted to the tests performed with the double-grip anchorage on the 0.5" and 0.6" diameter strands. The tests performed with single commercial grip will be discussed in the second subsection. The tests performed on the prenotched strand will also be discussed in the second subsection.

6.1.1 Dual-Grip Fatigue Tests. The tests performed with the 0.5" diameter strand will be presented first. The fatigue test results obtained with the steel, aluminum, and copper primary grips are presented in Tables 6.1, 6.2, and 6.3, respectively. S_R in the table is the stress range in ksi and S_{MIN} is the minimum stress level in ksi. These data are plotted in the Wohler Diagram of Fig. 6.1 along with the regression line obtained for this strand from reference [16].

TABLE 6.1 STEEL WEDGE RESULTS

S_R	S_{MIN}	Life
47.2[1]	157.7	87,290
47.2	157.7	59,700
47.2	157.7	53,430
33.8[1]	157.7	390,060
33.8	157.7	193,380
27.0[1]	157.7	2,873,960
27.0	157.7	450,230

[1]Test conducted with predeformed wedges.

TABLE 6.2 ALUMINUM WEDGE RESULTS

S_R	S_{MIN}	Life
47.2	157.7	157,640
47.2	157.7	143,900
47.2	157.7	135,870
47.2	157.7	83,230
47.2	157,7	79,620
47.2	157.7	79,610
33.8[1,2]	157.7	2,685,980
33.8	157.7	684,840
27.0	157.7	1,107,460

[1]Test conducted with predeformed wedges.
[2]Failure occurred in strand.

TABLE 6.3 COPPER WEDGE RESULTS

S_R	S_{MIN}	Life
47.2[1,2]	157.7	255,380
47.2[2]	157.7	232,830
33.8[1,2]	157.7	1,337,300
33.8	157.7	942,720
27.0[1,3]	157.7	10,342,540
27.0	157.7	3,327,150

[1]Test conducted with predeformed wedges.
[2]Failure occurred in strand.
[3]No failure. 10^7 cycles defined as a runout.

All of the fatigue tests which resulted in a failure in an anchorage zone failed at the lead-in section. The fatigue tests conducted with copper wedges serving as the primary wedge group resulted in the best performance. None of the tests performed with the pre-deformed copper wedges produced failures within the anchorage region. The test run at the 27.0 ksi stress range with the predeformed copper wedges was stopped at ten million cycles before any failure occurred.

The fatigue lives obtained with the predeformed copper wedges at the 33.8 and 47.2 ksi stress ranges will be used as a base for comparison of the results obtained with the other wedges. These fatigue lives represent the maximum lives obtainable at the corresponding stress ranges. It should be noted, however, that results from fatigue tests always contain a random component and no one fatigue life corresponds exactly to one stress range. Furthermore, the variation in fatigue life at a given stress range tends to increase with decreasing stress range becoming infinite at the endurance limit of the fatigue specimen.

Despite the uncertainty inherent in fatigue test results, some important observations can be made from the data. The effect of the various wedges types on the fatigue strength of the strand within the grip region can be seen in the bar graph of Fig. 6.2. The effect of the undeformed and pre-deformed wedges is measured as a percentage of the maximum obtainable fatigue life at 47.2 ksi stress range in the graph of Fig. 6.2. The values on the vertical axis were calculated by dividing the fatigue life (or average with replicates) by the fatigue life resulting from the predeformed copper wedges and multiplying by

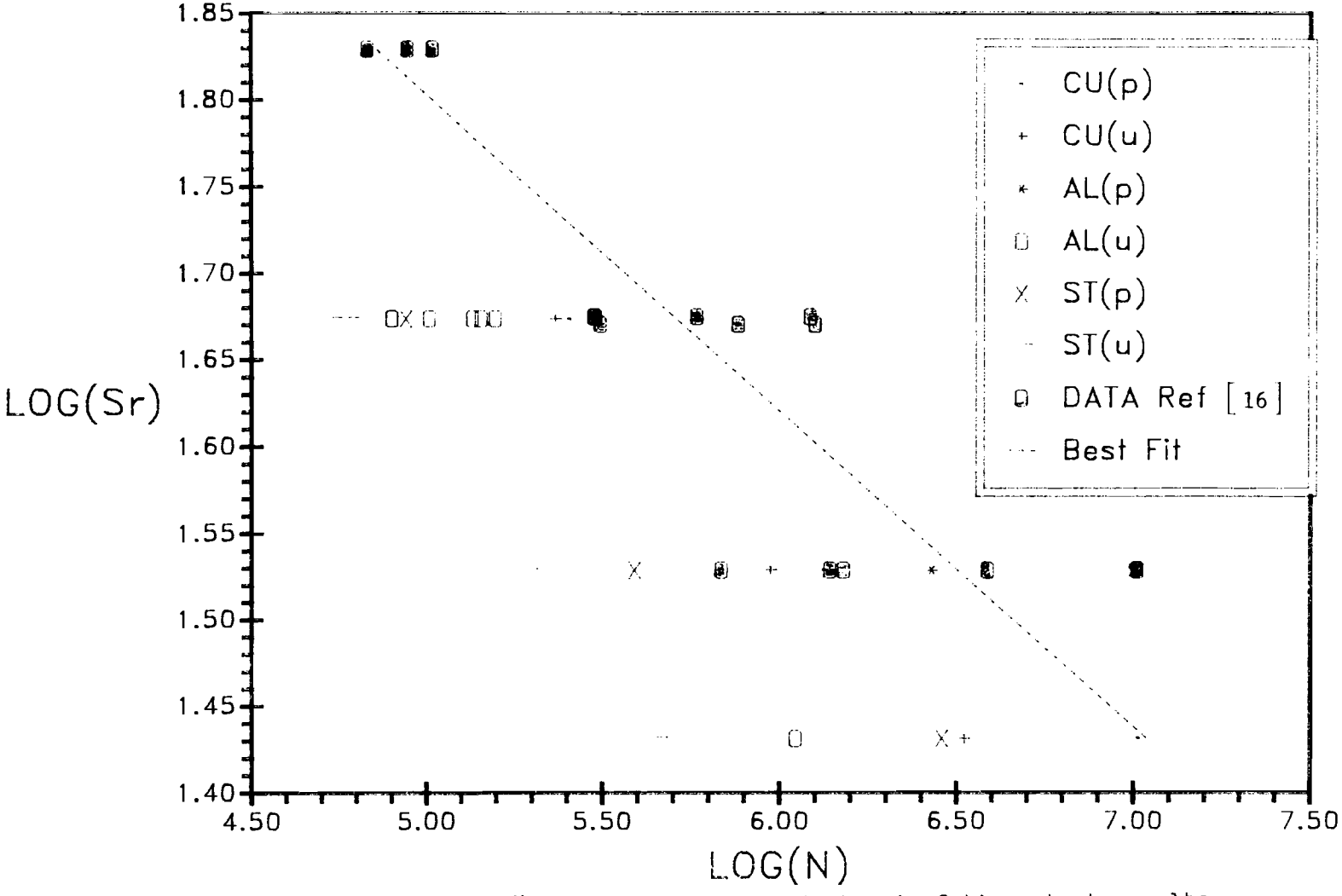

Fig. 6.1 Wöhler diagram of all dual-grip fatigue test results for 0.5" diameter strand

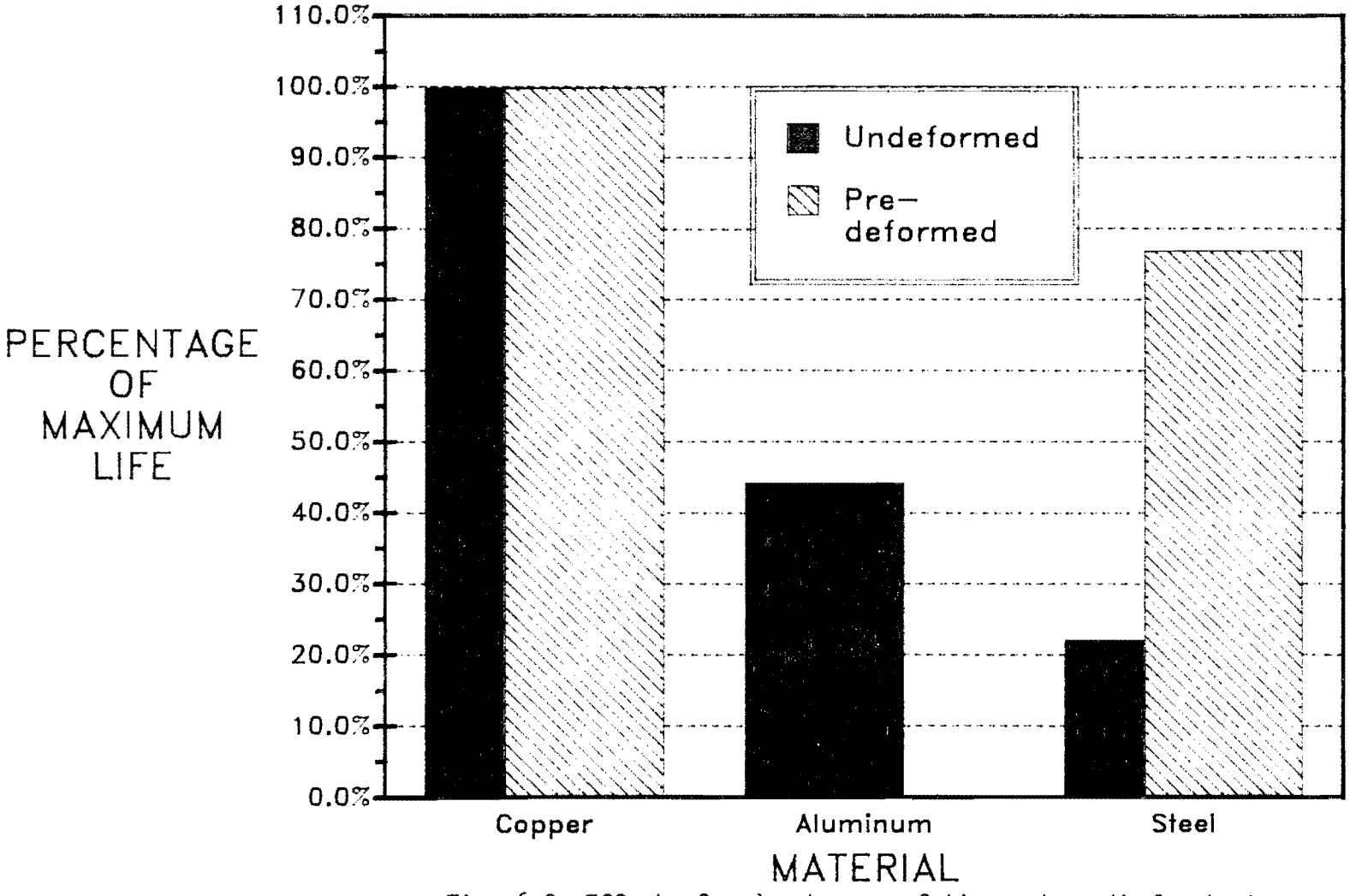

Fig. 6.2 Effect of wedge type on fatigue strength for tests performed at 47.2 ksi stress range

100%. The horizontal axis is labeled with each of the three primary grip materials tested for the 0.5 in. diameter strand. Two bars at each material differentiate between the undeformed and predeformed wedges. Immediately visible from the graph is the effect of the primary grip material on the fatigue life of the strand in the anchorage region. Another important observation is the difference in performance between the predeformed and undeformed wedges of a given material. The predeformed wedges consistently lead to higher fatigue lives.

The trends described for the 47.2 ksi stress range hold for the 33.8 ksi stress range as well. These trends are illustrated in the bar graph of Fig. 6.3. The graph is constructed similarly to that of the preceding figure. A similar graph cannot be constructed for the 27.0 ksi stress range since the test performed with the predeformed copper wedges did not result in a failure. However, the trends do appear to hold based on comparisons of the data in Tables 6.1 through 6.3.

Substantial variation in the fatigue life of the strand was shown to exist depending on the material from which the primary grips were fabricated and their geometry (whether undeformed or predeformed). Since the effect of the anchorage is limited to the surfaces of the outer six wires, the effect of the anchorage must also be limited to the crack initiation phase of the fatigue process. It is therefore apparent that significant improvement in the fatigue lives of prestressing strand can be achieved by concentrating on the crack initiation stage. This would not be true if crack propagation dominated the fatigue process. The lower the fatigue life produced by a given anchorage, the greater the accelerating influence on crack initiation that anchorage has. Anchorages composed of steel wedges tend to accelerate the crack initiation process while primary grips of copper wedges have little effect on crack initiation.

Fatigue tests were also performed on 0.6 in. diameter strand. No data representing the fatigue strength of the strand itself are available since all of the failures occurred in the anchorage zone. Three different wedges were tested in the primary grip: mild steel, heat-treated steel, and tungsten carbide-coated steel. The strand tested with the tungsten carbide-coated steel wedges failed, in tension, at the lead-in section upon application of the maximum load. The early failures are a result of the high local frictional stresses which develop at the lead-in section. The peak stresses were shown to increase with primary wedge hardness in the previous chapter. Since there was no evidence of plastic deformation of the tungsten carbide wedges, no stress redistribution along the outer wires could occur. Furthermore, the contact and frictional stress could not distribute around the wires either. The contact ratio for this case approaches the lower limit of zero, indicating the stress was distributed along a line and highly concentrated at the lead-in section. The early tensile

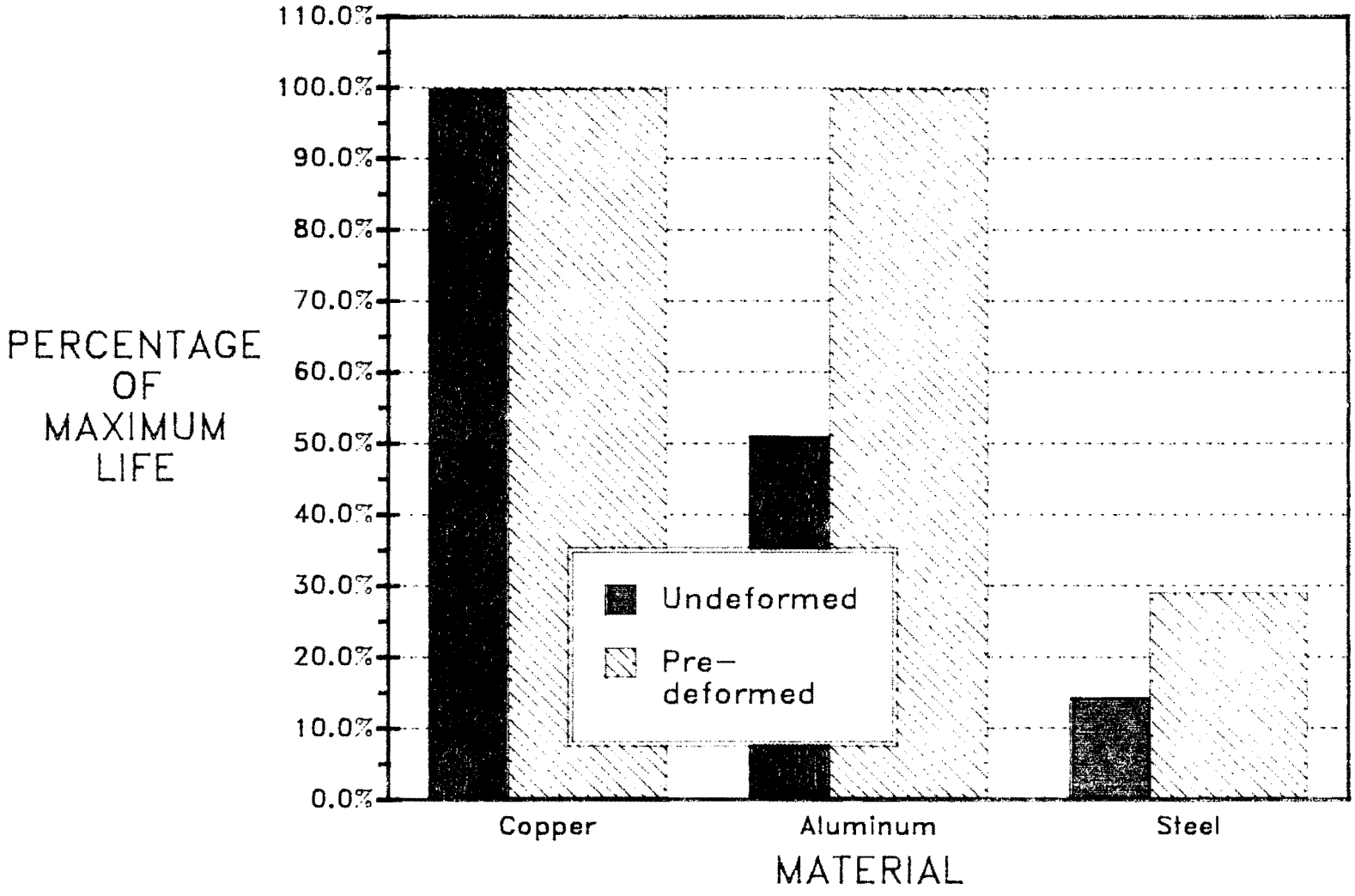

Fig. 6.3 Effect of wedge type on fatigue strength for tests performed at 33.8 ksi stress range

failures can be understood in light of the extreme nature of the stress state.

The heat-treated and mild steel did undergo some plastic deformation, however; and fatigue test results are available for these wedges. The results of the mild steel wedges are given in Table 6.4. The fatigue test results obtained with the heat-treated steel wedges are presented in Table 6.5.

TABLE 6.4 MILD STEEL WEDGE RESULTS

S_R	S_{MIN}	Life
47.2	157.7	112,950
47.2	157.7	83,730
33.8	157.7	181,740
33.8	157.7	177,660
27.0	157.7	720,900
27.0	157.7	595,160

TABLE 6.5 HEAT-TREATED STEEL WEDGE RESULT

S_R	S_{MIN}	Life
47.2[1]	157.7	156,610
33.8[1]	157.7	441,310
27.0	157.7	541,470

[1]Test required restarting.

The only variable in the series of tests performed on the 0.6 in. diameter was the hardness of the material since steel was the material used for both wedges. The data from Tables 6.4 and 6.5 are plotted together in the Wohler Diagram of Fig. 6.4. Also plotted in the graph are the least-squares regression lines for each of the data sets. The equations obtained from the least-squares regression are given below:

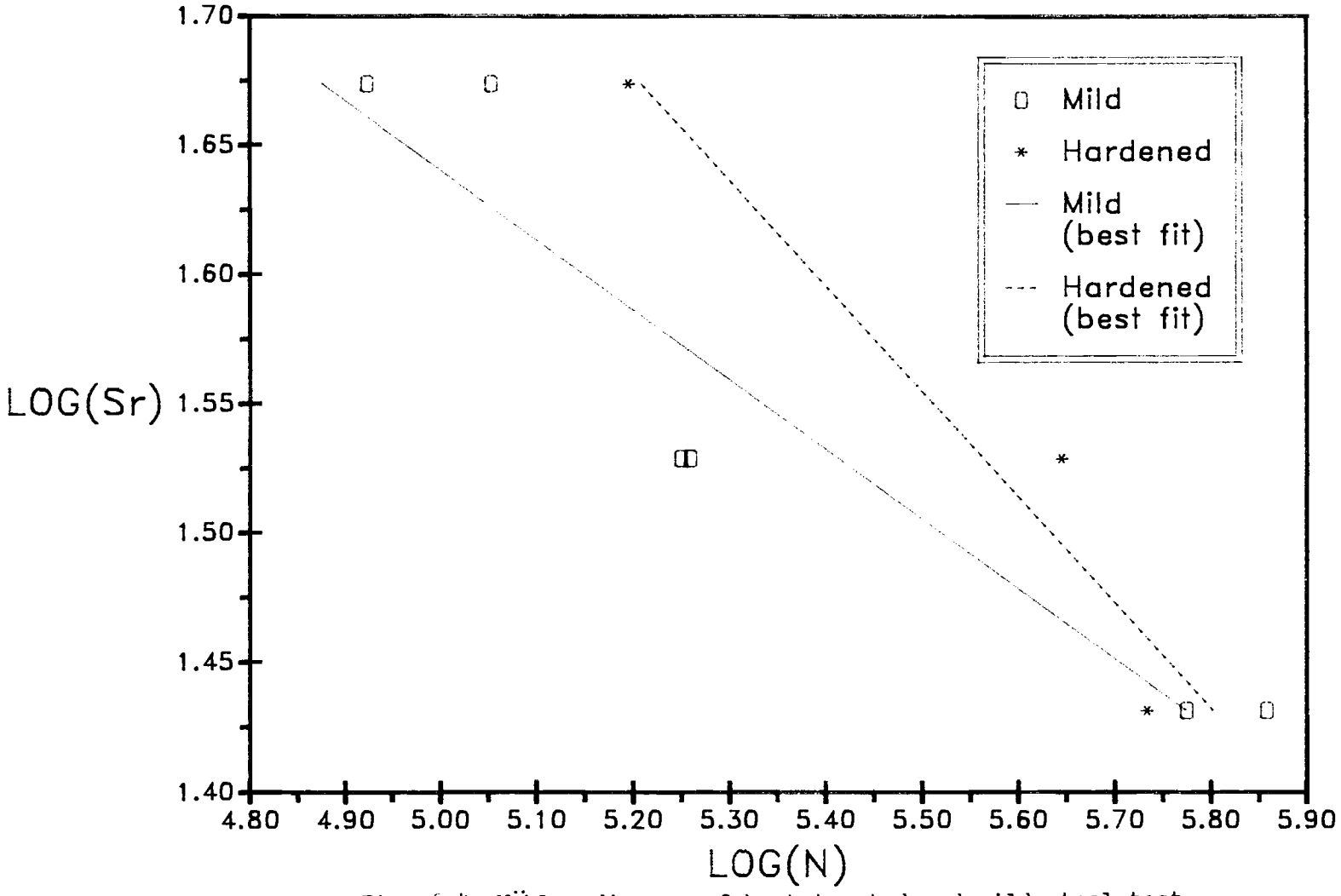

Fig. 6.4 Wöhler diagram of heat-treated and mild steel test results (0.6" ϕ)

Mild: $LOG_{10}(S_R) = 2.9895 - (0.2699)\ LOG_{10}(N)$

Heat-treated: $LOG_{10}(S_R) = 3.8028 - (0.4087)\ LOG_{10}(N)$

The data are difficult to interpret for several reasons. First, the heat-treated steel apparently produces better performance than the mild steel at the higher stress ranges but is exceeded at the low stress range. This discrepancy may be due to the fact that the two tests performed with the heat-treated wedges required restarting. These wedges would then be designated as "predeformed." Predeformed wedges were shown to produce better fatigue lives than corresponding undeformed wedges for the 0.5 in. diameter strand. The fatigue lives at the 33.8 and 47.2 ksi. stress range are therefore greater than would be expected for the undeformed heat-treated wedges. The apparent scatter in these results may be due to the variability inherent in fatigue testing. In any case, when comparing the regression lines, the differences do not appear to be significant.

A discussion of the fatigue tests performed on the 0.5 in. and 0.6 in. diameter strand was presented in this subsection. The influence of material on the fatigue lives was shown. Copper wedges were shown to have little effect on the crack initiation process while the steel wedges were shown to accelerate crack initiation. Also, predeformed wedges of a given material were shown to produce better fatigue performance than the corresponding undeformed wedges. The deformability of the primary wedge material was, therefore, also shown to be important. At one extreme, the tungsten carbide-coated wedges did not deform plastically and produced early tensile failures before any fatigue loading was applied. The copper wedges, on the other hand, were subjected to the largest amount of plastic deformation (large contact ratio) and lead to the best fatigue performance. The effect of deformability on fatigue life will be discussed in greater detail in Section 6.3.

6.1.2 Commercial and Prenotched Fatigue Tests. In addition to those tests performed with the double grip anchorage, tests were conducted with single commercial wedges at either end. These tests were run to investigate the fatigue sensitivity of these anchorages which served as the secondary grips in the two-part anchorages tested in this research program. To study the influence of the notches produced by the commercial wedges, tests were also performed on prenotched strand. The notches were produced in the free length of the strand by the commercial wedges and were, therefore, the same as those formed in the anchorage zone in the commercial tests. The results from both of these test series will be discussed in this subsection.

The fatigue test results, given in Table 6.6, are plotted in the Wohler Diagram of Fig. 6.5 with the results of the dual-grip fatigue tests. The results obtained with the commercial wedges were

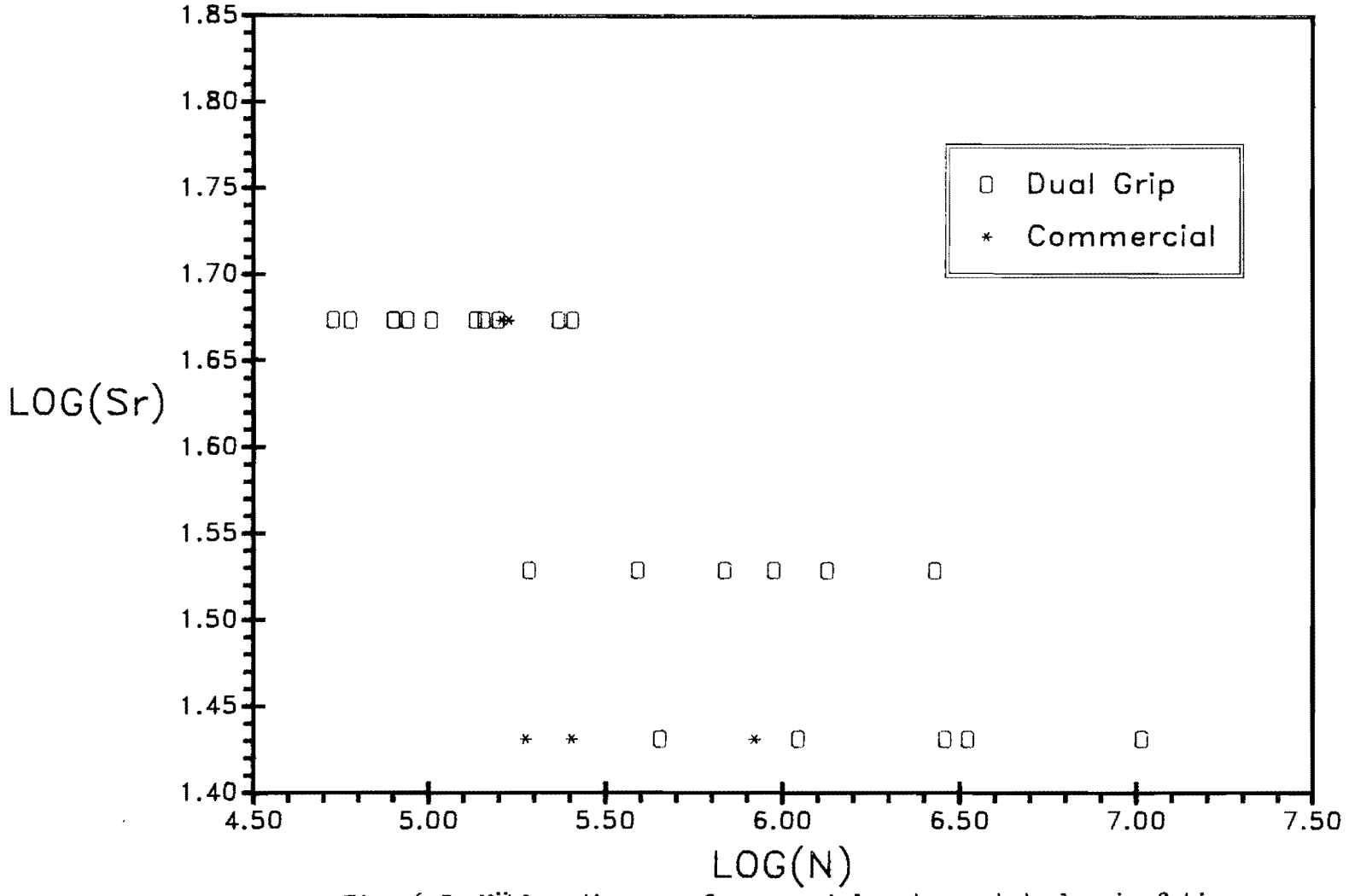

Fig. 6.5 Wöhler diagram of commercial wedge and dual grip fatigue test results

satisfactory at the 47.2 ksi stress range. The three tests performed at that level resulted in consistently longer fatigue lives than those obtained from the dual-grip anchors with steel and aluminum wedges. As the stress range decreases toward the service-load values (around 20 ksi or lower) the commercial wedges become more fatigue sensitive relative to the strength of the strand.

TABLE 6.6 COMMERCIAL WEDGE RESULTS

S_R	S_{MIN}	Life
47.2	157.7	222,690
47.2	157.7	169,280
47.2	157.7	161,570
27.0	157.7	833,670
27.0	157.7	253,970
27.0	157.7	188,860

The surprisingly good performance of the commercial wedges at the 47.2 ksi stress range confirm, to a certain extent, the results from the German research program [20] presented in Chapter 2. In summary, the Germans found that reducing the relative slip between the the wedge and the wire specimen resulted in improvements in fatigue lives. The researchers reduced the slip by designing wedges that would dig into the wire at the first and subsequent teeth. The commercial wedge performs in a similar manner. The first teeth in the commerical wedges are not full teeth, however, and digging in of the first few teeth is not possible. The digging in of the remaining teeth would reduce the slip to a certain extent and this accounts for the better-than-expected performance.

While the commercial wedge performed well at the high stress range, its performance relative to the strand worsened as the stress range decreased. Since service load stress ranges are typically in the range of 20 ksi or below, the commercial wedge used in this research program would be a poor choice to carry the fatigue loading alone. The commercial wedge can be defined as "fatigue sensitive" at low stress ranges.

The fatigue tests performed with prenotched strand did not result in significantly different lives from those obtained with the commercial wedges when compared in the Wohler Diagram of Fig. 6.6. These test results are presented in Table 6.7.

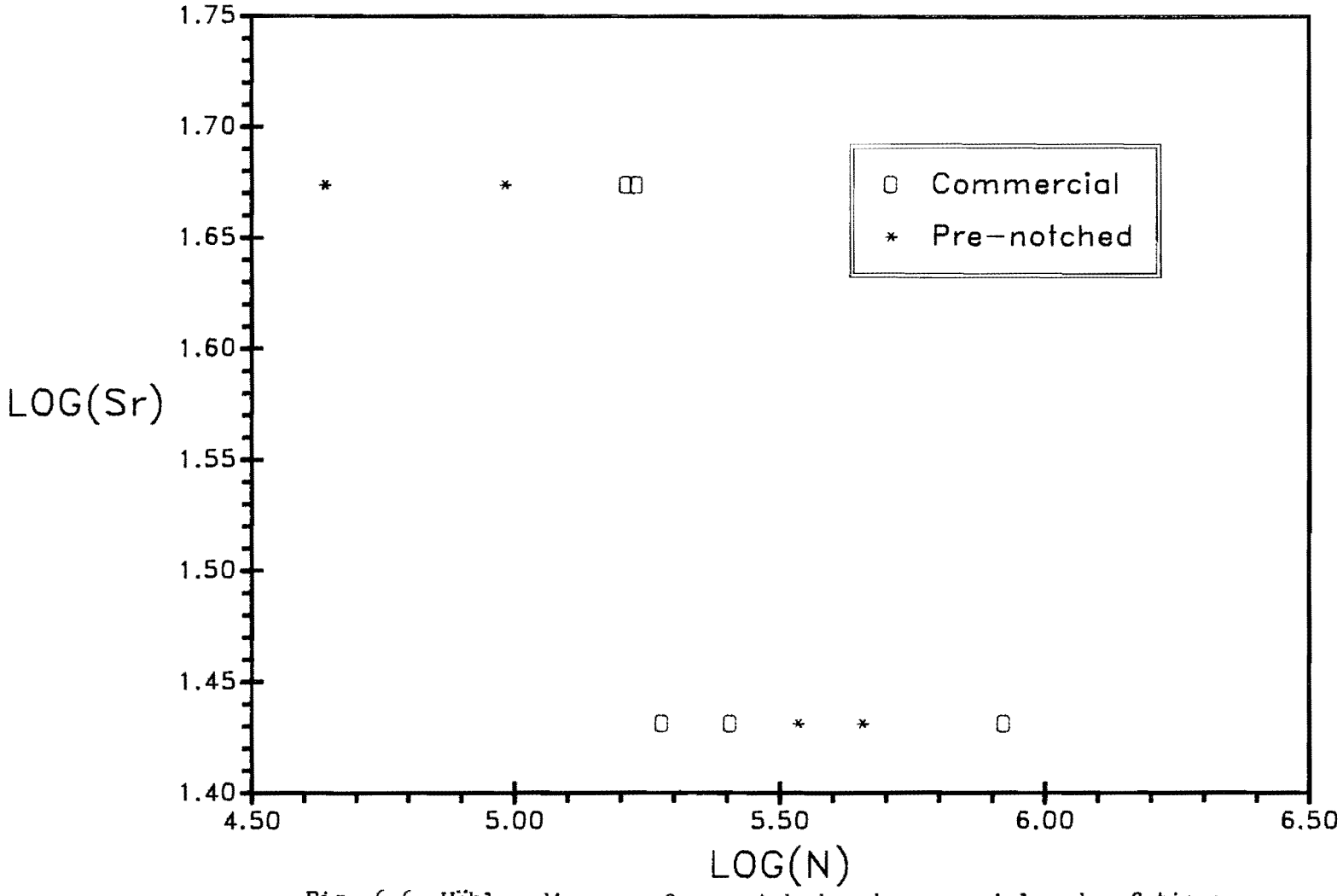

Fig. 6.6 Wöhler diagram of prenotched and commercial wedge fatigue test results

TABLE 6.7 PRENOTCHED STRAND RESULTS

S_R	S_{MIN}	Life
47.2	157.7	96,020
47.2	157.7	43,730
47.2	157.7	43,620
27.0	157.7	452,660
27.0	157.7	342,700

The strand consistently failed in the prenotched area although in a different location from that of the commercial wedge tests. In this series of tests, the strand failed in the deeper notches formed by the back end of the wedge. Failures consistently occurred in the strand at the base of the wedge in the commercial tests. The difference in failure location and lack of surface tractions for the prenotched strand indicate a different failure mechanism controlled the failure. In the case of the prenotched strand, the notches in the free-length served to accelerate the crack initiation stage and thus resulted in lower fatigue lives in the high stress range. There do not appear to be any systematic differences in the fatigue lives as shown in the Wohler Diagram (Fig. 6.6).

The results of the commercial tests and prenotched strand tests were discussed in this subsection. The commercial wedges were shown to perform poorly relative to the strength of the strand and were termed "fatigue sensitive" for typical service load stress ranges. The relatively good fatigue performance of the commercial grips at the high stress range was stated to be a result of the reduced slip at the strand/wedge interface. The prenotched strand produced shorter fatigue lives at the higher stress range. The failure of the prenotched strand occurred adjacent to the deepest notch. The electron micrographs in the next section show the location of crack initiation to lie away from the notched areas.

6.2 Electron Fractography

The purpose of the scanning electron microscopy was to determine the location of the fatigue crack initiation site in the failed wires. The cause of failure could then be attributed to some mechanism involving wedge/wire contact such as one of those presented in Chapter 3 or another mechanism altogether. The visual information provided by the electron microscope makes the determination of the

failure mechanism possible. The method of preparing the specimens and some of the electron micrographs will be presented and discussed in this section.

6.2.1 Specimen Preparation. After each fatigue failure in the laboratory, each of the surfaces of the failed wires was sprayed with a clear protective coating to guard against corrosion. Those wires selected for viewing under the microscope were cut from the strand and stored separately in a desiccator. Prior to microscopic study the protective coating was removed from the fracture surface by soaking the quarter-inch long specimen in an ultrasonic bath of acetone. The ultrasonic sound waves helped remove persistent contaminates and did not cause damage to the surface. The specimen was then ready to be studied under the microscope.

6.2.2 Selected Electron Micrographs. Before presenting some of the photographs taken with the electron microscope a general description of fatigued fracture surfaces will be presented. This discussion will be limited to the specimens tested in this research program.

The surfaces presented in this section have four common areas of interest: (1) the crack initiation site, (2) the crack propagation plane, (3) the final tensile-fracture zone, and (4) exterior surface damage. These four areas are illustrated in Fig. 6.7. Both the crack propagation plane and the final tensile-fracture zone lie on the fracture surface. The area of crack propagation can be identified by a "smooth" appearance while the tensile fracture area is generally much "rougher" in texture. The location of the crack initiation site is usually located at the center of a semicircular area. The crack initiation site lies, in general, on the border between the fracture plane and the exterior surface. It should be noted that fatigue cracks can initiate beneath the exterior surface and would then lie on the fracture surface. In this application, exterior surface damage is generally responsible for initiating fatigue cracks. The fourth area of interest, the zone of exterior surface damage, lies, as the name implies, on the exterior surface and is due to contact with the anchorage elements.

The electron micrographs for a given specimen will be presented in order of increasing magnification. This method of presenting the photographs permits the viewer to compare the previous photograph with the one of greater magnification and thus the location of a particular area of interest is easily found in relation to the overall view of the wire. The first photograph is always an overall view of the fracture surface.

The first series of four photographs is given in Figs. 6.8, 6.9, 6.10, and 6.11. The grip used in this test was composed of steel wedges. The first micrograph is a top view of the fracture surface.

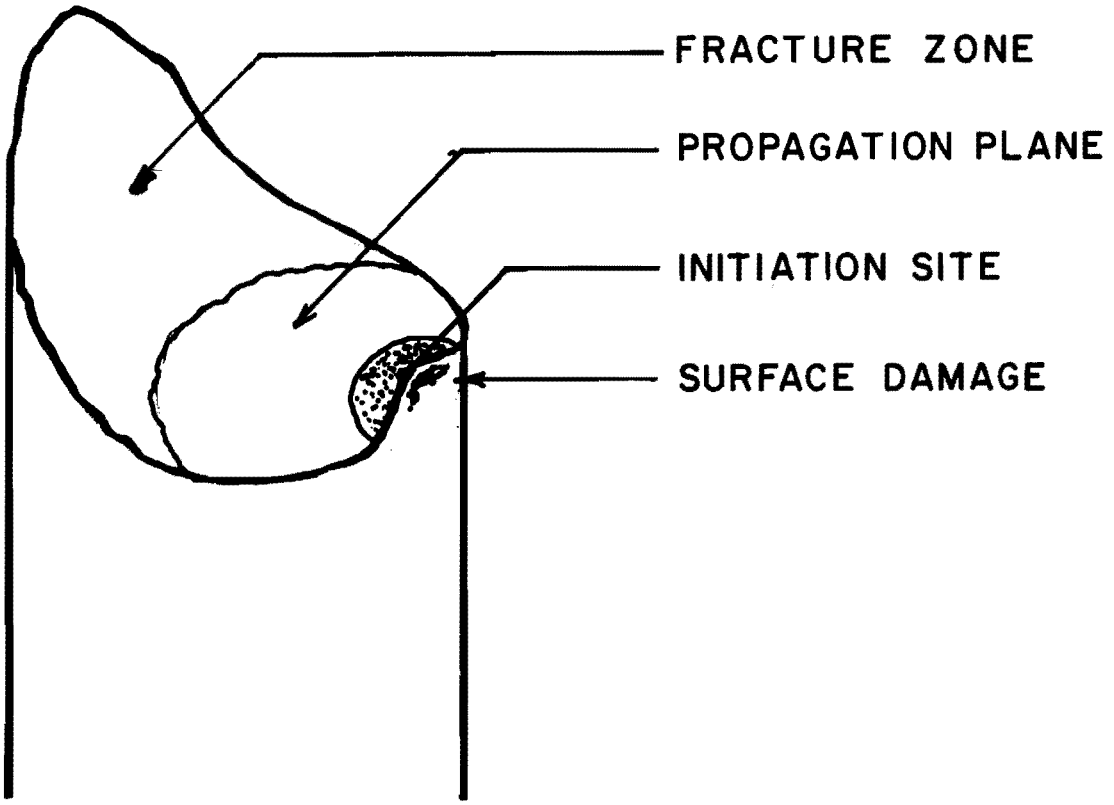

Fig. 6.7 Areas of interest on typical fatigue-fractured wire specimen

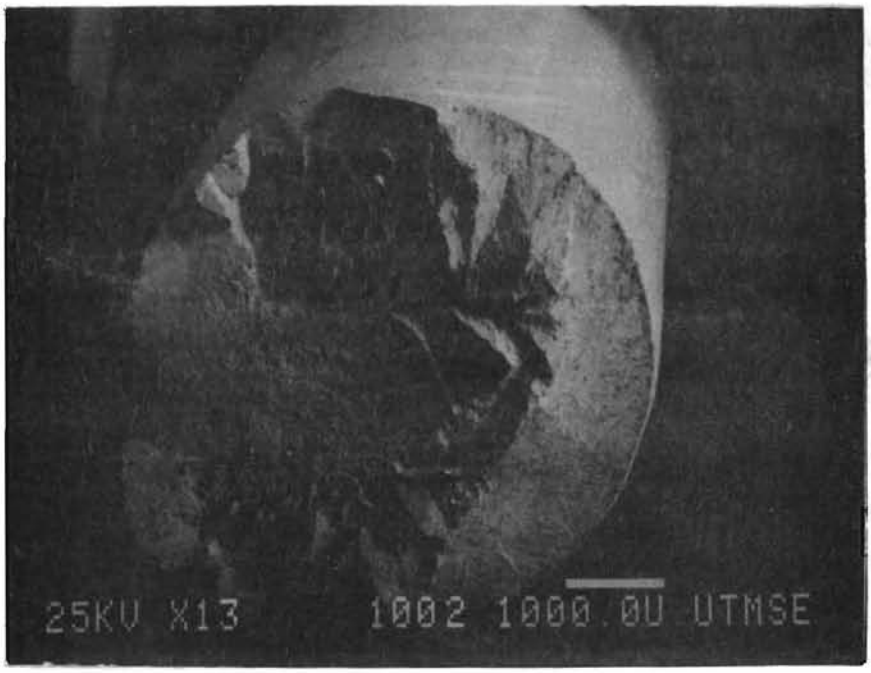

Fig. 6.8 Overview of fracture surface

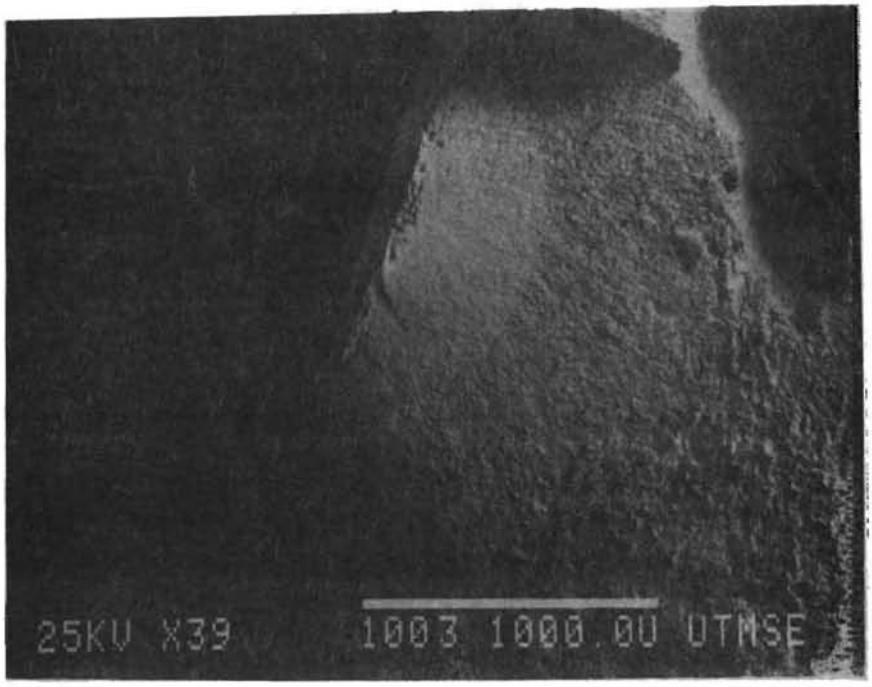

Fig. 6.9 Crack propagation plane

Fig. 6.10 Crack initiation site

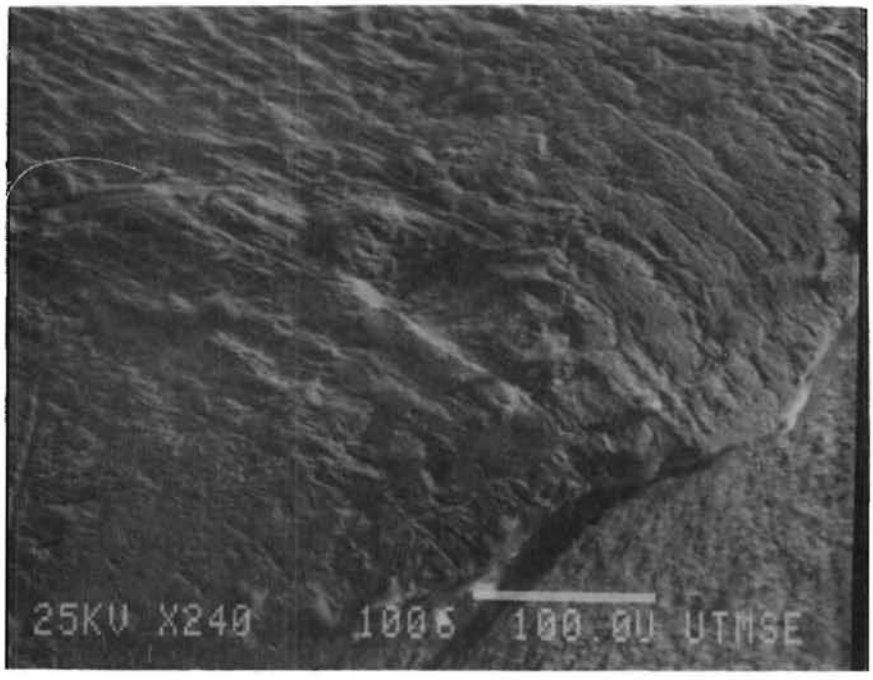

Fig. 6.11 Exterior surface damage

The location of crack nucleation can be seen along the edge of the surface at the left-center of the photograph. The relatively flat plateau in the photograph is the crack propagation surface. The remainder of the fracture surface is the final, tensile fracture zone.

The second photograph, Fig. 6.9, is a close-up of the crack propagation plane. The wire is turned "on edge" in the photograph of Fig. 6.10. The crack initiation site can be seen at the top of the rounded "chip." Scratches and pits are obvious at the crack nucleation site. A magnified view of the surface damage is presented in Fig. 6.11. An important feature of the surface damage is its confinement to the edge of the failure surface. This is a typical feature found in these photographs. The surface damage is localized and does not exist along the entire region of the primary grip contact.

The second series of photographs is from a test conducted with the commercial wedges alone. The point was made previously that fatigue failures obtained with the commercial wedges were not always due to the notches produced by the wedge. This series of photographs illustrates one such case. The photographs are presented in Figs. 6.12 through 6.15.

The overall view of the failure surface is presented in Fig. 6.12. The crack initiation site is not as obvious as that of the previous series and is just visible at the edge of the fracture surface on the left-hand side of the cross-section. Unusual in this photograph is the very pronounced shear lip at the lower left of the photograph. The shear lip is typically identified by a rise in elevation above the crack propagation plane (this corresponds to a decrease in elevation on the opposite failure surface). The surface of the shear lip is generally oriented at forty-five degrees to the propagation plane. In this instance, however, the shear lip rises almost vertically from the propagation plane. The relatively featureless crack propagation plane is shown in a close-up in Fig. 6.13. The crack initiation site is located on the edge at the end of the small step in the fracture surface at the top of the photograph. The step can be identified easily since it is lighter in color when compared to the surrounding propagation plane.

The remaining two photographs show the notches produced by the commercial wedge. Several of the the notches are shown in Fig. 6.14. The notches increase in depth as one moves back into the wedge. It is obvious from the photograph of Fig. 6.15 that the crack initiation site does not lie in one of the notches, but rather in front of the lead notch. Surface damage, such as that pointed out in the previous series of photographs, exists in the area of the crack initiation site.

The observations, while more qualitative than quantitative, are important. Three essential observations can be made from the

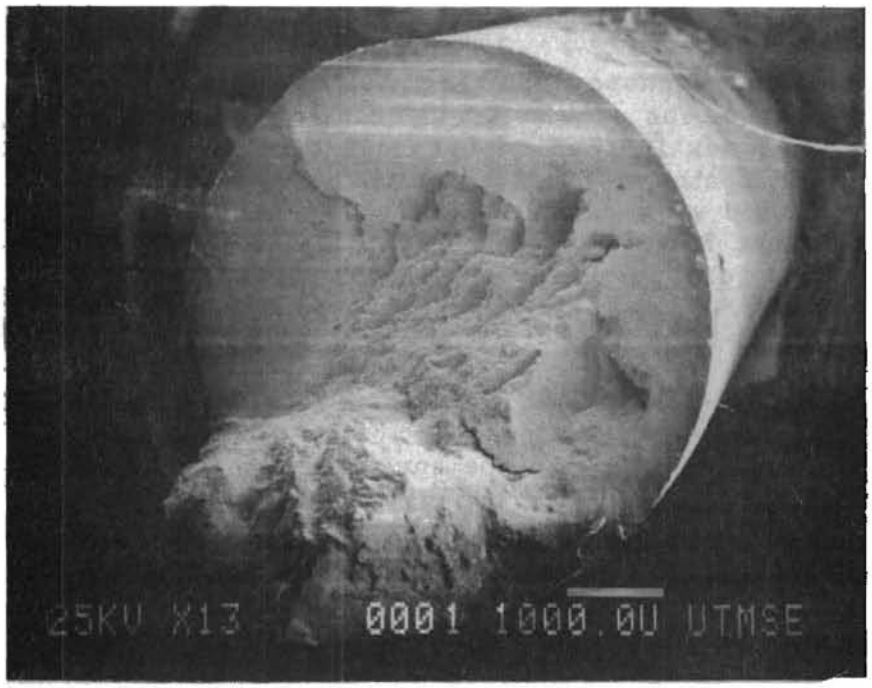

Fig. 6.12 Overview of fracture surface

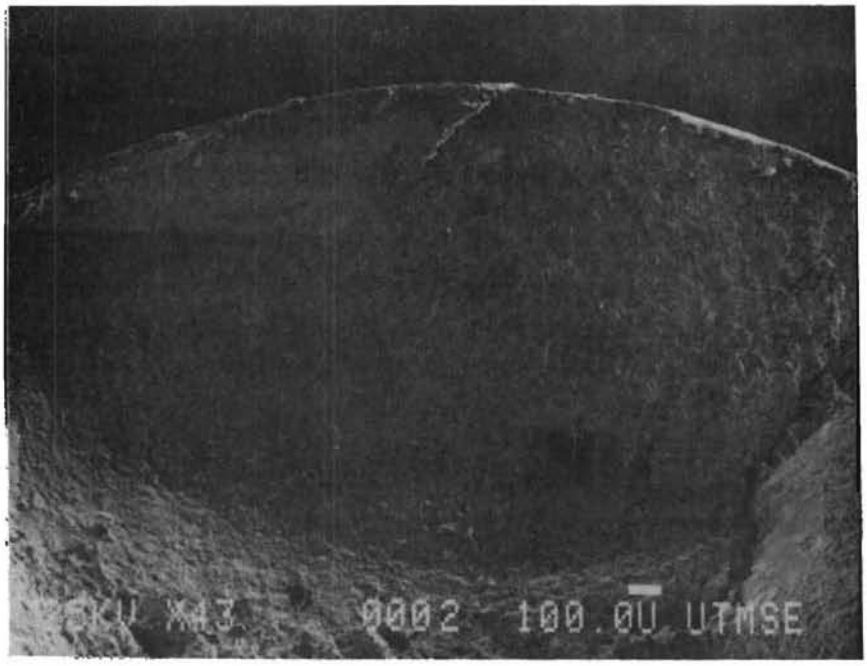

Fig. 6.13 Crack propagation plane

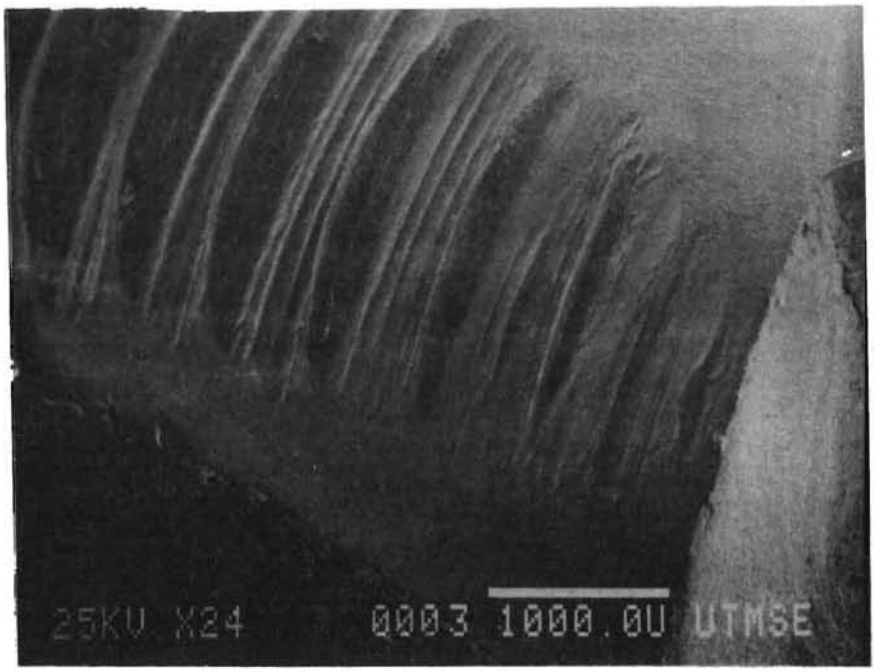

Fig. 6.14 Notches produced by commercial wedge

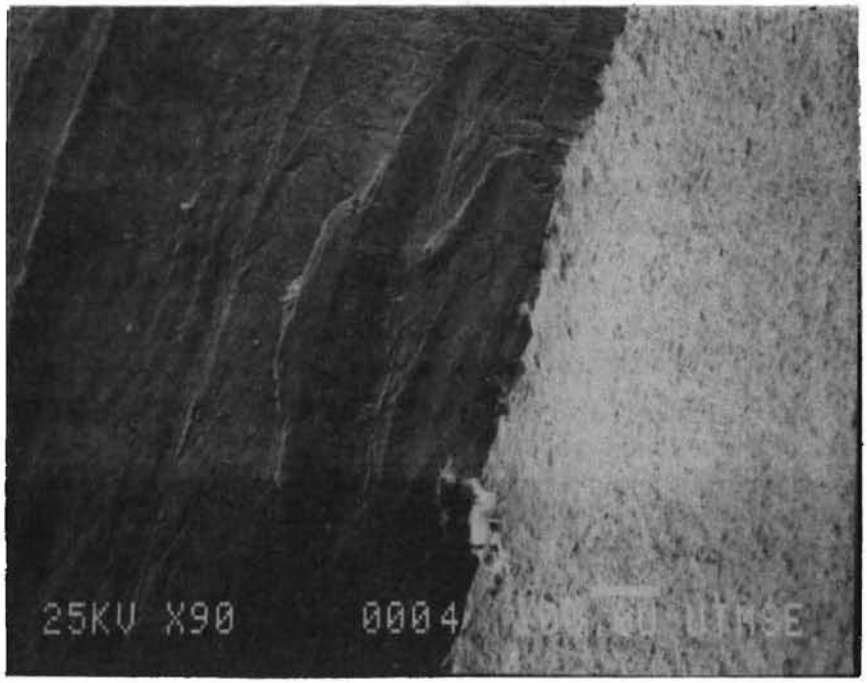

Fig. 6.15 Crack initiation site

photographs. The location of crack initiation, the visible factors leading to crack initiation, and the details of the crack propagation plane are important in determining the controlling failure mechanism.

The observed reduction in fatigue strength in the anchorage region of individual strands was assumed to be due to some detrimental influence of the anchorage technique. The failure mechanisms for individual strands were presented in Chapter 3. In each of the failure mechanism described, crack initiation was implied to occur at the interface between the strand and the anchorage material. The electron fractographs indicate the location of crack initiation to consistently occur at locations of contact between the strand and wedge.

Also, the crack initiation site consistently occurs at lead-in section where the strand enters the primary wedge group. This is important in light of the results of the finite element stress analysis discussed in the previous chapter. The largest magnitudes of frictional and normal stress were shown to occur at the lead-in section and decrease rapidly along the contact region. The influence of the frictional stress can be observed from the photographs. A cross section of a failure surface not subjected to surface tractions is illustrated in Fig. 6.16a. The crack propagation plane is flat and oriented perpendicular to the direction of the maximum tensile stress. The effects of surface tractions on the shape of the propagation plan are illustrated in Fig. 6.16b. The crack initiation site is typically at a higher elevation than the majority of the crack propagation plane. As the crack moves away from the surface, the influence of the surface tractions on the direction of crack propagation decreases and, finally, the crack grows perpendicular to the axis of the wire.

Another important observation with respect to crack propagation is the extent of the propagation plane. Most of the fracture surface is covered by the rough-textured metal indicative of final fracture. The smooth-textured propagation plane extends only over 30 to 40% of the surface. It can be seen that once a crack is initiated it need not grow far before final tensile fracture results in a failure of the wire.

The effect of the high frictional stresses has been discussed with respect to the crack propagation plane. However, the frictional and normal stresses are also responsible for early crack initiation. The effect can be seen in the surface damage on the outside surface of the wire at the intersection of the crack propagation plane. The accelerating effects of surface pits, scratches, etc. on crack initiation have been discussed in Chapter 3. The limited extent of the surface damage should also be noted. Exterior surface damage is very localized around the lead-in section.

The electron fractographs and their common characteristics have been presented in this section. Crack initiation and propagation

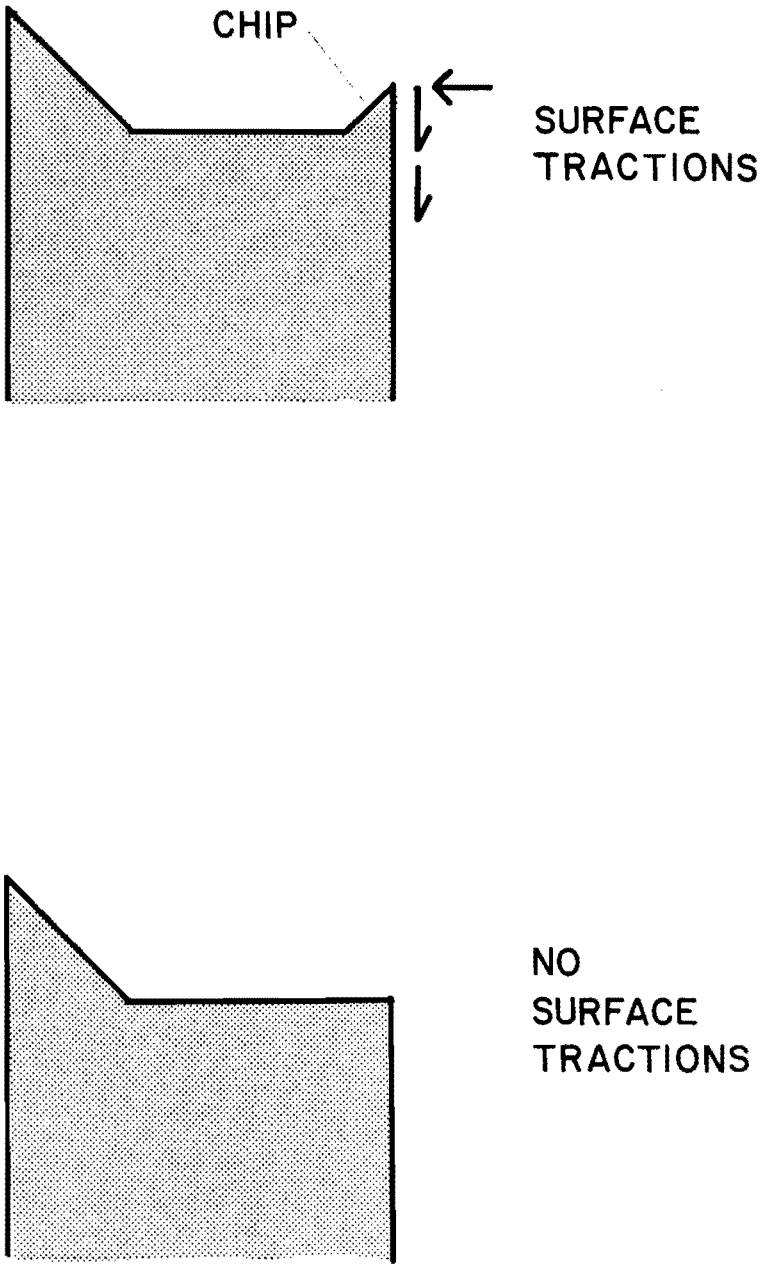

Fig. 6.16 Failure surface not subjected to surface tractions

were shown to consistently occur in regions of high normal and frictional stresses. The significance of these observations and those of the previous two sections will be discussed in relation to the fatigue test results in the next section.

6.3 Synthesis and Controlling Failure Mechanism

The results from each of the four separate investigations have been discussed in this and the previous chapter. Very little discussion was offered on the interrelationships existing between the investigations. The purpose of this section is two-fold. The first objective is to show that the results from one investigation directly influence those of another. Specifically, the effect of load and stress distribution on fatigue lives will be discussed. The fatigue test results will be shown to be significantly controlled by the load distribution characteristics of the anchorage used in the test. The second goal of this section is the presentation of the dominant failure mechanism. Each of the investigations will be discussed in relation to the failure mechanism.

6.3.1 Synthesis of Independent Investigations. Bar graphs were presented in the first section which illustrated the dependence of fatigue performance on the type of primary wedge used. In summary, the steel wedges were shown to produce the worst fatigue performance while the aluminum and copper lead to larger fatigue lives. In all cases, the predeformed wedge performed better than the undeformed wedge. The distribution of the tensile load in the strand between the primary and secondary grips was also shown (Chapter 5) to be dependent upon the material and whether the primary wedge group was composed of predeformed or undeformed wedges.

The two independent relationships imply a third relationship between the load distribution characteristics of an anchorage and the fatigue life obtained with that anchorage. The data from the two independent relationships are combined in Fig. 6.17. The trend illustrated in the figure is the influence of load distribution on fatigue life at stress ranges of 47.2 and 33.8 ksi. The load distribution ratio (the maximum load transferred by the primary grip divided by the maximum load carried by the strand: abreviated as LDR) is plotted along the horizontal axis while logarithm of the fatigue life at the given stress range normalized by the logarithm of the fatigue life of the strand (results of the tests conducted with the predeformed copper wedges) at the corresponding stress range is plotted along the vertical axis. It is seen from the graph that as the ratio of the tension carried by the primary grip to the total strand tension decreases, the fatigue life increases. Furthermore, the relationship is seen to be essentially independent of stress range.

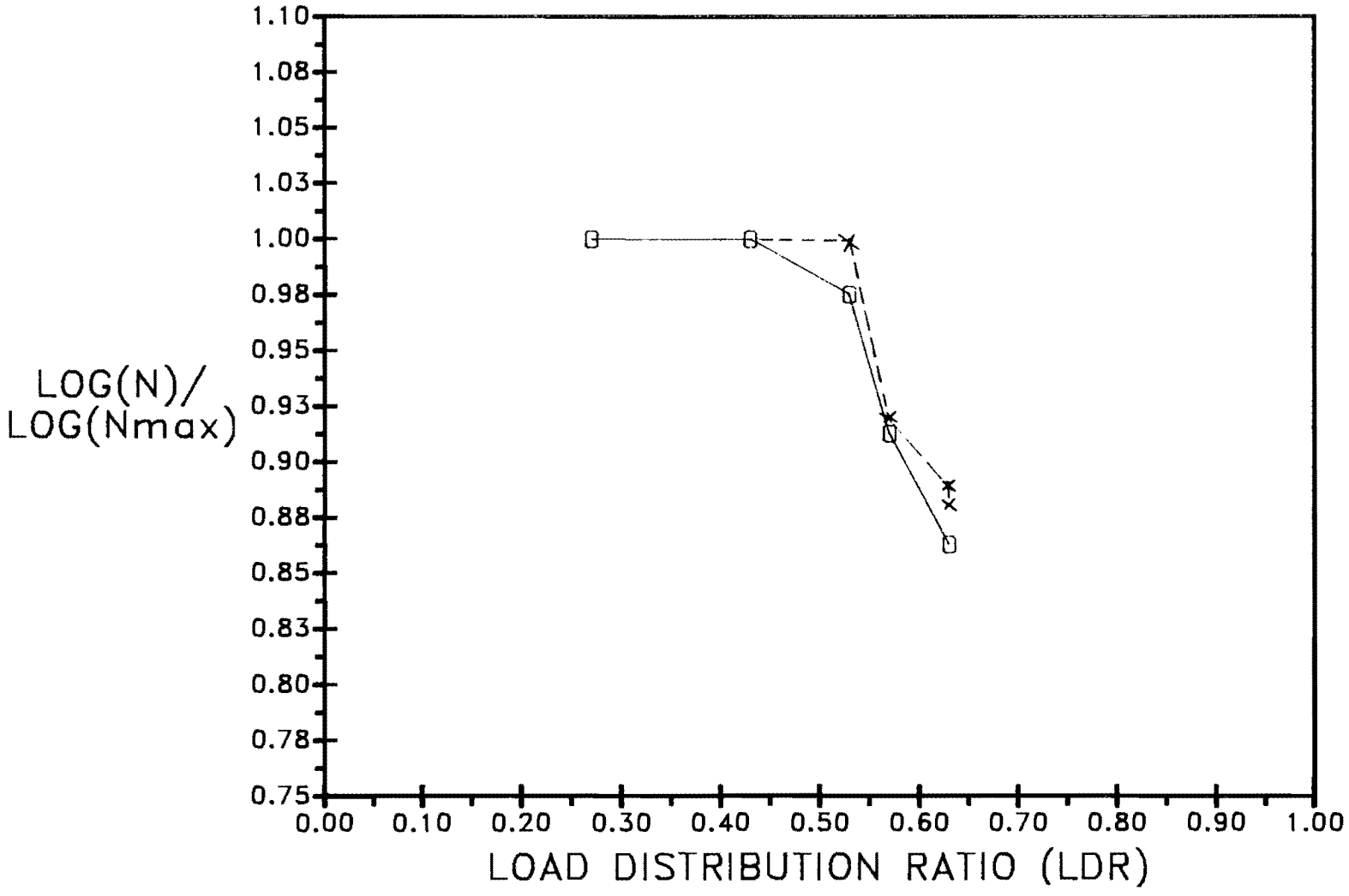

Fig. 6.17 Log (N)/Log (N_{MAX}) vs load distribution ratio (LDR) for 47.2 and 33.8 ksi stress ranges

The trend shown in Fig. 6.17, however, is composed of data from different materials. Material factors other than those influencing only the load distribution characteristics of the anchorage are also included in the graph. It was, therefore, necessary to to investigate the effect of the load distribution ratio on the fatigue life independently of any material variables. Three fatigue tests were performed with the predeformed steel wedges at varying load distribution ratios. The test results are presented in Table 6.8. All of the failures occurred at the lead-in section of the strand. The load distribution ratio was changed by preloading the specimen to different preloads while maintaining a constant load range and minimum load.

TABLE 6.8 EFFECT OF LOAD DISTRIBUTION

S_R	S_{MIN}	Life	LDR
32.7	65.4	6,816,770	0.18
32.7	65.4	8,415,120	0.39
32.7	65.4	1,051,290	0.52

The logarithm of the resulting fatigue lives is plotted as a function of the load distribution ratios in Fig. 6.18. The same general trend is observed independent of material variables. This is not to say that other material variables play no role, only that their role is subordinate to that of the load distribution ratio.

The fatigue life obtained at the midrange value of the load distribution ratios exceeded that obtained at the lowest load distribution ratio. Theoretically, this should not occur. However, it should be kept in mind that fatigue data is subject to variation, especially at combinations of low stress range and mean stress. This inherent variation accounts for this discrepancy in performance.

The final relationship to be discussed in this subsection is the influence of the stress distribution within the primary grip on the surface of the strand. Since fatigue failures consistently occurred at the lead-in section of the primary grip and the contact and frictional stresses were shown to be maximum at that section, it appears reasonable to focus this discussion on the lead-in section as well.

Adhesion, abrasion, and fretting were discussed in Chapter 3. The influence of the contact load on each was also presented. In each case, adhesion, abrasion, and fretting increase

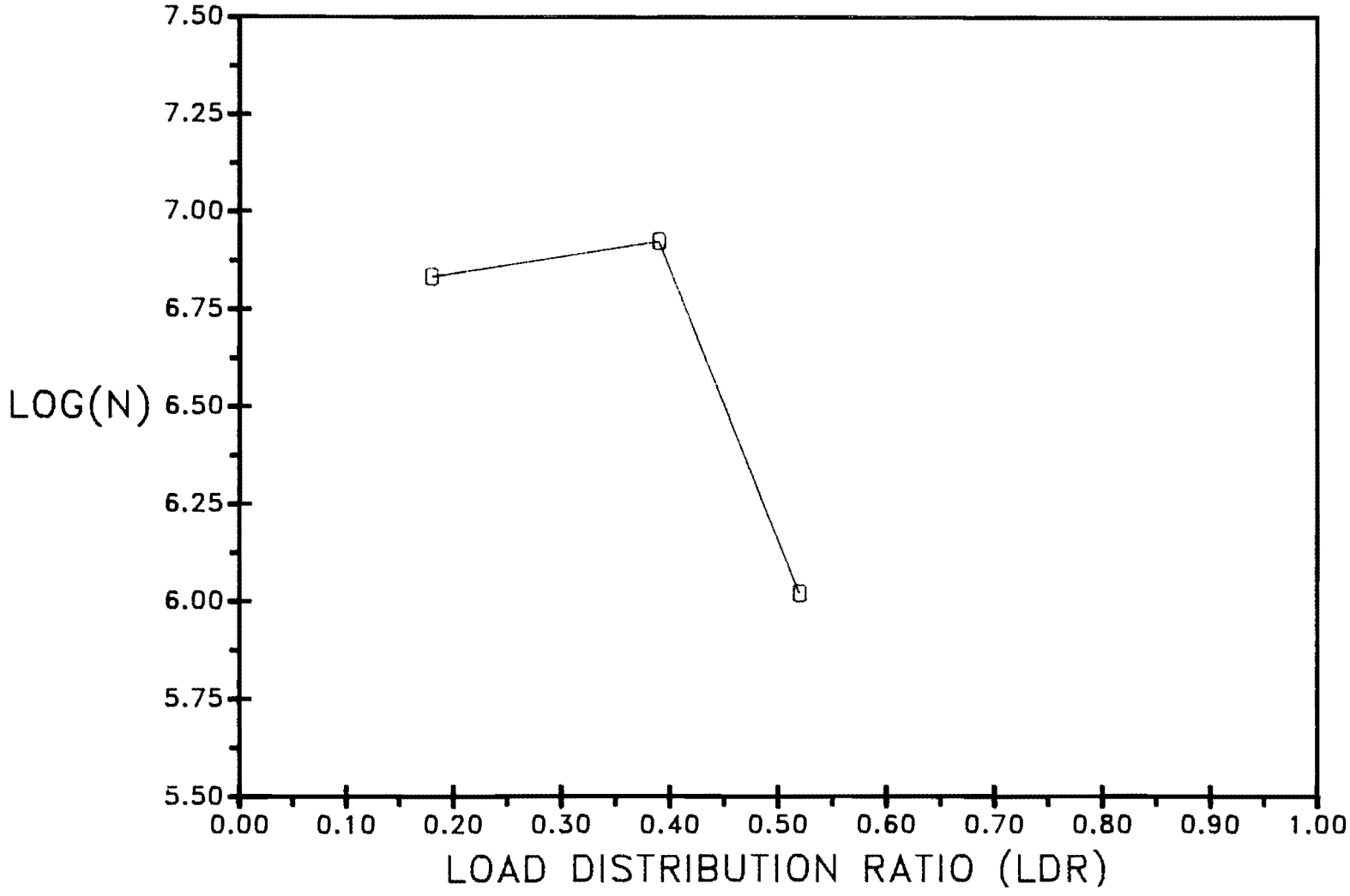

Fig. 6.18 Log (N) vs load distribution ratio (LDR) (predeformed steel wedge only)

with increasing contact load. Larger normal stresses lead to increases in the rates of wear. The effect worsens with a simultaneous increase in the frictional stress.

The dependency of the fatigue life on the behavior of the anchorage was demonstrated in this subsection. The fatigue life was shown to be closely related to the load distribution ratios of the anchorages used in the tests. The relationship between the load distribution ratios and the stress distribution in the primary grip was discussed in the previous chapter. The influence of the stress distribution on the surface of the strand was then presented. These three relationships imply another relationship between the surface of the strand and the fatigue performance. This relationship is a synthesis of all relationships and is defined as a "failure mechanism" and is presented in detail in the next subsection.

6.3.2 Controlling Failure Mechanism. The important interrelationships existing between the various independent investigations were discussed in the preceding subsection. These relationships can be further synthesized into a conclusive mechanism explaining the influence of the strand anchorages on the fatigue lives. Understanding the controlling failure mechanism is crucial if fatigue resistant anchorages are to be developed. This failure mechanism will be presented and discussed in this subsection.

In terms of the mechanisms discussed in Chapter 3, the controlling mechanism appears to be a combination of the asperity contact mechanism and the friction-generated cyclic shear stress mechanism. According to the friction-generated cyclic shear stress theory, an array of microcracks would tend to form in front and behind the contacting surfaces. The shear stress is transferred by friction across the interface.

The asperity contact model, as discussed in Chapter 3, is somewhat different from the friction-generated shear stress model. In this model, microcracks would be expected to form over the entire region of contact at the bases of contacting asperities. The microcracks are assumed to develop as a result of shear stresses transferred across the interface by adhesion between the wedge and the strand.

Elements of both of these mechanisms appear to be most predominate at the interface between the strand and wedge. The surface damage resulting from wedge/strand contact was shown in the electron fractographs to be limited to the lead-in section of the wire. This localization of the damage is consistent with the predictions of the friction-generated cyclic shear stress theory. However, the damage itself is a result of particle removal in the area. The frictional stresses, alone, are not responsible for the damage.

The surface damage visible in the electron micrographs is a result of wear processes in the area. Abrasion cannot be responsible for the particle removal since the hardness of the strand was greater than the hardness of the wedge material. The wear process of adhesion can produce pitting in the harder of two surfaces, however, and must be responsible for the surface damage of the strand in this case. Evidence of adhesion can also be supported from direct unaided visual inspection of the surfaces of the outer six wires. Discoloration of the outer six wires is due to the adherence of particles removed from the surface of the wedge. Adhesion, therefore, acts in conjunction with friction. The surface cyclic shear stresses would be transferred across the interface through friction and adhesion. Since adhesion is known to exist at the interface and surfaces, in general, are never truly flat, the asperity contact mechanism must also be considered.

The exact microcrack initiation mechanism can not be exactly defined. Elements of both, the friction-generated cyclic shear stress mechanism and the asperity contact mechanism, were discussed and shown to be active at the interface. Based on this evidence a microcrack initiation mechanism can be proposed which explains the influence of the various load and material parameters on the fatigue performance of the strand in contact with the anchorage. This mechanism will be presented and discussed in relation to the various test results already presented.

In a broad sense, the purpose of defining a controlling crack initiation mechanism is to show a relationship between the material, and to a certain extent, the geometry of the anchorage and the fatigue performance. To facilitate the discussion, the physical crack initiation model will be presented first, followed by a discussion of the influence of material, geometric, and load parameters on crack initiation.

The discussion of the physical model will be presented for the general case of a surface (a single wire of a seven-wire strand) with nonzero values of normal and tangential stress. This situation is illustrated in Fig. 6.19a. The normal and tangential stress components are labeled N and T, respectively. The surface is assumed to be free of contact at point A. Point B represents the first point of contact and point C is at some location within the contact region. The two stress components are added vectorially and shown in Fig. 6.19b as a single vector labeled F. The angle of attack of the stress vector is dependent upon the relative magnitudes of normal and tangential stress. As the tangential stress increases relative to the normal stress the angle decreases.

Fatigue failures have been observed to consistently occur at a location corresponding to the point B in the previous figure. The surface in the immediate vicinity of B is shown in Fig. 6.20. The material just beneath the surface is subjected to compressive stresses

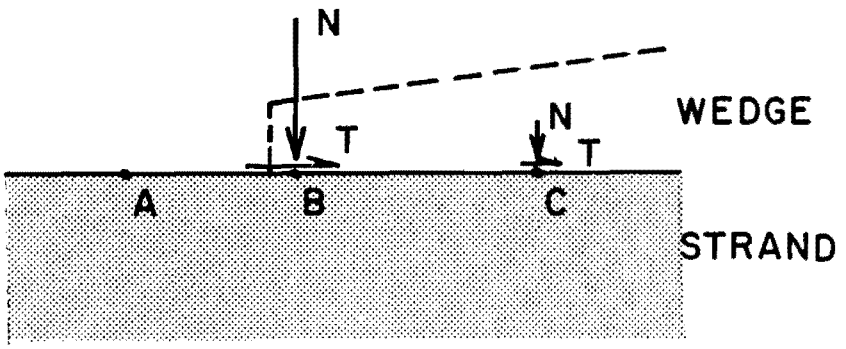

Fig. 6.19 (a) Surface tractions on single wire

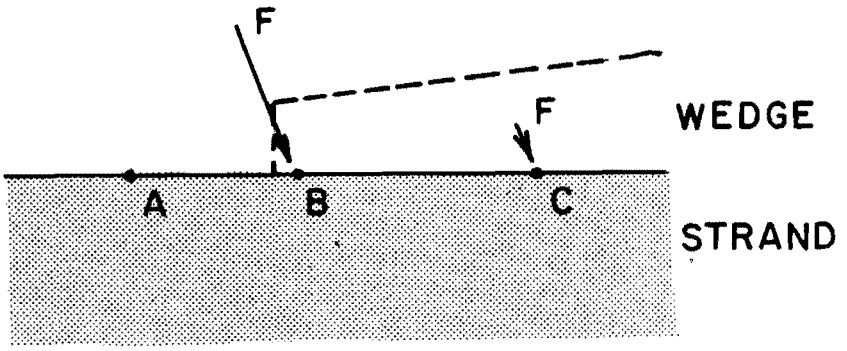

Fig. 6.19 (b) Vectoral sum of surface tractions

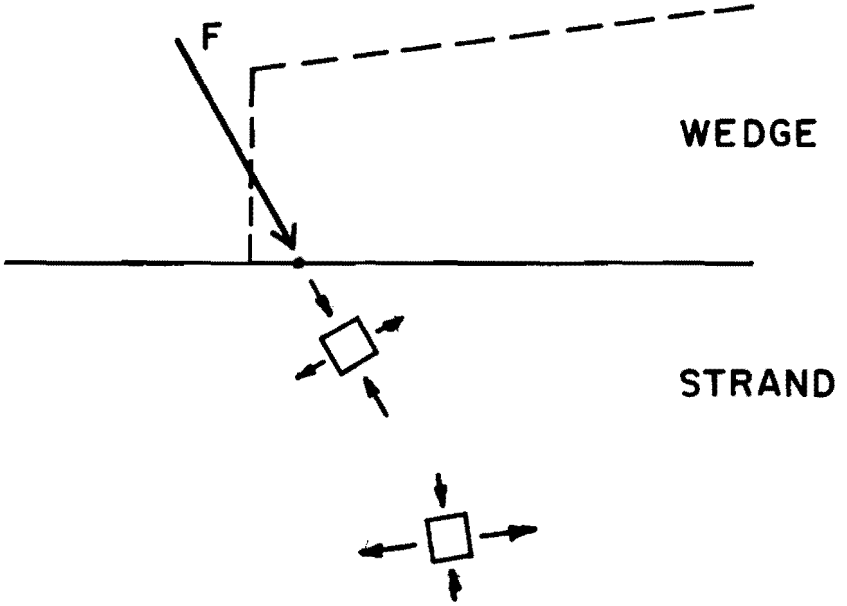

Fig. 6.20 Surface of wire at wedge/strand contact

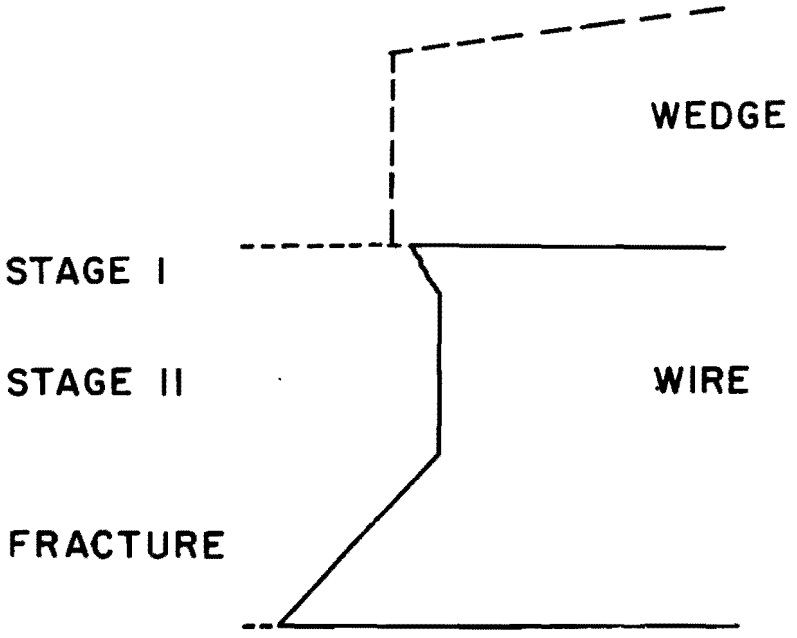

Fig. 6.21 Propagation path of fatigue crack

oriented along the line of the applied surface stress F. Acting perpendicular to these compressive stresses are tensile stresses. A representative stress block showing the stress components is shown beneath the surface line in Fig. 6.20. This stress block is valid at locations near the surface where the surface stress F has its maximum effect. At locations further below the surface, the axial stress in the wire begins to dominate and the stress block rotates as shown in the figure.

The larger the value of F the greater the tensile stresses in the stress block and therefore the greater the probability of local overstresses and material failure. If the surface material fails locally, it will tend to crack perpendicular to the tensile stress. The surface stress F has led to the development of a microcrack parallel to the stress F.

The propagation path of this crack is shown in Fig. 6.21. The propagation of the crack is divided into Stage I crack growth and Stage II crack growth. The final section of "crack growth" is the fracture or overload zone. The Stage I crack growth is that portion of the crack propagation phase influenced primarily by the surface tractions. Stage II crack growth represents that portion of crack growth essentially unaffected by the state of stress at the surface. The failure surface traced in the previous figure is drawn in isometric form in Fig. 6.22. A comparison of this drawing and the electron fractographs presented earlier in this chapter reveals many similarities. Specifically, the initial, angled, part of the crack propagation plane is explained.

The effect of the two surface stress components was discussed in the presentation of the crack initiation model above. The two stress components have already been discussed in relation to the load distribution ratio characteristics of an anchorage. The relationship will be briefly reviewed. First, a base normal stress is assumed to exist for load distribution ratios equal to zero. As the load distribution ratio increases, the normal and tangential stresses increase as well. Increases in the two stress components increase the probability of local material failure and hence microcrack initiation. The relationship between the time (number of cycles) required for crack initiation and the load distribution ratio was presented earlier in this chapter. The decreases in fatigue life with increases in the load distribution ratio support the claim that increases in the surface stress components lead to reduced fatigue lives (i.e. faster crack initiation).

Material variables also influence the crack initiation phase of crack growth. The effect of the hardness of the wedge material has already been discussed and will not be repeated. The contact ratio was also shown to be a function of material hardness. The lower the contact ratio the higher the contact stress and therefore the higher

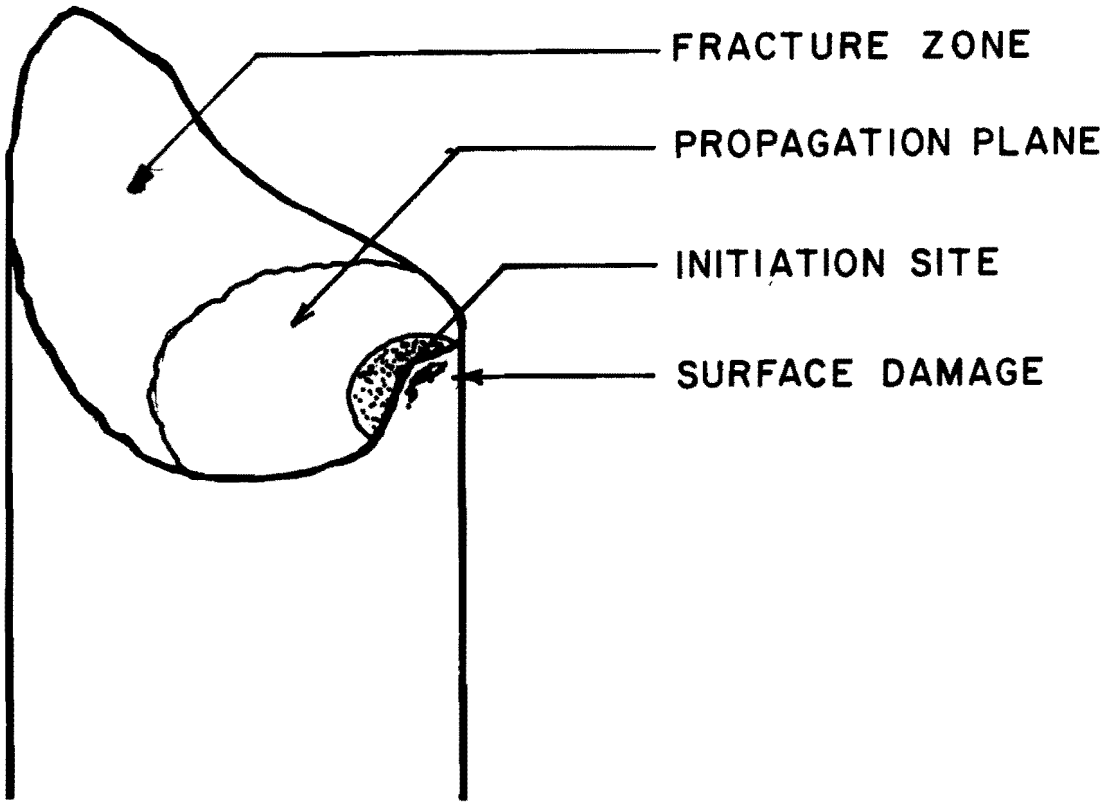

Fig. 6.22 Isometric of resulting fracture surface

the force at some point within the region of contact. The amount of adhesion between two surfaces is directly related to the force pressing the two surfaces together. A large clamping force produces greater adhesive bonds. The increased number of adhesive bonds translates directly into greater tangential stress when the two surfaces are displaced relative to one another as during the fatigue process.

A crack initiation mechanism has been proposed to explain the observed effects of the various material and load parameters on the fatigue performance. In general, any effect which increases the normal and tangential stress components on the surface leads to faster crack initiation and therefore poorer fatigue performance. Fatigue cracks and hence fatigue failures consistently develop at the lead-in section because the stress components are greatest at that location.

CHAPTER 7

CONCLUSIONS AND APPLICATIONS

The results and observations of the research program are summarized in this chapter. This research program has illustrated that a simple fatigue resistant anchorage is possible for prestressing strand loaded in fatigue. The predeformed copper and aluminum wedges were both shown to be capable of providing a fatigue resistant anchorage. The important observations made during the research program will be summarized in the first section of this chapter. Applications of the simple anchorage will be presented in the final section of the chapter.

7.1 Conclusions

The purpose of this research program was to investigate the possibility of the fatigue resistant anchorages which allowed for the visual inspection and replacement of component strands for use in cable-stayed applications. Limitations exist in some of the current anchorage methods currently available. Those anchorages which require grouting do not allow for the inspection or replacement of the component strands. Also, since grout tends to creep over time, a portion of the dynamic load carried, initially, by the grout will reach the more fatigue sensitive static load anchors possibly resulting in early fatigue failures. The objective of this research program was the development of an anchorage method that answered these specific problems.

It was decided in the initial stages of this research program that fatigue testing should be performed on single seven-wire prestressing strands. Diameters of 0.5 in. and 0.6 in. were selected for testing. Two practical methods of gripping the single strand were considered: a clamp system and a wedge system. The wedge-type anchorage was selected for ease of application. The clamp anchorage required the monitoring of both the normal clamping force and the applied tension. The wedge-type anchorage, however, has the advantage of automatically applying a normal force for any tension applied to the strand as long as friction exists between the strand and wedge.

Following the selection of the test specimen and the general anchorage type, the mechanisms responsible for early crack initiation in similar situations were reviewed. The number of cycles required for fatigue crack initiation was assumed to be greater than the number of cycles required for full crack propagation since the crack initiation

mechanisms had the most profound effect on the crack initiation phase. Consequently, increasing the number of cycles required for microcrack initiation was selected as the best method of improving the fatigue performance within the gripped area. Based on the failure mechanisms discussed, only material variables were selected for this research program. Wedges were designed and fabricated from steel, aluminum, and copper for the 0.5 in. diameter strand and from mild and heat-treated steel for the 0.6 in. diameter strand. Also, a modification to the typical wedge-type anchorage was made. The complete anchorage used in this testing program was a two-part anchorage composed of a primary wedge group and a secondary wedge group made up of the commercial wedges currently in use in the post-tensioning industry.

The material variables selected for testing proved to have a significant effects on the fatigue life. In general the materials with the higher values of hardness produced the lowest fatigue lives. The relationship between the primary wedge hardness and the resulting fatigue life was illustrated through the use of the load distribution tests. Harder materials tended to deform less and, consequently, their serration patterns were more effective in providing frictional resistance. As a result, primary grips composed of harder materials carried more of the total strand tension than primary grips composed of "softer" materials.

The better fatigue performanece was observed with anchorages composed of soft primary grip materials primarily because of the lower frictional and normal contact stresses resulting from the lower load distribution in the region of the primary grip. Furthermore, the finite element study indicated that any factor which increased the stiffness of the primary grip (modulus or geometric parameter) produced larger components of the contact stresses. The finite element study also gave the distribution of the contact stresses along the wedge/strand interface. The maximum (or peak) stresses occurred at the lead-in section of the primary grip. All fatigue failures which occurred within the anchorage region developed at the lead-in section of the anchorage. The effects of the surface tractions on the crack propagation planes of the fracture surfaces was observed in the photographs taken with the aid of a scanning electron microscope.

The fatigue test results supported by the load distribution and finite element stress analyses led to the development of a refined crack initiation mechanism for this particular case which was discussed in detail in Chapter 6. The primary grip material was shown to have a significant effect on the fatigue life of the strand within the anchored region. Since the influence of the primary grip is limited to the surface of the strand, its influence must also be limited to crack initiation. It is therefore possible to conclude that the predominate process in the fatigue of wedge-gripped strand is the crack initiation process. Based on the crack initiation model and the

various relationships presented in detail earlier it should be possible to "optimize" the grip for fatigue loading.

7.2 Applications

It was implicitly assumed that the analysis and discussion presented in the previous chapter applied only to the specific anchorages used in the testing program. The observed trends, however, may be applied, within reason, to anchorages not tested. The purpose of this section is two-fold. One objective is to summarize the desired qualities of a single-strand anchorage. The second objective is to demonstrate how a single-strand anchorage might be used in a multiple-strand stay cable.

7.2.1 Single-Strand Anchorage. The primary goal in the design of any single-strand anchorage for use in fatigue-load situations is the retardation of fatigue crack initiation within the anchorage zone. The controlling crack initiation mechanism for single seven-wire strands gripped with wedge-type anchorages was presented in the previous section. The critical section was shown to be the lead-in section where the normal and tangential interface stresses are a maximum. Any "treatment" which tended to cause an increase in the two stress components was shown to produce a decrease in the fatigue performance. Therefore, only those treatments which reduce the two interface stress components should be considered. Other factors such as corrosion will be discussed in the next subsection.

There are two geometric parameters that influence the normal and tangential stress components at the lead-in section of the anchorage. These two variables, the tip thickness and the angle between the inner and outer surfaces of the wedge, were investigated in the finite element stress analysis described in Section 5.3. The peak stresses (at the lead-in section) were shown to decrease with increasing tip thickness. The peak stress was also shown to decrease for increasing angles. However, decreases were small for angles greater than seven degrees (an angle of seven degrees is common in wedges manufactured in many countries including the U.S.).

Based on the stress analyses a wedge with the same angle as those currently in use and a tip thickness greater than those in service should provide better performance. It is difficult to specify a value for the optimum tip thickness as no "flattening" of the peak stress versus tip thickness graph was observed within the range of tip thicknesses studied. The possibility of a shear failure of the wedge itself must also be considered when increasing the the tip thickness. A tip thickness of approximately 0.25 in. would probably be safe for the 0.5 in. strand wedges.

Significant increases in fatigue performance can be achieved through changes in the primary wedge material alone as indicated in the results of this testing program. Reductions in the modulus of elasticity of the primary wedge material below that of the surrounding strand and collar were shown to lead to reductions in the peak stress in the finite element study. The hardness or yield stress was also shown to have a significant effect on the fatigue performance through its influence on the load distribution ratio and the contact ratio. The softer materials have the best performance.

Some limits on the softness of the primary wedge material must be observed. There is some evidence that as the hardness of the primary wedge material decreases the constant load plateau of the secondary grip load distribution diagram becomes less stable (i.e. not constant) thereby introducing fatigue loading in the fatigue-sensitive secondary grip. The possible influence of hardness on the constant load plateau can be seen by comparing the B legs of the predeformed copper, aluminum, and steel wedge load distribution diagrams. The change in slope is small in the range between copper and steel however. It should be noted that "fatigue sensitive" dead-load anchors are not "required". The dead load anchors used in this application were required to provide full resistance against slipping of the primary grip. As such, the dead-load anchors were designed (by commercial designers) to dig into the strand and provide positive resistance to movement by the primary grip.

Materials which exhibit creep deformation (such as lead) should also be avoided. Long-term deflections would tend to shift load into the secondary grip. Eventually the secondary grip would be subjected to relatively significant fatigue loads, thus risking premature failure in the secondary grip area. Materials of approximately the same hardness as that of the copper tested in this program should provide an optimum performance. The constant load plateau is long enough to accommodate substantial stress ranges and is also flat enough so that little if any fatigue load reaches the secondary grip. Zinc would be a possible alternative to copper. Zinc also possesses the desirable characteristic of being anodic to steel and would therefore protect the strand in electrolytic environments.

Only the fatigue results of those anchorages actually tested can be discussed with absolute confidence. However, the trends observed in the test results do allow for some "extrapolation" with a certain degree of confidence. This being the case, an "optimum" single-strand anchorage can be suggested for further experimental exploration. The wedge could be fabricated from zinc with a tip thickness of approximately 0.25 in. and an angle of seven degrees. The length of the wedge is not too important since the critical section is at the lead-in section of the wedge. However, 2 in. is recommended (the same as that tested). It should be noted that the copper wedge tested in this research program performed as well as could be expected

and the only real advantage which exists if one selected the zinc over the copper would be in conditions where galvanic corrosion is a serious threat. Both the predeformed copper and aluminum anchorages yielded fatigue failures in the strand away from the grip. Consequently, without further optimizing, these two types of wedges can be used as part of a simple fatigue resistant stay anchorage.

7.2.2 Stay Cable Anchorage. Since a parallel element stay cable for cable-stayed bridges is simply composed of many (up to about 90) single strands, each of which is individually anchored, the single-strand anchorage described in the previous subsection should be ideal. There are several factors which are different, however, and those will be discussed here.

First, an individual strand cut to length for use in a cable stay would be much longer than the lengths tested in this research program. A decrease in the fatigue strength of the strand on the order of 35% can be expected for extremely long lengths [12]. This reduction is due to the laboratory-observed length effect. The longer the strand, the greater the probability of a large material inclusion. Since the length effect affects only the free length of the strand, the anchored length becomes less important.

Another factor found in cable-stayed bridge cables not included in this research program is possibility of corrosion. Galvanic corrosion is particularly important since salt water is an electrolyte. The proposed zinc anchorage would be ideal for this application since zinc would act as the anode and corrode before the strand. If copper wedges were to be used a small zinc disc could be placed at the lead-in section to provide cathodic protection.

A third possibility in cable stayed applications is beneficial effect of initially overtensioning the strand. Overtensioning the strand forces the secondary grip to carry more of the load in relation to the primary grip when the load is reduced to the in-service maximum. This process is most applicable in bridges with many cables so that the overtensioning of a single cable does not produce overstressing the other structural members.

Finally, and perhaps most importantly, the use of the individual anchorages allows for the inspection of the individual strands contained in the socket. Some of the strands of large anchorages could be destressed separately from the remaining strands and inspected. Any required replacement could be performed on an "as-needed" basis. After the inspection process and any required replacements the destressed strands could be restressed to their original load. A specially designed end plate would be required to allow for partial destressing of component strands. Inspection is not possible in anchorage systems which require grout. The corrosion

protection function of the grout could easily be handled by oil. The oil could be drained prior to inspection then replaced.

The practical advantages inherent in the individual anchorage of strands comprising a stay cable are obvious. The results of the fatigue tests performed in this research program indicate that individual anchorages can be fatigue resistant as well.

R E F E R E N C E S

1. Waterhouse, R. B. Fretting Corrosion. Pergamon Press, 1972.

2. Waterhouse, R. B. ed. Fretting Fatigue. Applied Science Publishers, London, 1981.

3. Collins, J. A. Failure Of Materials In Mechanical Design. John Wiley & Sons, New York, 1981.

4. Deutsche Gesellschaft Fur Metalkunde. Metalurgical Aspects of Wear. DGM, Germany, 1981.

5. David A. ed. Fundamentals Of Friction And Wear Of Materials. American Society For Metals, Ohio, 1980.

6. Fuchs, H. O. and Stephans, R. I. Metal Fatigue In Engineering. John Wiley & Sons, New York, 1980.

7. Calaud, R. Fatigue Of Metals. Chapman and Hall Ltd., London, 1953.

8. Rabinowicz, Ernest. Friction And Wear Of Materials. John Wiley & Sons, New York, 1965.

9. Sarker, A. D. Wear Of Materials. Pergamon Press, Oxford, 1976.

10. Tung, P. P.; Agraival, S. P.; Kumar, Arun; and Kitcher, Micheal. Fracture And Failure: Analysis, Mechanisms And Applications. American Society For Metals, Los Angeles, 1980.

11. Broek, David. Elementary Engineering Fracture Mechanics. Suthoff & Noordhoff, The Netherlands, 1978.

12. Leonhardt, Fritz and Zellner, Wilhelm. Cable-Stayed Bridges: Report On Latest Developments. Canadian Structural Engineering Conference, 1970.

13. Aeberhard, H. U.; Fischli, F.; Luthi, K.; and Schuler, W. VSL Stay Cables For Cable-Stayed Bridges. VSL International Losinger Ltd., 1984.

14. Podolny, W. and Scalzi, J. Construction and Design Of Cable-Stayed Bridges. John Wiley & Sons, New York, 1976.

15. Troitsky, M. S. Cable-Stayed Bridges: Theory And Design. Crosby Lockwood Staples, London, 1977.

16. Paulson, Conrad. A Fatigue Study Of Prestressing Strand. Thesis presented to the Graduate School of the University of Texas at Austin in partial fulfillment of the requirements for the degree of Master of Science in Engineering. The University of Texas at Austin, 1982.

17. Dykers, Scott Robert. Cable-Stayed Bridges: The Cable and Its Fatigue Resistance. Thesis presented to the Graduate School of the University of Texas at Austin in partial fulfillment of the requiremeents of the degree of Master of Science in Engineering. The University of Texas at Austin, 1984.

18. Frost, N. E., Marsh, K. J., and Pook, L. P. Metal Fatigue. Clarendon Press, Oxford, U.K., 1974.

19. Rehm, G., Nurnberger, U., Patzak, M. "Keil-und Klemmverankerungen fur Dynamischg Beanspruchte Zugglieder aus Hochfesten Drahten." Der Bauingenieur 52, 1978.

20. Nurnberger, U. "Spannstahlen in Keilverankerungen Under Statischer Belastung." Der Bauingenieur 56, 1981.

21. Task Committee on Cable-Suspended Structures of the Committee on Special Structures of the Committee on Metals of the Structural Division. "Tentative Recommendations for Cable-Stayed Bridge Structures." ASCE Journal of the Structural Division, pp. 929-939, May 1977.

22. Task Committee on Cable-Suspended Structures of the Committee on Special Structures of the Committee on Metals of the Structural Division. "Commentary on the Tentative Recommendations for Cable-Stayed Bridge Structures," ASCE Journal of the Structural Division, pp. 941-950, May 1977.

23. Podolny, Walter, and Fleming John. "Historical Development of Cable-Stayed Bridges," ASCE Journal of the Structural Division, pp. 2079-2095, September 1972.

24. Faulkner, L. L., and Menkes, S. B. Corrosion and Corrosion Proection Handbook, Marcel Dekker, New York, 1983.

25. Fontana, M. G., and Greene, N. D. Corrosion Engineering, McGraw-Hill, New York, 1978.

26. Uhlig, H. H., and Revie, W. R. Corrosion and Corrosion Control, John Wiley & Sons, New York, 1985.

27. American Society for Metals. Fatigue and Microstructure, American Society for Metals, Cleveland, Ohio, 1979.

28. American Society for Metals. Metals Handbook, American Society for Metals, Cleveland, Ohio, 1948.

29. Hibbit, Karlsonn, and Sorrenson Inc. ABAQUS, a general purpose finite element analysis program.